University of Nottingham

UK | CHINA | MALAYSIA

OIL PALM FIBRE FILLED POLYMER COMPOSITES FOR AIRCRAFT INTERIOR

BY

ONG THAI KIAT

THESIS SUBMITTED TO THE UNIVERSITY OF NOTTINGHAM FOR THE DEGREE OF DOCTOR OF PHILOSOPHY

SEPTEMBER 2023

Abstract

This study aimed to assess the feasibility of using natural fibre reinforced thermoplastic composites for aircraft interior components. Currently, aircraft interior components like seats, interior panels, floor coverings, and linings are primarily made from polymeric materials and composites. Synthetic fibre thermoset composites are commonly used due to their excellent mechanical and thermal properties as well as compliance with airworthiness standards. However, recycling thermoset composites is environmentally challenging compared to thermoplastics.

The study involves investigating the mechanical performance and flammability of natural fibre composites after applying fibre surface treatment, coupling agents, and flame retardants. The goals are to enhance mechanical properties of oil palm fibre (OPF) reinforced acrylonitrile-butadiene-styrene (ABS) composites and ensure compliance with Federal Aviation Regulations (FAR) standards.

First, the optimum process parameters for melt blending used in the fabrication of OPF/ABS composites were justified through visual inspection, tensile test result and melt plastogram analysis. Visual inspection highlighted colour changes at high processing temperatures, while melt plastogram data indicated temperature control challenges at varying rotor speeds and mixing times. Mechanical test result revealed that ultimate tensile strength (UTS) and impact strength of ABS reduced by 20% and 30% respectively. This decline in performance can be attributed to oxidative degradation of ABS, which exposed at high temperatures for extended period.

Second, nanocellulose was extracted from oil palm fibres and used as a reinforcing filler for ABS composites. The material was characterized by Fourier Transform Infrared Spectrometry (FTIR) analysis, Scanning Electron Microscopy (SEM) observation and particle size measurements. FTIR analysis revealed that nanocellulose isolated from OPF and commercial cellulose nanocrystals (Celluforce NCC) have similar FTIR spectra. The Zeta particle size test result showed that average particle size of nanocellulose isolated from OPF and Celluforce NCC are 175.19 nm and 125.42 nm respectively. Tensile tests demonstrated that, with suitable coupling agents (silane and maleic anhydride) and 3 wt. % Celluforce NCC, ultimate tensile strength of ABS composites improved by up to 18.61%. The SEM images also verified the reinforcing mechanism of NCC.

In the third phase, chemically treated oil palm fibres were introduced into ABS composites to study their effects on mechanical properties of ABS composites. The research indicated that fibre surface treatment and coupling agents significantly improved mechanical properties of OPF/ABS composites. Maleic-treated and silane-treated oil palm fibres increased ultimate tensile strength of raw OPF/ABS composites by up to 35.59%, while chemically treated oil palm fibre/ABS composites also marginally enhanced the tensile

properties of neat ABS by 2.38%. The SEM images showed reduced gaps at the interface between chemically treated OPF and ABS.

In the fourth phase, ammonium polyphosphate (APP), alumina trihydrate (ATH), Zinc borate (ZB) and expandable graphite (EG) were added to investigate their effects on mechanical properties and flammability of OPF/ABS composites. Expandable graphite is proven as the most effective flame retardant in OPF/ABS composites. 25 wt. % EG filler able to help OPF/ABS composite to achieve V-0 rating in the vertical burning test. Other flame retardants (APP, ATH and ZB) are unable to help OPF/ABS composites achieve self-extinguish properties. 15 wt.% of APP, ATH and ZB only able to slow down the burning rate of OPF/ABS composites in horizontal burning test. Limiting Oxygen Index (LOI) test result revealed that LOI values increased with addition of flame retardants and APP is the most effective flame retardants. Furthermore. no synergistic effects among flame retardants were observed in the burn test and LOI test. In addition, the tensile properties of OPF/ABS composites were compromised after incorporating of 15 wt. % flame retardants.

Overall, this study explored the potential of natural fibre-reinforced thermoplastic composites for aerospace interior components. The investigation encompassed various aspects including the determination of optimal processing parameters. mechanical properties and flammability. It is feasible to utilize OPF/ABS composites with an appropriate amount of flame retardants for use as aircraft interior materials. However, it is crusial that OPF/ABS composites also pass the heat release rate test and smoke test which prescribed in FAR Part 25. Compliance with stringent safety and flammability standards are required for aerospace applications.

List of Publications

1. **T. K. Ong**, K. Y. Tshai and P. S. Khiew, "Brabender Mixing Parameters on Compounding and Melting Behaviour of Palm Fibre Filled Acrylonitrile Butadiene Styrene," 10th International Materials Technology Conference and Exhibition (IMTCE2016), 16th – 19th May 2016, Kuala Lumpur, Malaysia
2. **T. K. Ong**, K. Y. Tshai, P. S. Khiew, and E. H. Yap, "Thermal and mechanical properties of chemically treated oil palm fiber filled acrylonitrile butadiene styrene composites," Materwiss. Werksttech., vol. 50, no. 3, pp. 240–247, Mar. 2019.
3. **T. K. Ong**, K. Y. Tshai, H. L. Choo, P. S. Khiew, and S. L. Chung, "Mechanical performance and biodegradability of polyvinyl alcohol nanocomposite films," *Materwiss. Werksttech.*, vol. 51, no. 6, pp. 740–749, Jun. 2020

Acknowledgements

The author would like to express his heartfelt gratitude to his supervisor, Dr. Albert Tshai and Dr. Khiew for their support, guidance and expertise during the preparation and completion of the thesis.

The author is grateful to the Faculty of Engineering, University of Nottingham, Malaysia Campus for the use of facilities and Tunku Abdul Rahman University of Management and Technology for their financial support.

Lastly, special thanks to author's family.

Table of Contents

Contents

List of Figures

List of Tables

Chapter 1: Introduction

The increasing demand for new aircraft interior materials to satisfy economic benefits and enhance process efficiency without compromising safety is the thrust to draw researchers and engineers' attention in the past decades. According to the market research report written by Marketandmarkets™, the main driving force of global aircraft cabin interior market is attributed to growing applications in the new generation aircraft, rising environmental concerns and upgrade work of existing aircraft fleets. It was expected that global aircraft cabin interiors market worth USD 32.7 billion by 2025 at compound annual growth rate (CAGR) of 13.2% from 2020 – 2025 [1].

The evolution of aircraft materials indicated that implementation of composite materials in aircraft manufacturing is recent trend. For example, 50 wt.% of Boeing 787 Dreamliner is made from composites and new Airbus A350 even consumed composites in aircraft manufacturing up to 53 wt.%. Hence, the demands of composites in aircraft industry will continue to expand as composites manufacturing technology became more mature [2] [3].

Certain part of aircraft cabin does not need cutting-edge materials to produce as they have limited service life and refurbishment is needed to comply with safety standard of the aircraft. Furthermore, rising fuel prices and incorporation of aviation emissions into the European Union Emission Trading Scheme which started in Year 2012 had facilitated the development of new cabin materials to compensate the above impacts.

Polymer composites are potential substitutes of metallic cabin materials as they are lighter, stronger and less prone to corrosion when compared to conventional metals, alloys and polymers. However, one of the biggest challenge is material cost of advanced polymer composites. Carbon fibre as reinforcement, is still expensive and hence it is only used in structural components for saving cost. On the other hand, consistency in part quality for advanced polymer composite materials is another concern. Failure of certain aircraft components during their service life could cause enormous loss.

In order to reduce overall material cost, enhance part quality and consistency as well as comply with airworthiness standard, researchers and engineers are still exploring new materials. Perhaps, natural fibre reinforced polymers could be one of the alternatives.

Natural fibre filled polymer composites have been used extensively in industries such as automobile, construction, furniture and consumer product due to their distinctive advantages in weight and cost saving, environmentally friendly and potential material properties enhancements. Thermomechanical properties of natural fibre filled polymer composites are highlighted because they influence the potential application of natural fibre filled polymer composites. Broader application can be exposed once the properties enhancements were verified.

There are quite a number of researches focused on fire performance of synthetic fibre reinforced thermoset composites. Synthetic fibres such as glass fibre and carbon fibre offer better flame resistance during combustion due to their uniform dimension and stable thermal properties. In addition, thermosets are network polymers that become permanently hard during their formation. They do not soft upon heating due to covalent crosslinks between adjacent molecular chains. Hence, thermosets are generally harder and stronger in comparison with thermoplastics. This caused synthetic fibre reinforced thermoset composites as one of the well accepted composite materials for aircraft application [4].

Natural fibres exhibited different characteristics in contrast with synthetic fibres. Natural fibre does not promote heat transfer and they decompose at low temperature. It caused them to ignite at shorter time. Furthermore, formation of levoglucosan during decomposition of natural fibres further deteriorates their flame retardancy. In spite of that, natural fibres able to form char as barrier layer to inhibit flame propagation. The heat released during combustion also much lower as compared to many plastic materials. Thus, incorporation of natural fibre into thermoplastics could possibly improves fire resistance of composites [5].

In this study, various approaches on enhancing thermomechanical properties of natural fibre filled polymer composites are studied through literature review and a series of identified methodologies were employed in fabrication of the oil palm fibre (OPF) filled acrylonitrile butadiene styrene (ABS) OPF/ABS composites specimens in the current research work. At present, ABS is employed in the production of aircraft interior components. The utilization of OPF shows potential as a means to reinforce polymer composites. In compliance with airworthiness standard, thermomechanical properties of natural fibre filled polymer composites shall be better or on par with the thermomechanical properties of neat polymer.

1.1 Problem Statement

To date, consumption of aircraft materials has increased drastically as a result of rising demand in the aerospace industries. Using advanced composites in aircraft manufacturing is the current trend as advanced composites possess distinct characteristics such as light weight, excellent specific strength and dimensional stability while fulfilling stringent flammability standard.

From the economic perspective, aircraft manufacturers are keen to seek potential substitutes to reduce their material and manufacturing cost. Therefore, natural fibre reinforced polymers have come into consideration. Natural fibres are significantly cheaper than synthetic fibres, which are widely used in aircraft interior. Moreover, natural fibres are easier to recycle than synthetic fibres because of their biodegradability, renewability and lower energy consumption. Explore the feasibility of natural fibre reinforced polymers for certain aircraft components has drawn attention to researchers [6][7][8]. In order to achieve optimum combination between natural fibre and polymer matrices, there are several factors that should be considered when designing natural fibre reinforced polymer composites.

The primary objective of manufacturing polymer composites is enhancing their specific strength. High strength fibres are always incorporated into polymer matrix for better properties enhancement. However, there are several factors such as fibre loading, fibre size, fibre orientation, interfacial bonding mechanism, processing method as well as properties of fibre and matrix phases which may influence the effectiveness of the potential reinforcement property within the composites [9]. Many studies were conducted in the past and their results showed that fibre characteristics, additives and coupling agents used in natural fibre reinforced polymer composites capable of enhancing the mechanical, physical, electrical and thermal properties of the composites [10][11].

Nanocelluloses have been considered as reinforcing agents in polymer composites for several reasons. They are extremely lightweight yet possess remarkable mechanical properties. Additionally, they offer an environmentally friendly alternative to traditional synthetic fillers. This aligns with the growing demand for sustainable and eco-friendly materials in various industries [12][13] [14].

Acrylonitrile Butadiene Styrene (ABS) was chosen as a polymer matrix for aircraft interiors due to its exceptional properties. ABS is a lightweight material known for its high impact resistance and toughness. It can withstand significant stress and mechanical impacts, making it suitable for high-traffic areas in aircraft interiors. Reducing the weight of components enhances fuel efficiency and overall aircraft performance. Furthermore, ABS can be easily moulded and fabricated into complex shapes and designs, providing versatility for various components and allowing for efficient manufacturing processes.

ABS is available in various colours and finishes and can be easily painted or coated for aesthetically pleasing designs. It can also be modified to meet the stringent fire safety standards required in the aerospace industry. Additionally, ABS exhibits good resistance to a variety of chemicals, including many cleaning agents used in aircraft maintenance, ensuring the longevity and durability of interior components. Overall, ABS offers a combination of mechanical properties, ease of processing, aesthetic flexibility, and compliance with safety standards, making it an excellent choice for aircraft interior applications [15][16][17][18].

Interfacial bonding is amongst the key factor influencing mechanical properties of natural fibre composites. The interface is responsible for transmitting the load from the matrix to the load-bearing fibres. Weak interfacial bonding will lead to failure such as fibre pull-out and hence lowering reinforcing efficiency. Voids may exist in the interface of fibre and matrix. Presence of voids could increase moisture absorption rate and tend to induce stress concentration within composites. Furthermore, fibre agglomeration and fibre loading could lead to adverse effect and thus affect reinforcement efficiency. In order to enhance interfacial bonding, hydrophilic natural fibre and hydrophobic polymer matrix phases need to be modified and coupling agents are often added into composites to graft the fibre and polymer. Hence, a comprehensive literature review and research work should be conducted to study the effects of various factors such as fibre surface treatment and coupling agents on the thermomechanical properties of natural fibre composites.

Parameters of surface treatment and concentration of coupling agents need to be justified to find out optimum composition of oil palm fibre/ABS composites. A series of material characterisation test, mechanical and flammability test need to be conducted to justify the outcome.

In order to comply with stringent fire, smoke & toxicity numbers (FST) stated in Federal Aviation Regulations (FARs), flame retardants were added into natural fibre composites. Flammability tests such as burn test, limiting oxygen index test and thermal stability via thermogravimetric analysis will be carried out to justify the effects of additives and whether natural fibre composites could be an alternative for making aircraft interior components.

1.2 Research Objectives

The objectives of this study are

(i) To investigate the effects of natural fibre surface treatment and coupling agents on the thermal mechanical properties and flammability of OPF/ABS composites.

(ii) To synthesize and characterize nanocellulose extracted from oil palm fibre as reinforcement in ABS composites.

(iii) To study the flammability of oil palm fibre reinforced polymer composites as a function of various flame-retardants and to justify the

potential application of natural fibre reinforced thermoplastic composites for aerospace interior

1.3 Research Hypothesis

The theoretical strength of microfibrils of natural fibre can reach up to 7.5 GPa. Therefore, natural fibres could be effective reinforcing agents for polymer composites [19]. However, there are numerous factors such as chemical components of natural fibres, interfacial bonding mechanism, processing method as well as properties of fibre and matrix phases which may influence the effectiveness of the potential reinforcement property within the composites. If the above factors are to be studied systematically, it is found that the oil palm fibre/ABS composites should have better mechanical properties than neat ABS resin.

It is envisaged that fibre surface treatment should be able to modify the physical appearance and chemical properties of oil palm fibres to achieve better reinforcing efficiency while incorporating into the polymer matrix. In addition, inclusion of coupling agents in natural fibre composites should be able to enhance bonding strength at fibre matrix surface interface. The experimental procedure conducted shall provide positive outcome, and the natural fibre reinforced polymer composites possessed the potential of becoming one of the candidate aircraft interior materials in the near future.

Characteristics of natural fibre and addition of flame-retardants are expected to play key roles in fire resistance of natural fibre composites. Natural fibre not only led to a reduction of peak heat release rate (PHRR) but also may increase char yield of composites which form a barrier layer during combustion. Flame retardants such as ammonium polyphospate (APP), alumina trihydrate (ATH) and zinc borate (ZB) should be able to increase limiting oxygen index (LOI) and time-to-ignition of composites. If synergistic effects occur among constituents of composites, the composites may exhibit self-distinguished.

The in-depth literature review can help to identify the most effective initial guiding procedure for improving the thermal-mechanical and flammability properties of natural fibre thermoplastic polymer composites. Application of the optimum formulations of constituent composition coupled with an effective composite fabrication route capable of producing lab scale natural fibre composite potentially applicable in aircraft interior components.

Chapter 2: Literature Review

2.1 Introduction

In the view of aircraft design, weight is always one of the most important factor. Aircraft designers and engineers have continuously strived to improve the lift to weight ratio of aircrafts over the years. Thus, use of composite materials such as carbon fiber-reinforced epoxy, glass fiber-reinforced epoxy and aramid fiber-reinforced epoxy have played a huge role in the reduction of the overall weight of aircrafts. In addition, composites also provide deisn flexibility, high specific stiffness and strength, excellent corrosion resistance etc. Therefore, the use of composite materials to replace metal materials in aerospace applications has been rapidly growing over the past decade [20]. Figure 2-1 illustrates that one of the best available commercial aircraft on the market, the Boeing 787 Dreamliner is made of 50 % composite materials by weight or 80 % composites by volume [21] [22].

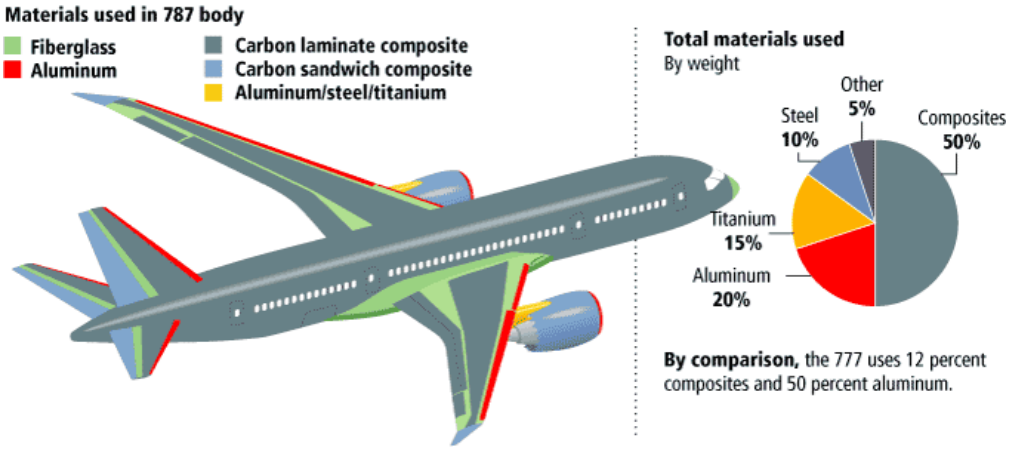

Figure 2-1: Materials used in a Boeing 787 Dreamliner by weight [21]

As part of the current drive towards improving sustainability along with performance in the aerospace industry, environmentally friendly composites are constantly being introduced into the industry as substitutes in aircraft component construction. One of these substitutes that is widely discussed are natural fibre polymer composites (NFPC). Due to the similarity of natural fibre composites with glass fibre composites, NFPC can be used in airraft indoor structure such as aircraft flooring, closets, seating, air ducts, cargo liners, insulating applications and various other cabin interior parts [23].

2.2 Existing Materials Used in Aircraft Interior

The aircraft cabin is an important section of the interiors of a plane. The interior components should meet the basic design, production and functional requirements of the aircraft manufacturers while considering aesthetic properties and serviceability. Materials used in aircraft are independent of types of aircraft. However, they should meet all the standards prescribed in FARs. The fire-worthiness requirements for materials used in aircraft interior are clearly stated in FAR Part 25.853 compartment interiors.

Certain types of aircraft interior components are suitably made from polymeric materials or polymer composites with enhanced flame retardancy. These advanced plastic materials must able to meet flame, smoke and toxicity (FST) requirement as specified in Appendix F to FAR Part 25 [24]. Apart from fulfilling flammability requirement, aircraft interiors generally have less demanding structurally if compared to airframe parts. The interior components do not need to sustain very high structural load or high service temperature. Thus, they could be made from polymeric materials and composites to improve their comfortability as well as reduce their overall weight and cost.

Figure 2-2 illustrates some of the main components in aircraft interior. They are stowage bins, ceiling panel. Wall panels, partition, flooring, galley, lavatory and window. Table 2-1 summarised common materials used in different aircraft interior components. It can be noted that aircraft interior components such as aircraft seat, interior panel structures, floor covering, lining and windows are mainly fabricated by polymeric materials and composites [25].

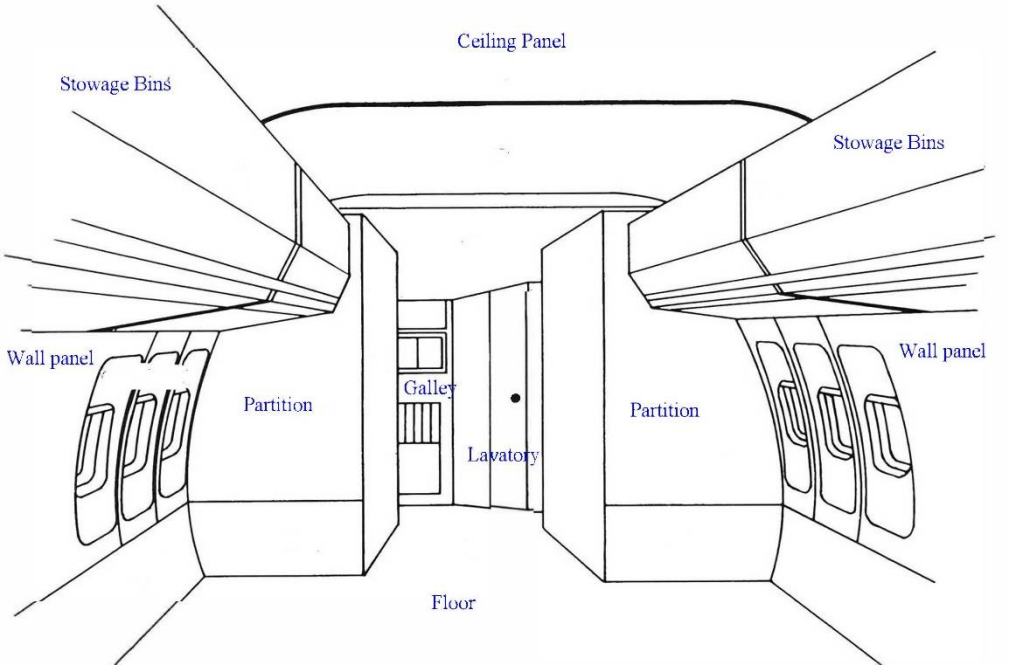

Figure 2-2: Typical main cabin [25]

Table 2-1: Materials used in different aircraft interior components [25]

Application	Components	Materials Used

Aircraft Seat	Foam Cushions	I) The plastics materials used to make foam cushions are depending on requirement. Open Cell urethane foams is the most common material. For emergency safety purpose, polyethylene foams are chosen. II) In the absence of fire-blocking textiles, neoprene, silicone & modified urethane foams can be used for cushions to meet FAR 25.853 (c) .
	Upholsteries	I) Fabrics such as zirconium / wool blends, wool / nylon blends, leather, fire-retarded (FR) polyester, FR nylon, FR wool and vinyl are typical materials for upholstery.
	Fire-Blocking Textiles	I) Polybenzimidazole (PBI), Aromatic polyamides, woven glass are used as fire blocking layers.
	Plastic moulding	I) Polycarbonate (PC), acrylonitrile-Butadiene-Styrene (ABS), decorative vinyls are used to fabricate plastic part of aircraft seat.
	Structure	I) Seat structure are made by aluminium or carbon composites for weight saving.
Interior Panel Structures	Face sheets	I) Fibre reinforcements could be made by fiberglass, aromatic polyamides or graphite/carbon. II) Epoxy and phenolic are used as resin system.
	Core	I) Aluminium honeycomb is used for cabin interior. II) Aramid honeycomb is used for ceiling panel and floor panels.
	Adhesives	I) Epoxy and modified phenolic film adhesives used to bond face sheet to core.
	Decorative coverings for panel	I) PVF (Tedlar) are used due to its good cleanability, colourfastness and low heat release. II) It is suitable for galley and lavatory surfaces that face the aisle, ceilings, baggage racks, lavatory interiors and door liners.
Floor coverings	Galley and lavatories	I) Plastic floor coverings are used in galleys and lavatories due to its excellent water-repellent characteristic.
	Cabin floor	I) Carpets in cabin floor are made by natural fibre or synthetic fibre with addition of fire retardant to enhance fire resistance and noise suppression of yarns.
Windows		I) Stretched cast polymethylmethacrylate

One of the main aircraft interior components are panels. Interior panels are made of face sheets, adhesives, core and decorative coverings as illustrated

in Figure 2-3. They are sandwich structure which used for ceilings, galleys, lavatories, sidewalls, baggage racks, floors, partition and closets. For instance, stowage bins are made from panel with decorative plastic laminate. Partition and floor are made from panel with different decorative cover.

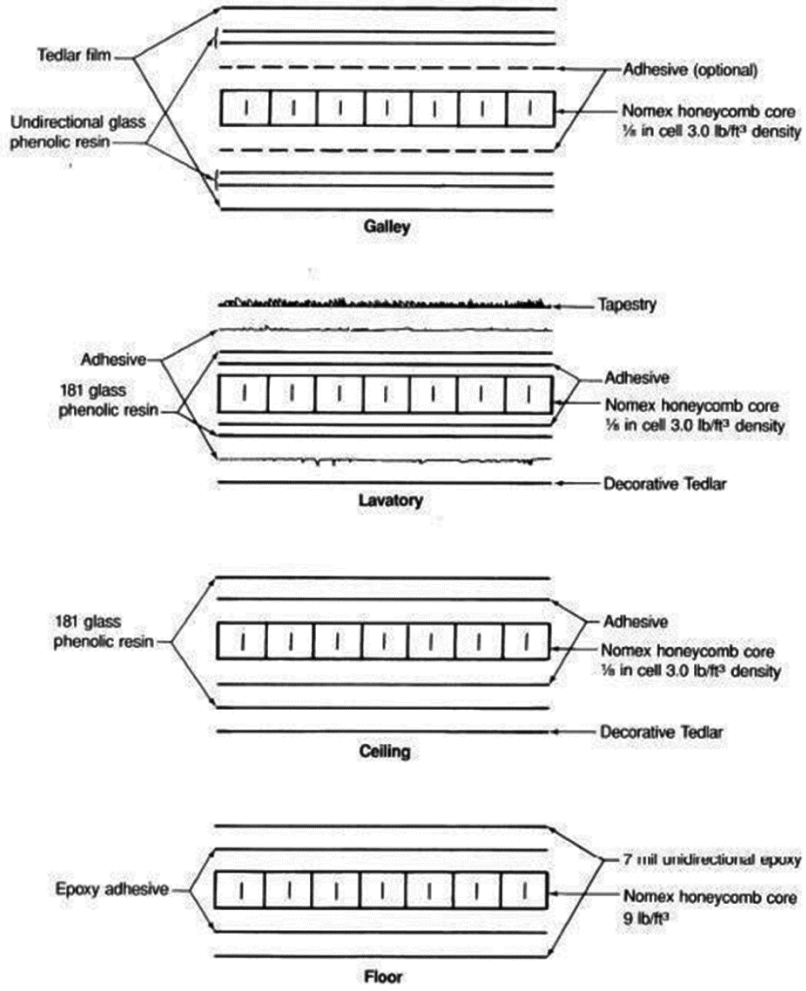

Figure 2-3: Typical panel installation [25]

All panel faces are made up by polymer resin and fibre reinforcement. Epoxy and phenolic are common polymer resins used in making face sheets. Depend on materials selection criteria, epoxy has higher strength compared to phenolic but phenolic can provide superior fire resistance and lower smoke emissions. Moreover, fibreglass, aromatic polyamides, graphite and carbon are used as fibre reinforcement in the form of unidirectional or woven. They possess high specific strength and excellent fire resistance.

The core is most often a honeycomb structure which can be processed into both flat and curved composite structures without excessive mechanical force or heating. Honeycomb cores are available in a variety of materials for sandwich structures. Nomex honeycomb core is an aramid-based paper coated with phenolic resin to stabilise the paper. It is widely used for lightweight interior panels for aircraft in conjunction with phenolic resins in the skins. It is famous due to its unique combination of properties such as high strength, high

stiffness and very good fire resistance. Thus, it is suitable for high performance aircraft structures. Aluminium honeycomb can produce one of the highest strength to weight ratio of any structural material. Its properties can be tailored by varying the foil thickness and cell size. However, Aluminium honeycomb may face potential corrosion problem and it has low resilience.

Adhesives is needed to bond face sheets to core and panel face sheets with decorative coverings. Decorative coverings are laminated on panel face sheets with a layer of adhesives to cover surface flaws. Polyvinyl fluoride (PVF) is typical plastic films used in panel installation due to its good cleanability.

2.3 Potential Application of Natural Fibre Reinforced Polymer Composites in Aircraft Interior

Composite materials especially carbon fibre reinforced polymers had played a key role in the current and potentially future aircraft manufacturing. The percentage of usage of composite materials increased dramatically in the past few decades. At present, 50 wt. % of the Boeing 787 Dreamliner was made up by composites. Most of its primary structures were made of composites, particularly the fuselage, as shown in Figure 2-4. Composites provide irresistible properties as compare to conventional aircraft materials such as metals and aluminium alloys [3][26].

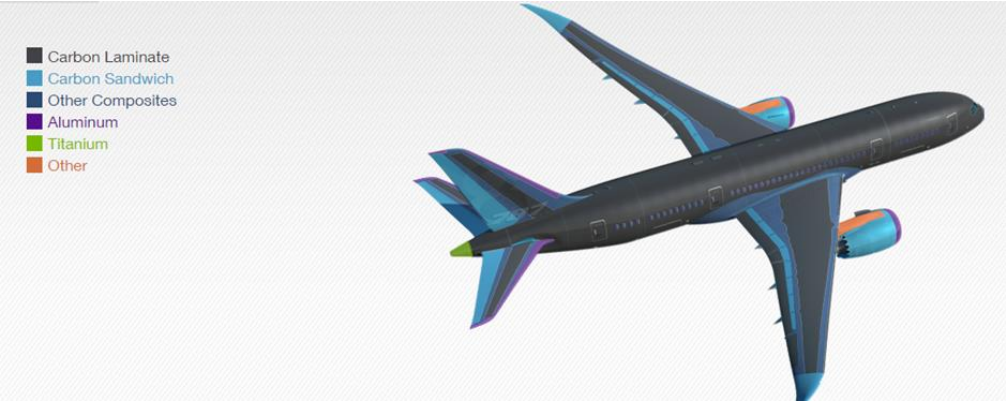

Figure 2-4: Materials used in Boeing 787[21]

Aircraft composites materials should have light weight, excellent strength, dimensional stability, and corrosion resistance as well as fulfilling stringent fire, smoke & toxicity requirements (FST) as defined by FAA. Polymer matrix composites (PMCs) are suitable to be used in aircraft manufacturing. They have lower densities and hence reduce part weight. Consequently, it improved fuel economy and performance. They also have excellent specific properties such as strength and stiffness, thus improved structural performance. In addition, they have better corrosion resistance and fatigue performance than metal and therefore reduce part maintenance cost.

Moreover, one piece-composite components lead to lower manufacturing and assembly cost compared to multiple parts made from metallic materials. Part consolidation resulting in lower product and manufacturing costs. On the other hand, PMCs is superb thermal and sound

insulators. It may improve ride performance due to reduced noise, vibration and harshness.

In spite of the above-mentioned features, there are some challenges need to be solved when designing polymer matrix composites for aerospace industry. PMCs have little plasticity especially thermosets matrix. Therefore, they may lack of damage tolerance. Damage tolerance is a structural property relating to its ability to sustain defects safely until repair can be effected. The properties of polymer composites also greatly affected by environmental degradation. Apart from that, consistent and high quality fabrication process is essential to avoid fabrication defects such as void formation, poor bonding and alignment of fibres, wrinkling of fibres and delamination.

Aircraft interior components include aircraft seats, insulating materials, panel structure, floor coverings, draperies, non-metallic air ducting, linings, electrical components, fire walls and windows. They are made up with various type of materials. Certain type of materials is irreplaceable due to their unique characteristics. For instance, materials selection criteria for windows require materials to have excellent transparency while aircraft seat should be made from thin and flexible materials. Generally, natural fibre reinforced polymer composites are opaque and have higher modulus than thermoplastics.

Nevertheless, certain types of aircraft interior components can be suitably made from natural fibre filled polymer composites with enhanced flame retardancy. Table 2-2 shows a summary of aircraft interior components which potentially could be replaced by natural fibre reinforced polymer composites.

Table 2-2: Aircraft interior component

Aircraft Interior Components	Existing Materials used
Interior panels (ceiling panels, wall panels, galleys, lavatories, sidewalls, overhead luggage compartments and partition)	The face sheets are made from glass fibre / carbon fibre reinforced epoxy/phenolic
Floor covering	Thermoplastics and fibreglass reinforced polymers
Non-metallic air ducting	Fibre glass reinforced thermosets
Compartment lining	Fibreglass reinforced polymers and thermoplastics
Insulating cover	Polymers, fibre glass and ceramics
Plastic moulding of aircraft seat, food tray	Thermoplastics

Thermoplastics such as ABS and polycarbonate (PC) already used in making cargo compartment lining, plastic moulding of aircraft seats and food tray. They can be improved in term of properties and cost when suitable reinforcement is added.

Glass fibre / carbon fibre reinforced epoxy / phenolic have been widely used in aircraft manufacturing. High specific strength, light weight and excellence flame resistance make synthetic fibres favourable choice. However, natural fibres such as oil palm fibre can be incorporated into polymer matrix and possess the potential to replace synthetic fibres in making non-structural aircraft interior components. Natural fibre has lower density and it is fully biodegradable as compared to synthetic fibre. The raw materials cost and processing cost also relatively lower when compared to synthetic fibre. However, natural fibre has lower thermal stability and microbial resistance, and higher moisture absorption. Furthermore, inconsistent size i.e., length and diameter, and hydrophilic nature of natural fibre also may lead to reduction in properties of natural fibre reinforced polymer composites [23].

Aircraft manufacturers prefer thermosets to thermoplastics as polymer matrix because thermosets give better mechanical properties, excellent resistance to solvents and corrosives, and higher heat distortion temperature. However, thermoplastics have distinct characteristics. They can be recycled and they are more environmentally friendly as compared to thermosets. If the thermoplastics incorporated with appropriate reinforcement, their usage can be extended to the aircraft interior and even replace thermoset materials in certain applications. For example, high-performance thermoplastics such as Polyetherketoneketone (PEKK) that has excellent impact resistance and short processing time may be used in load-bearing components that requires good impact strength.

Most of PMCs are fibre reinforced polymer composites and the common synthetic fibres used to reinforce polymer matrices are glass fibre, aramid fibre, boron fibre and carbon fibre. Thermosets are naturally in liquid state and hence they are easier to impregnate fibres. Thermoset composites can be produced by hand layup technique, vacuum bagging process, filament winding, pultrusion and etc. Since the above techniques can hold the fibres in place and long fibres able to improve strength of composites more effectively, it is suitable to reinforce thermosets with long fibres. On the other hand, most of the thermoplastics are granules in form and they require sufficient heat and pressure to shape them into final product. If thermoplastics are reinforced with short fibres or particulate fillers, ease of processing is an added advantage.

Custom designed composition and formulation of natural fibre reinforced polymer composites can replace virgin polymers to improve their properties and achieve cost saving. The service life of aircraft interior components is around 3 – 7 years. The needs for periodic refurbishment of old planes encourage manufacturer seeking new raw materials. Therefore, their distinct properties such as recyclability and lower materials cost make them an alternative option [27].

One of the potential application of natural fibre reinforced thermoplastics is making face sheet for sandwich panel. Currently, most of the face sheet is made by synthetic fibre reinforced thermosets. Rajesh et al. had

done a preliminary research. Their result showed that, with proper flame retardant treatment, natural fibre based sandwiched honeycomb structures are promising materials for aerospace application [28]. Thus, thermoplastics having low Limiting Oxygen Index (LOI) and Heat Release Rate (HRR) could replace thermosets such as phenolic and epoxy in making face sheet. Boegler et al. reported that replacement of aluminium 7000 with ramie fibre composites for making wingbox of airbus A320-200 could help to save 12-14% of weight without compromising structural integrity [29].

Aerospace industry key player, Airbus collaborates with South African Council for Scientific and Industrial Research (CSIR) in search for new aircraft interior materials. Coherent with the future materials development at Airbus, they study the potential application of natural fibre-based materials for making sidewall and ceiling panels, insulation blankets and other less load-bearing parts [30]. As aerospace pioneer, Airbus is exploring bio-composites as tomorrow's materials for future aircraft.

Another leading aircraft manufacturer, Boeing Research and Technology Europe (Madrid, Spain) works together with Invent GmbH (Braunschweig, Germany), Aimplas (Valencia, Spain) and Lineo (St.-Martin du Tilleul, France) to develop environmentally-friendly interior panels made with flax and eco-friendly polymer. Their product is about 35 % lighter than carbon fibre / epoxy prepregs. They also develop flax / epoxy sandwich panel, which can be used for cabin sidewalls of Boeing 737 through vacuum bagging process. They recognized that the biggest challenge of natural fibre is fire resistance. Hence, halogen-free flame retardants are used to comply with FAA and EASA fire resistance requirements [31].

2.4 Airworthiness Authorities, Regulations

2.4.1 Airworthiness Standards and Test Criteria

Federal Aviation Administration (FAA) is part of the United States Department of Transportation (DOT) and it is the national aviation authority of the United States. It holds the responsibilities to regulate Federal Aviation Regulations (FARs) and Airworthiness Standards for different types of aircraft to govern all aviation activities in the United States. FARs are issued by the FAA to implement the provisions of the Federal Aviation Act. All FAA operating procedures must be in accordance with the Federal Aviation Act. Compliance with the FARs is mandatory to obtain the certificates or approvals to which the particular FAR applies.

Among these FAR standards, FAR Part 25: Airworthiness standards: Transport category Airplanes, Subpart D section 25.853 compartment interior is the main section that related to the current study. It clearly describes the flammability requirement and testing procedures of aircraft interior materials [25][32]. Aircraft interior materials used for making different aircraft interior components are required to meet different test criteria as prescribed in Part I –

VII of Appendix F to FAR Part 25 [25]. Part I, part IV and part V of Appendix F to FAR Part 25 are the main components related to the current study.

Part I of Appendix F to Part 25 stated burn test criteria and procedures to compliance with the requirements of FAR 25.853 (a). Burn tests are conducted to determine the resistance of materials to flame. Different types of burn test are conducted to test different interior compartments materials. The materials used to make interior panel structures need to meet applicable test criteria and procedures prescribed in Part I of Appendix F to Part 25 as summarised in Table 2-3.

60-seconds vertical Bunsen burner test (ASTM F501) are conducted for interior compartments such as interior ceiling panels, interior wall panels, partitions, galley structure, large cabinet walls and structural flooring. 12-seconds vertical Bunsen burner test are conducted for floor covering, textiles (including draperies and upholstery), seat cushions, padding, decorative and non-decorative coated fabrics, leather, trays and galley furnishings, electrical conduit, air ducting, joint and edge covering, liners of Class B and E cargo or baggage compartments, floor panels of Class B, C, D, or E cargo or baggage compartments, cargo covers and transparencies, moulded and thermoformed parts, air ducting joints and trim strips (decorative and chafing). 15-second Horizontal Bunsen Burner Test (ASTM F776) are conducted for clear plastic windows and signs, parts constructed by elastomeric materials, seat belts, shoulder harnesses, cargo and baggage tie down equipment [25].

Table 2-3: Part I of appendix F to part 25 [24]

Test Name	Test Criteria
60-second Vertical Bunsen Burner Test	I) They must be self-extinguishing when tested vertically. II) The average burn length may not exceed 152 mm. III) Average flame time after removal of the flame source may not exceed 15 seconds. IV) Drippings from the test specimen may not continue to flame for more than an average of 3 seconds after falling.
12-second Vertical Bunsen Burner Test	I) They must be self-extinguishing when tested vertically. II) The average burn length may not exceed 203 mm. III) The average flame time after removal of the flame source may not exceed 15 seconds. IV) Drippings from the test specimen may not continue to flame for more than an average of 5 seconds after falling.

15-second Horizontal Bunsen Burner Test	I) Average burn rate may not greater than 2.5 inches per minute when tested horizontally.

As tabulated in Table 2-4, Part IV of Appendix F to Part 25 showed the test method and criteria to determine heat release rate (HRR) from cabin materials when they exposed to radiant heat. Heat release rate (HRR) test is conducted to determine the heat release rate to compliance with the requirements of FAR 25.853. The Ohio State University (OSU) heat release rate test is often used as it is compliance with ASTM E906. HRR is a measure of the rate at which heat is generated by fire. HRR is used to characterize fire and its hazard. Heat release rate is the driving force for the fire. Thus, high HRR means that toxic gases, smoke and other types of fire hazards will increase. HRR should be monitored cautiously to prevent fire hazards and minimise the threat to life and property [25].

Part V of Appendix F to Part 25 described the test method and criteria to determine the smoke emission characteristics of cabin materials. Smoke test can be conducted according to ASTM E662 to determine the smoke generating characteristics of airplane passenger cabin interior materials to demonstrate compliance with the requirements of FAR 25.853 (d).

Table 2-4: Part IV and part V of appendix F to part 25 [24]

Test Name	Test Criteria
Heat Release Rate Test	I) The average maximum heat release rate during the 5-minute tests will not exceed 65 kW/m^2. II) The average total heat released during the first 2 minutes will not exceed 65 $kW\ min/m^2$.
Smoke Test	I) The average specific optical smoke density, D_m during the 4-minute test shall not exceed 200.

2.4.2 UL-94 Tests for Flammability of Plastic Materials for Parts in Devices and Appliances

Most plastics are carbon-based materials which will burn and release smoke and gases when subjected to a flame. Flammability, generally refers to the propensity of a substance to ignite easily and burn rapidly with a flame [33].

UL 94 (Underwriters Laboratories test standard UL 94) is the Standard for Safety of Flammability of Plastic Materials for Parts in Devices and Appliances testing, released by Underwriters Laboratories of the United States. It is one of the most widely used flammability tests for determining relative flammability for plastic materials. It measures the ability of plastic part to either extinguish or spread the flame after ignition and its dripping behaviour in response to a small open flame or radiant heat source under controlled laboratory conditions. The tests results can be used as a preliminary indication

of suitability of the materials with respect to flammability for a particular application [34].

(I) Horizontal Burning Test (94HB)

The horizontal burn test is used with polymer materials, with the test specimen oriented in the horizontal direction. This test determines the rate of burning of a material as the flame front progresses between two benchmarks as shown in Figure 2-5. The flame is applied to the free end of the specimen for 30 seconds. The length of the test specimen is 125mm with benchmarks at 25mm and 100mm position. The time for the flame front to move between the benchmarks is measured.

$$Linear\ burning\ rate, V = \frac{60L}{t}$$ ---------- Equation 1

L = burn length, max is 75 mm, t = elapsed time

This is the easiest burn test to pass. A material will be classified 94HB if it fulfils one of the criteria as follow:

1) A material having a thickness between 3 and 13mm will be classified as a HB material if it does not have a burning rate exceeding 40 mm per minute.
2) For material with thickness less than 3mm the burning rate should not exceed 75mm per minute.
3) The material will also be rated as HB if it ceases to burn before the 100mm mark independent of thickness.

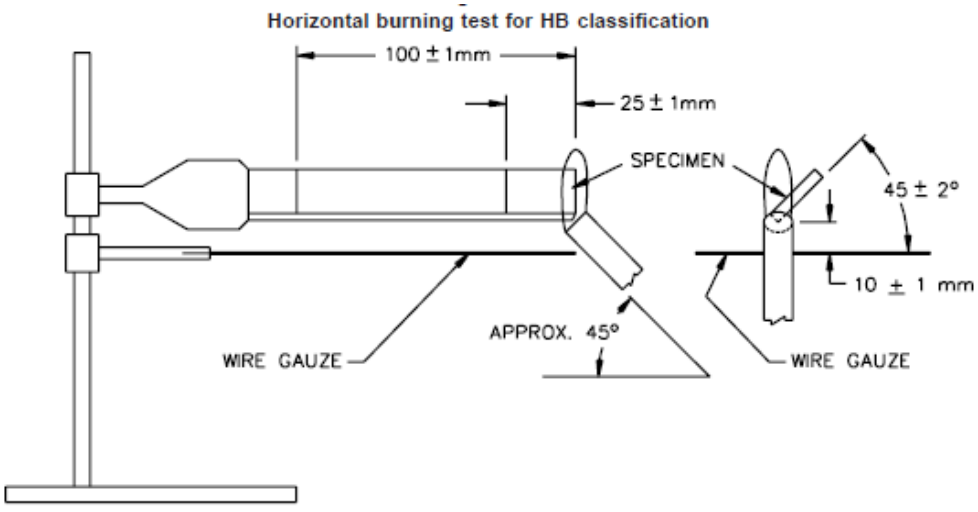

Figure 2-5: Setup of horizontal burning test (94HB)

(II) Vertical Burning Test (94V)

Vertical burning test is more demanding test than horizontal burn test. The specimen is tested in the vertical orientation as illustrated in Figure 2-6. A

test flame is applied to the lower end of the test specimen for 10 ± 0.5 seconds and afterflame time, t_1 is measured. As soon as afterflaming of the specimen ceases, test flame is applied to the lower end of the test specimen for another 10 ± 0.5 seconds and afterflame time, t_2 is measured. 94V requires materials to be self-extinguishing to pass the test. Observation on whether or not specimens drip flaming particles and whether the particles ignited the cotton indicator is needed to help classify materials according to test criteria stated in Table 2-5. If the test samples are unable to meet the test criteria, they are unable to be classified V-0, V-1, or V-2.

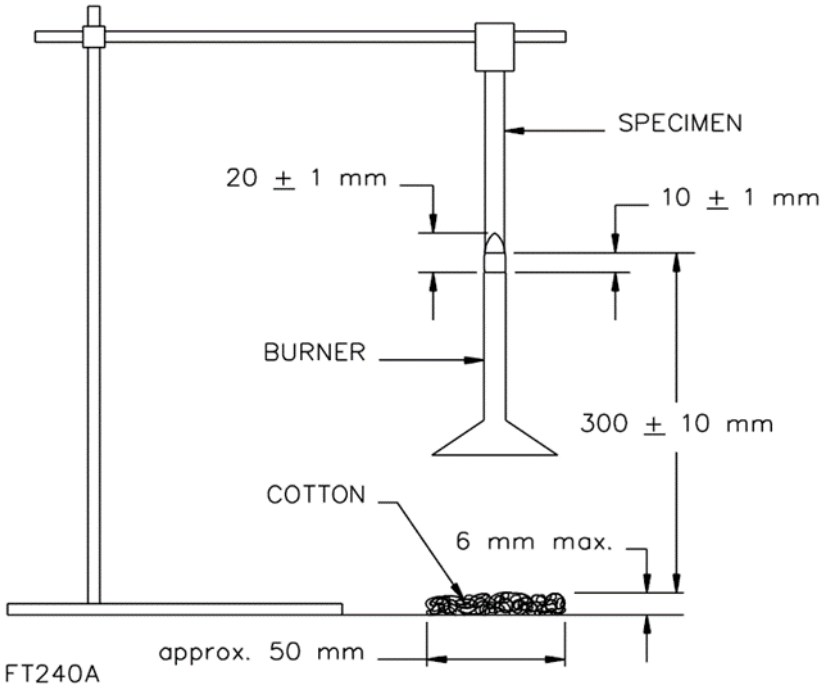

Figure 2-6: Set-up of UL-94 vertical burning test (94V)

Table 2-5: Test criteria of vertical burn test (VB)

Criteria conditions	V-0	V-1	V-2
After flame combustion time for each independent samples t_1 or t_2	≤ 10 seconds	≤ 30 seconds	≤ 30 seconds
Total after flame time for any condition set (t_1 + t_2) of 5 specimens	≤ 50 seconds	≤ 250 seconds	≤ 250 seconds
Flaming and glowing combustion for each specimen after second burner flame application (t_2 or t_3)	≤ 30 seconds	≤ 60 seconds	≤ 60 seconds
Cotton indicator ignited by flaming drops from any samples	No	No	Yes
Presence of glowing or flaming after combustion of any samples up to holding clamp	No	No	No

As compared to horizontal Bunsen burner test and vertical Bunsen burner test stated in FAR 25.853, UL 94 flammability tests (94HB and 94V) use same test flame (50W) and similar test setting as well as samples conditioning method. However, the test procedure and test criteria are different. The criteria stated in vertical burning test (94V) is more stringent than FAR 25.853. V-0, V-1 and V-2 materials need to show self-extinguishing behavior within stipulated time.

(III) Limiting Oxygen Index Test

Fire triangle as illustrated in Figure 2-7 stated the three basic components for combustion. Heat is ignition source to raise the material to its ignition temperature. Different materials have different flash points. Fuel refers to materials that is flammable. Oxygen is essential component of fire to initiate and propagate combustion. When the three elements are co-existed in the right proportions, a fire will take place. If any of the three elements are removed, the fire is extinguished.

The objective of the Limiting Oxygen Index (LOI) test is to measure the relative flammability of plastics and composite materials by burning them in a controlled atmosphere consisting of a mixture of oxygen and nitrogen. The Limiting Oxygen Index represents the minimum level of oxygen in the atmosphere that can sustain flame on a polymer. If materials have higher LOI value, the materials have lower flammability. LOI values of polymer composites can be affected by flammability of fibre types and fibre loading, properties of matrix and flame retardants.

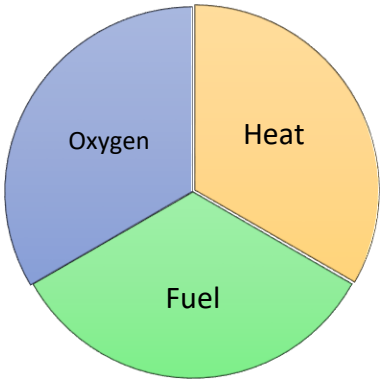

Figure 2-7: Fire triangle

2.4.3 Mechanical properties of aircraft interior materials

There is no specific FAR standard discuss about the mechanical properties requirement of aircraft interior materials. In aerospace material market, commercial FR plastics such as SIMONA Boltaron Series (Simona AG), Kydex® Thermoplastic Sheet (Sekisui), Elastollan® Series (BASF) and Radel® R-7000 Series (Solvay S.A) are popular thermoplastics that able to meet demanding FST requirements. However, they have some limitations. SIMONA

Boltaron 9000 and 4000 Series and Kydex® Thermoplastic Sheet are only suitable for thermoforming process. ElastollanÂ® Series is thermoplastic polyurethane that has been designed for soft touch application such as seat cushion while Radel® R-7000 Series and Pro-Mirror™ are suitable for making aircraft mirror [35][36][37].

Compared with other aircraft interior materials, FR grade ABS have its distinct advantages in term of process flexibility while fulfilling stringent FST standard. Flame retarded ABS can be used for overhead luggage storage compartment and cabin interiors. Generally, it consists of 15% of flame retardants. Table 2-6 summarised mechanical properties of FR grade ABS available in market.

Table 2-6: Mechanical properties of FR grade ABS available in market [38] [39] [40][41]

Mechanical Properties	Value
Tensile Strength (MPa)	33.1 – 44.8
Impact Strength (J/m)	49 - 746
Flexural strength (MPa)	53.1 – 54.9

Considering the FR grade ABS, natural fibre ABS composites have great potential to be used as alternative materials for the interior components such as cargo compartment lining, plastic moulding of aircraft seats and food tray. These products could be fabricated by injection moulding, extrusion or thermoforming process. Natural fibre ABS composites able to provide lower materials cost and manufacturing flexibility on top of fulfilling mechanical, thermal, and flammability requirement of FAR.

2.5 Introduction to Natural Fibres

Natural fibres can be defined as substances produced by plants or animals that can be spun into filament, thread or rope and in the downstream processes be woven, knitted, matted or bound.

As shown in

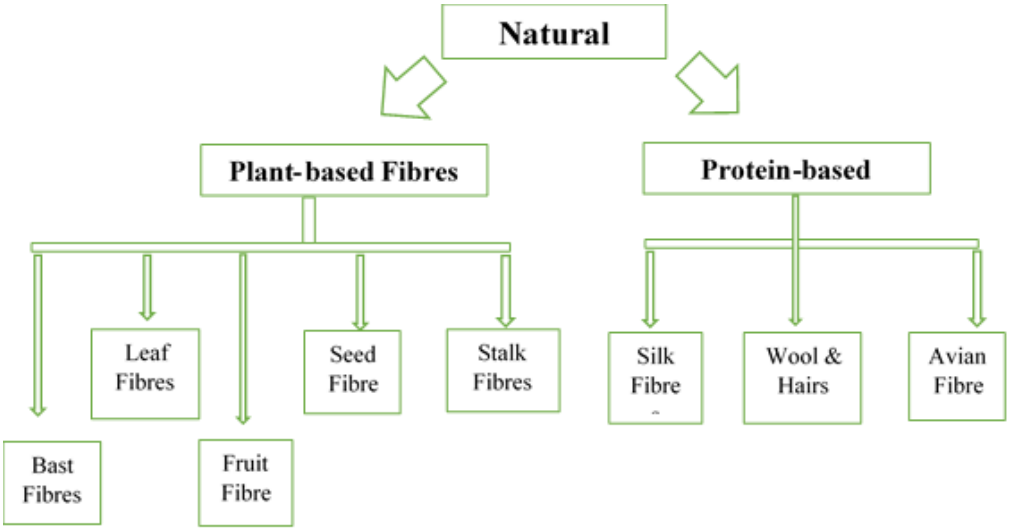

Figure 2-8, natural fibres can be classified into two main groups according to their origin. There are plant-based fibres and protein-based fibres. Based on their origin within the plant, plant-based fibres (vegetable fibres) can be further divided into few subgroups. Cotton and kapok are examples of fibres originating as hairs borne on the seeds. Flax, hemp, kenaf, jute, and ramie are examples of bast fibres which are collected from the skin or bast surrounding the stem of plant. Abaca, pineapple, sisal and henequen are leaf fibres. Coir is example of fruit fibres which originated from inner wall of fruit and examples of stalk fibres are corn, wheat, bamboo and miscanthus. [42]

Protein-based fibres (animal originated fibres) generally consist of proteins such as collagen, keratin and fibroin. Three subgroups of animal fibres are silk fibres, avian fibres and wool & hairs. Avian fibres are the fibres from bird's feathers. Silk fibres are extruded by the larvae of moths and are used to prepare their cocoons. Wool & hairs were taken from animals or hairy mammals. Example includes sheep's wool which is widely used in textile application.

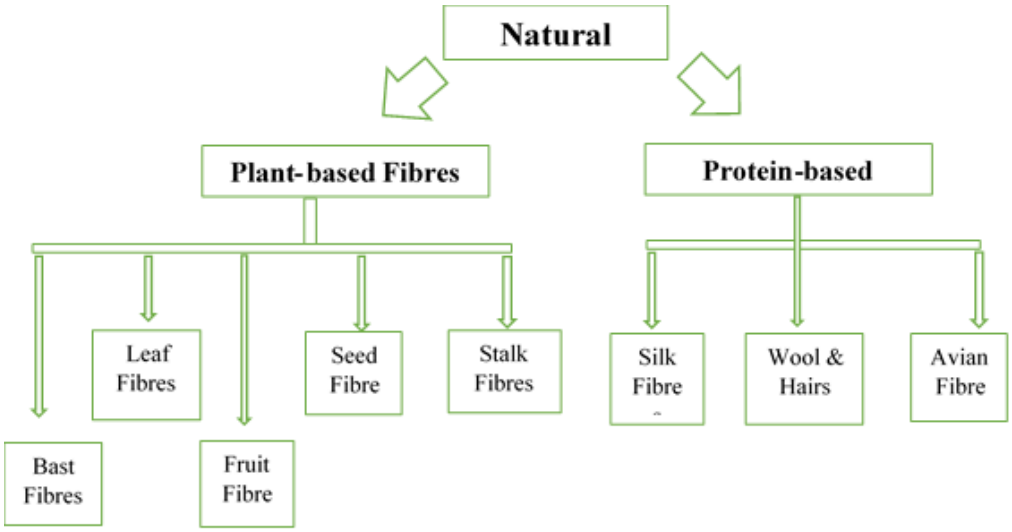

Figure 2-8: Classification of natural fibres

Chemically, all plant-based fibres consist mainly of cellulose, varying amounts of hemicellulose, lignin, pectin, and waxes. Cellulose is an insoluble organic compound with the formula, $(C_6H_{10}O_5)_n$. It is a long chain of linked sugar molecules that gives wood its remarkable strength. Due to its long chain and crystalline structure, cellulose has excellent chemical resistance. It is also the main constituent of the cell walls in most plants and the basic building block for many textiles [43].

Hemicellulose belongs to a group of heterogeneous polysaccharides. It contains some molecules other than sugars. The solubility and susceptibility to hydrolysis of hemicellulose are greater than cellulose because hemicellulose has amorphous structure and lower molecular weight. Lignin is an amorphous, highly complex organic polymer deposited in the cell walls of many plants and make them rigid and woody. Lignin and cellulose work together to provide a structural function in plants. It is much less hydrophilic compared to cellulose and hemicellulose. Furthermore, lignin also forms an effective barrier against attack by insects and fungi.

The chemical composition of plant-based fibres affects the mechanical properties of plant-based fibres reinforced composites. Cellulose has better strength due to its crystalline structure. On the other hand, hemicelluloses tend to have higher water absorption rate and lower temperature degradation as compared to lignin and cellulose. Thus, it may limit the upper service temperature of their composites [44][45][46].

Lignin has better thermal stability among lignocellulosic components, but it is susceptible to ultraviolet degradation. Figure 2-9 shows the structure of plant-based fibres and the amount of different chemical composition of plant-based fibres are shown in

Table 2-7.

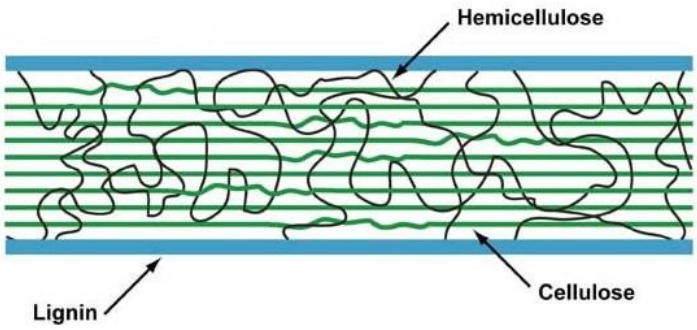

Figure 2-9: Main components in plant-based fibres [47]

Table 2-7: Chemical composition of plant-based fibres

Plant-based fibres	Chemical Composition			Ref.
	Cellulose (%)	Hemicellulose (%)	Lignin (%)	

Oil Palm Fibre	41 - 65%	17.1 - 33.9%	13.2 - 25.31%	[10][48] [49][50]
Cotton	85-90	1-3	7-16	[44]
Jute	61-72	13.6-20.4	12-13	[44]
Flax	64-71	18.6 – 20.6	2-5	[44]
Hemp	70.2-77	17.9-22.4	3.7-5.7	[44]
Kenaf	44-57	21-23	15-19	[42][44]
Ramie	68.6-76.2	13.1-16.7	0.6-0.7	[44]
Sisal	66-78	10 -12	8 - 14	[49][51]
Coir	32-43	0.15-0.25	40-45	[44] [49]
Henequen fibre	60-78	4-26	8-13	[42]
Pineapple leaf fibre	81.5	-	12.7	[49]

2.5.1 Characteristics of Natural Fibres

Natural fibres are widely used in many applications such as textile manufacturing, reinforcement for composite materials, etc. They possess few competitive advantages over synthetic fibres. Original natural fibres are biodegradable and ease of recyclability and combustibility.

The low raw materials cost is attributed to the abundant resources of natural fibres that may come from agricultural waste, plantation, and farm. However, processing cost of natural fibres need to take into consideration. To ensure the consistent quality of natural fibres, some processing steps such as washing, contamination removal, pulverising, fibre treatment etc. need to carry out. Furthermore, the quality and price of natural fibres may vary from batch to batch and depend on geographical location and weather as well. Natural fibres are generally non-abrasive to processing equipment. This led to lesser machine abrasion and further save the equipment maintenance cost. On the other hand, it also restricts natural fibres for light non-abrasive applications only.

From the economic point of view, utilizing natural fibres to the greatest extent especially natural fibres come from agricultural waste, it does not only bring higher profits to the industries, but it may help to promote environmental friendliness and hence facilitate society towards long-term sustainability as natural fibres contain minimum health hazards.

All natural fibres are particularly susceptible to microbial decomposition. Cellulosic fibres can be decomposed by aerobic bacteria and fungi. With the presence of high humidity environment and exposure to higher temperature, cellulose mildews and decomposes more rapidly. Furthermore, some insects such as moths, carpet beetles, termites and silverfish may attack natural fibres.

Hence, chemical modification or surface treatment of fibres were used to protect against microbial damage and insect attacks.

Both vegetable fibres and animal fibres also have an affinity for water. Therefore, it may produce swelling effect due to uptake of water. This characteristic facilitates fibre dyeing process in watery solutions, but it is also a critical drawback for natural fibre reinforced composites. Polarity characteristic of natural fibre creates incompatibility problems with many nonpolar polymers and hence lower the properties of natural fibre reinforced polymer composites. In addition, hydrophilic nature of fibres makes fibres tend to agglomerate into bundle due to forming of hydrogen bonds.

If natural fibres were added into polymer matrices, the polymer composites may possess good acoustic and thermal insulation properties. Due to low density of natural fibres, they are preferred in application that weight is crucial materials selection criteria. On the other hand, natural fibres are restricted to low temperature applications due to their thermal characteristics. Unlike most of the synthetic fibres, natural fibres do not soften when heat is applied. They also would not turn brittle when cooled to freezing point. However, natural fibres may tend to yellowish when exposure to sunlight and moisture. Generally, natural fibres have lower melting temperature and decomposition temperature compared to synthetic fibres. Natural fibres may not be suitable for applications which required higher processing temperature as their limited thermal stability may cause thermal degradation during processing.

As showed in .

Table 2-8 and Table 2-9, natural fibres are lighter than glass fibre and hence it is suitable for application which required low density. In terms of performance, natural fibres are still lower than synthetic fibres. Synthetic fibres have tensile strength of 2000 – 4000 MPa while natural fibres have tensile strength of 50 -1500 MPa.

Natural fibres tend to have lower durability, impact strength, bending strength and poor fire resistance. In order to improve performance of natural fibres, chemical modification, surface treatment and use of additives are common practise in industries [42][43].

Table 2-8: Physical and mechanical properties of natural fibres

Fibre Name	Density (g/cm^3)	Elongation (%)	Tensile strength (MPa)	Elastic modulus (GPa)	Ref.
Oil Palm fibre	0.7 - 1.55	4 – 18	50 - 400	0.57 - 9	[10] [48][51]
Cotton	1.5 - 1.6	3.0 – 10	400	5.5–12.6	[44][52]
Jute	1.3 – 1.46	1.5–1.8	393 – 800	10 – 30	[44][52]

Flax	1.4 – 1.5	2.7–3.2	500–1500	27.6 – 80	[44][52]
Hemp	1.47 – 1.48	1.6 – 40	690	70	[44][52]
Kenaf	1.45	1.6	930	53	[52]
Ramie	1.5	2 –3.8	400–938	44 –128	[44][52]
Sisal	1.33 – 1.5	2.0– 3	511– 700	9.4– 38	[44][52]
Coir	1.2 – 1.25	15 – 30	220 – 593	4.0–6.0	[44][52]
Softwood kraft pulp	1.5	4.4	1000	40	[52]
Abacca	1.50	-	980	-	[44]
Pineapple	-	2.4	640	-	[49]
Banana	-	3	540	-	[49]

Table 2-9: Physical and mechanical properties of synthetic fibres

Fibre Name	Density (g/cm^3)	Elongation (%)	Tensile strength (MPa)	Elastic modulus (GPa)	Ref.
Carbon (Std. PAN-based)	1.78	1.4–1.8	4000	230	[52][4]
E-glass	2.55 – 2.58	0.5 – 3	2000 – 3500	72.5 – 73	[44] [52] [4]
S-glass	2.5	2.8	4570	86	[52][4]
Aramid (Kelvar 49)	1.44	3.3–3.7	3000 – 3150	131	[52][4]
UHMWPE	0.94	350 - 525	38.6 – 48.3	0.69	[52][4]

2.5.2 Chemical Components of Oil Palm Fibres (OPF) and Their Thermal Properties

The chemical components of oil palm fibre are composed of α-cellulose, hemicellulose, lignin, extractives and ash. Generally, oil palm fibre consists of 41 – 65 % of cellulose, 17.1 – 33.9% of hemicellulose and 13.2 – 25.31% of lignin.[10][51][48] Various types of oil palm fibres have various chemical

components. According to research work done by M. S. Sreekala, oil palm empty fruit bunch fibre (EFB) consist of approximately 41 % of cellulose, 24 % of hemicellulose and 21.2 % of lignin [49].

Different chemical components show different characteristics. *α*-cellulose is the preferable chemical component in this study. α-cellulose is composed of long straight chain of glucose units. Its structure contains highly crystalline region and higher degree of polymerization. Hence, *α*-cellulose possesses the highest strength and lowest moisture absorption rate amongst other compound within EFB fibres. The tensile strength of microfibrils can reach up to 7.5 GPa[19]. Besides that, α-cellulose has better resistance to photochemical degradation compared to hemicellulose and lignin.

Hemicellulose is a complex, branched and heterogeneous polymeric network. It has lower degree of polymerization compared to α-cellulose. Hemicellulose is highly hydrophilic and susceptible to biological and thermal degradation. It can be hydrolysed by dilute acids and bases easily. Hemicelluloses start to degrade at temperature range between 200-260 °C and evolve non-combustible gases and tar during pyrolysis.

Lignin is amorphous, highly complex hydrocarbon polymer of phenyl-propane units. It holds cellulose and hemicellulose together. Lignin possesses the lowest strength among chemical components of wood fibres and it is susceptible to photochemical degradation. [46] Lignin is more thermally stable compared to holocellulose. In spite of that, lignin may start to degrade earlier than hemicellulose and it decomposes slowly over a broad temperature range of 200 – 500 °C. This is attributed to the thermal stability of various oxygen functional groups in its structure. Those components have different decomposition pathways. Hence, the exothermic peaks of lignin occurred between 225°C and 450°C [53][54].

Thermogravimetric analysis is often conducted to study the decomposition characteristics and compositional analysis of natural fibres as a function of temperature in a controlled atmosphere. Table 2-10 summarised the findings reported by researchers on the decomposition temperature of natural fibres. It can be seen that hemicellulose decomposed at temperature range from 200 – 270 °C and maximum decomposition rate of natural fibres happened at temperature between 270 to 330 °C due to degradation of cellulose.

Table 2-10: Decomposition characteristics of natural fibres

	Onset Degradation Temperature of hemicellulose / °C	Maximum Decomposition Rate of Cellulose / °C	Ref.
Bamboo fibre	214.1 – 270	300 – 330	[19][55][56]
Arunda fibre	275	320	[57]
Toquilla straw	250	330	[58]

Bagasse	222.3	299.3	[56]
Cotton stalk	221.6	293.4	[56]
Hemp	205.1	282.3	[56]
Jute	205.1	283.1	[56]
Kenaf	219	284.1	[56]
Rice husk	223.3	297.4	[56]
Rice straw	228.5	273.6	[56]
Maple	220.9	308.3	[56]
Pine	234.6	311.5	[56]

Determination of decomposition temperature of hemicellulose, cellulose and lignin through various natural fibres pyrolysis may be used as reference but it is not able to reveal the absolute composition. Varying amount of chemical composition in natural fibres will affect their thermal stability. Ramli et al. reported that thermal stability of OPF are attributed to the concentration of hemicellulose and lignin [11]. Higher content of hemicellulose in natural fibres resulted in lower onset of degradation temperature. The maximum loss rate of cellulose is influenced by the crystallinity of cellulose. Highly crystalline cellulose not only enhance strength of natural fibre composites but also improve thermal properties [59].

Thurs and Haiping Yang et al. conducted TGA on hemicellulose, cellulose and lignin of biomass respectively. The result showed that the weight loss of hemicellulose mainly happened at 220 – 315 °C, while cellulose is at 315 – 400 °C. The maximum mass loss rate of hemicellulose and cellulose occurred at 268 °C and 355 °C respectively. After heated to 900 °C, the solid residue left for hemicellulose and cellulose are approximately 20% and 6.5% respectively [60].

Characteristic Bands of FTIR spectra of natural fibres were summarised in Table 2-11. The main constituents of the fibres such as cellulose, hemicelluloses, lignin and pectin can be verified by referring to the peaks at various wavenumbers range. Functional groups were assigned in accordance with the peaks at various wavenumbers. It can be noted that eight peaks indicated in the FTIR spectra are found to be related to cellulose of natural fibre. Three to four peaks at specific wave number range are relevant to the lignin. Specific peaks represent the existence of pectin and hemicellulose.

Table 2-11: Characteristic bands of FTIR spectra of the natural fibres

Wave Number Range (cm^{-1})	Functional Groups	Component	Ref.

3300-3400	O-H stretching	cellulose	[60][61][62][63]
2850-2970	C-H stretching vibrations	cellulose	[60][61][62][63]
1700-1740	C=O stretching of acetyl or carboxylic acid	hemicellulose	[60][61][62][63] [64][65][66][67]
1645-1650	COO, C=C	pectin	[61] [63]
1613	C=C stretching	lignin	[60]
1510-1560	C=C stretching of the aromatic ring	lignin	[60][61][63][64] [65][66][68]
1430-1470	O-CH_3, C-H asymmetric bending in CH_3	lignin	[60][68]
1426-1430	-CH_2 scissoring	cellulose	[61][63][68]
1360-1375	C-H asymmetric deformation, O-H bending vibrations (in plane)	cellulose	[61][62][68]
1317-1343	CH_2 wagging, -OH bending vibration	cellulose	[61] [68]
1240-1250	C-O-C stretching	Lignin / hemicellulose	[60][62][63][65] [66] 60][68]
1155-1163	C-O antisymmetric bridge stretching	cellulose	[61][68]
1033-1060	C-O stretching and C-O deformation	cellulose	[60][63][65][68]
890-900	C-H stretching, asymmetric, out of phase ring stretching	cellulose	[60][61][63][65] [68]

2.6 Characteristics of Acrylonitrile-butadiene-styrene (ABS)

Acrylonitrile-butadiene-styrene (ABS) is a block terpolymer of acrylonitrile, butadiene and styrene as shown in Figure 2-10. Generally, ABS consists of 15 – 35 % of acrylonitrile and 40 – 60 % of styrene to form a continue phase (SAN) that copolymerised to 5 – 30% of dispersed butadiene phase. Combination of these three components makes ABS one of commercial engineering thermoplastics. Styrene provides shiny and impervious surface as well as ease of processing. Acrylonitrile contributes to high strength and

excellent thermal & chemical stability while butadiene gives excellent impact strength and toughness to ABS.

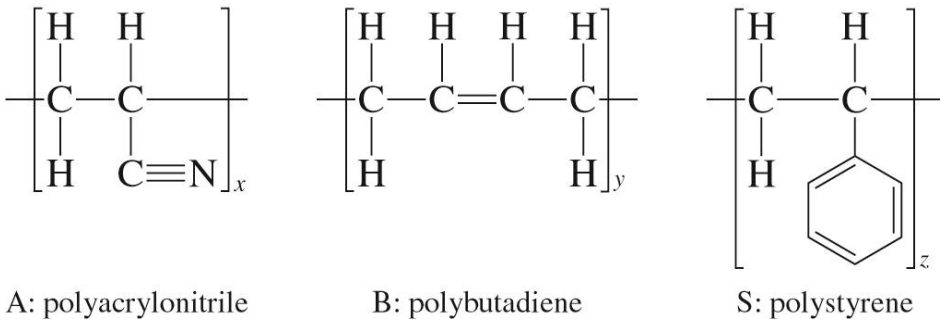

Figure 2-10: Chemical formula of acrylonitrile-butadiene-styrene

ABS is a lightweight opaque thermoplastic that are synthesized from petrochemical compounds. Hence, it is not biodegradable but it can be easily recycled. It is also suitable for surface treatment such as painting, electroplating and polishing. Different grades of ABS are produced based on different composition of acrylonitrile, butadiene and styrene. Its price is relatively high compared to commodity plastic but quite competitive among engineering plastics. Versatility of ABS made the material a suitable candidate for making automotive components, pipe and fittings, Lego bricks, housings for appliances and etc [69].

Nevertheless, ABS is susceptible to degradation under elevated processing condition. Thermal degradation of polybutadiene phase in ABS occurred in the presence of oxygen at high temperature over a long period of time. Moreover, ABS has poor resistance to hydrocarbons and organic solvents. When ABS exposed to heat source, it could lead to high smoke generation during combustion. Apart from that, their poor weathering resistance and fatigue resistance also impede its application. Owing to the excellent processibility of ABS, its drawbacks could be overcome by incorporating various additives such as reinforcing fibres, UV stabilizers and flame retardants during melt blending process. ABS can also be melt-blended with other thermoplastics such as polycarbonate, polyamide and polyvinyl chloride to tailor properties for specific application.

In order to open door for ABS and their polymer composites to be used in specific application such as the aerospace industry, comprehensive study on the properties of ABS and its relation to additives is essential. Masanori Suzuki et al conducted TGA and FTIR analysis to investigate the thermal degradation behaviours of polystyrene (PS), polybutadiene (PBD), polyacrylonitrile (PAN), styrene-acrylonitrile (SAN) and acrylonitrile-butadiene-styrene (ABS). As summarised in Table 2-12, the authors reported that individual polymer resin showed lower onset degradation temperature as compared to ABS terpolymer. Thermal degradation of ABS commences at 340°C due to degradation of polybutadiene. Then followed by decomposition of styrene at 350°C and evolution of polyacrylonitrile at 400°C. Tong et al conducted thermal decomposition studies of ABS resin using TA instrument SDT Q600 under

nitrogen environment. They reported that degradation commences at 410°C [70][71].

Table 2-12: Thermal degradation of constituents of ABS [70][71]

	PBD	PAN	PS	SAN	ABS
Onset temperature	290 °C	290 °C	360 °C	370 °C	340
End temperature	500 °C	480 °C	450 °C	530 °C	490
Residues	9 wt. % residue at 600 °C	56 wt. % residue at 800 °C.	No residue	No residue	4 % residue at 600 °C

Sara Aid et al and Peydro et al conducted FTIR spectra analysis on the ABS resin whose trade name as Terluran® GP-22, their result showed that GP-22 exhibits characteristic peaks as tabulated in Table 2-13. The sharp peaks appeared at 966 cm^{-1}, 1603 cm^{-1} and 2239 cm^{-1} are attributed to butadiene moieties, styrene moisties and nitrile moieties respectively. The FTIR spectra was verified by using Spectrum 65 FT-IR Spectrometer and the result is shown in Figure 2-11. It was found that FTIR spectra of GP-22 is similar to the investigation done by Sara Aid et al and Peydro et al. [72][73].

Table 2-13: Characteristic bands of FTIR spectra of GP-22

Peaks (cm^{-1})	Functional Groups	Ref.
843 cm^{-1}	C-H	[72]
966 cm^{-1}	Trans-2-butene-1, 4-diyl (butadiene)	[72][73]
1455 cm^{-1}	Chin butadiene	[72]
1494 cm^{-1}	Aromatic C	[72]
1603 cm^{-1}	Styrene moieties	[73]
2239 cm^{-1}	C Ξ N (nitrile moieties)	[72][73]
2855 cm^{-1}	C-H	[72]
2922 cm^{-1}	CH_2	[72]

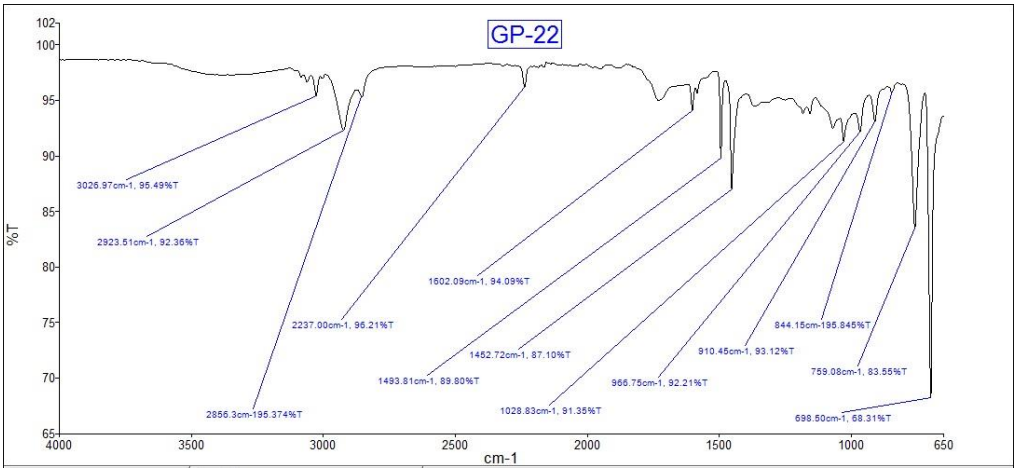

Figure 2-11: FTIR spectra of GP-22

2.7 Surface Treatment of Oil Palm Fibres

Natural fibres are highly polar and hydrophilic due to the hydroxyl groups in their structure. Fibre treatment is essential to enhance its compatibility with polymer resins. Fibre treatment is not only able to improve wettability with the polymer matrix, but also can reduce moisture absorption of polymer composites. Chemical treatment such as acetylation, mercerization and silane treatment could change the hydrophilic fibre surfaces to hydrophobic and thus lead to better dispersion of fibres in polymer matrix.

Mercerization, which also called alkali treatment of natural fibre, is a fundamental and widely used fibre surface treatment. Mercerization breaks down fibre bundle and turn it into smaller fibrils. It does not only make the surface of natural fibre rougher but also increase the aspect ratio and reactive sites of fibres. Hence, mercerization helps to enhance fibre-matrix interfacial adhesion. Table 2-14 summarised the parameters of alkali treatment used in fibre reinforced composites by different researchers. Their works had proven that alkali treatment could modify the natural fibre surface and enhance the mechanical properties of natural fibre composites effectively.

Moshiul Alam et al. studied the efficiency of alkali treatment on oil palm empty fruit bunch (EFB) fibre reinforced poly(lactic acid) composites. They reported that ultrasound-alkali treated oil palm empty fruit bunch fibre able to increase the tensile strength and tensile modulus of EFB/PLA composites by 23.5% and 52 % respectively as compared to raw empty fruit bunch fibre [74]. Maya Jacob et al. reported that sisal fibre and oil palm fibre treated with 4 wt % sodium hydroxide solution able to improve storage modulus of hybrid fibre-reinforced natural rubber composites due to increased crosslinking and formation of a strong fiber/matrix interface [75].

Tran Huu Nam et al. treated coir fibre with 5% sodium hydroxide solution at room temperature and then added alkali-treated coir fibre into poly(butylene succinate). The tensile test result showed that the mechanical

properties of the above composites are significantly higher than those of untreated fibres [76].

Table 2-14: Parameters of alkali treatment used in fibre reinforced composites

Concentration of NaOH Solution	Treatment Temperature (°C)	Treatment Time (Hour)	Type of Fibre	Polymer Matrix	Ref.
17.50%	20 °C	2	Oil palm fibre	Polypropylene	[50]
3 %	80 °C	1.5	Oil palm fibre	Polylactic acid	[74]
4%	room temperature	1	Sisal / Oil palm fibre	Natural rubber	[75]
2%	100°C	0.5	Oil palm fibre / glass fibre	Polyester	[77]
5%	room temperature	72	Coir	Poly(butylene succinate)	[76]
20%	25°C	0.5	Coir	Ethylene dimethylacrylate	[78]
5%	300°C	1	Coir	Polyester	[79]
6%	40°C	24	hemp	Polylactic acid	[80]
5%	30°C	5	pineapple leaf	Polycarbonate	[81]
22%	10°C	1	Hemp	Epoxy	[82]
29%	20°C	0.33	Flax	Polypropylene	[82]

2.7.1 The effect of Coupling Agents on the Properties of Polymer Composites

Chemical coupling agents can be divided into three types, which are organic coupling agents, inorganic coupling agents and organic-inorganic coupling agents. Each enhances compatibility between natural fibre and polymer by different coupling mechanism.

Organic coupling agents such as maleic anhydride and acetic anhydride were recommended to add into OPF filled ABS to act as bridges to link OPF and ABS by covalent bonding or hydrogen bonding. The hydroxyl group of OPF was activated after conducting alkali treatment. Organic coupling agents could chemically react with hydroxyl group of OPF while another functional group of coupling agents can copolymerise with polymer matrix. As a result of stronger adhesion at the interface, stress can be transferred to fibre more effectively and lead to mechanical properties enhancement [83].

Organic-inorganic agents are hybrid organic-inorganic compounds. Silanes such as γ-methacryloxy propyl trimethoxy silane and γ-amino propyl trimethoxy silane had proven that they could improve coupling efficiency. By a proper surface and/or bulking treatment with silanes, the normally hygroscopic natural fibres can be converted into a hydrophobic reinforcement for non-polar polymer matrices. Hydrophobation treatments can weaken the hydrogen bonds between natural fibres and the agglomeration of fibres is thus reduced during compounding with non-polar polymer matrices.

Coupling agents could further enhance the grafting efficiency of natural fibre composites in the presence of free radical initiator. Hence, peroxides are incorporated into natural fibre composites during compounding.

Inorganic coupling agent such as sodium silicate could act as dispersing agent to help uniform dispersion of OPF in polymer matrix. They counteract surface polarity of wood fibre and thus improve the compatibility between natural fibre and polymer.

2.7.2 Maleic Anhydride Treatment

Bonding Mechanism

As shown in Figure 2-12, organic coupling agents such as maleic anhydride ($C_4H_2O_3$) contain multifunctional groups in their molecular structure. Refer to FT-Raman spectra of maleic anhydride provided by Sigma – Aldrich as shown in Figure 2-13 and Table 2-15, a weak peak detected at 3100 - 3150 cm^{-1} was attributed to C-H stretching. A sharp peak found at 1800 - 1900 cm^{-1} was corresponding to C=O carbonyl groups. Vibration peaks at the range of 1700 - 1800 cm^{-1} are associated with C=O stretching. An intense peak found at 1560 - 1590 cm^{-1} was assigned to C=C stretching. Few vibration peaks found at 1240 - 1250 cm^{-1} are associated with C-O stretching.

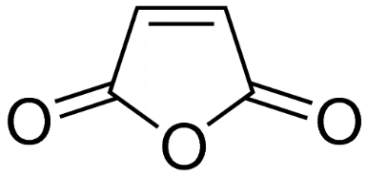

Figure 2-12: Chemical structure of maleic anhydride ($C_4H_2O_3$)

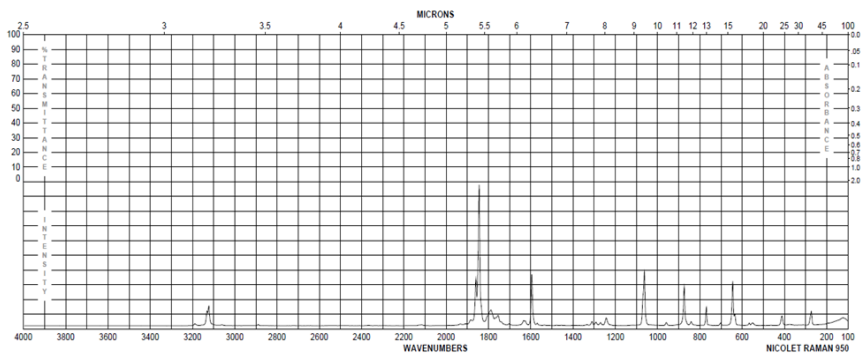

Figure 2-13: FT-Raman spectra of maleic anhydride [84]

Table 2-15: Characteristic bands of the FTIR spectra of maleic anhydride

Wave Number Range (cm^{-1})	Functional Groups	Ref.
3100-3150 cm^{-1}	C-H Stretching	[84]
1800-1900 cm^{-1}	C=O carbonyl groups	[60][61]
1700 – 1800 cm^{-1}	C=O stretching	[60][61]
1560-1590 cm^{-1}	C=C Stretching	[60]
1240-1250 cm^{-1}	C-O Stretching	[85]

The carboxylate groups (-COO-) of maleic anhydrides could react with polar groups such as hydroxyl groups (-OH) of fibre and form covalent bonding. This may form more ester groups on the natural fibre surface. Their reaction is illustrated in Figure 2-14. Furthermore, organic coupling agents could help to modify polymer matrix by graft copolymerization and thus result in strong adhesion between natural fibre and polymer matrix. FTIR spectra of treated OPF and OPF/ABS composites could help to verify the effectiveness of maleic anhydride as compatibilizer in OPF/ABS composites.

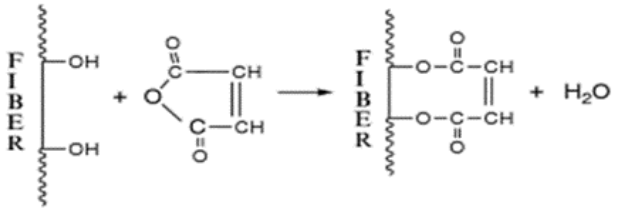

Figure 2-14: Reaction of maleic anhydride and nature fibre

Maleic anhydride is an effective coupling agent due to its conjugated structure. The graft reactivity of maleic anhydride with the polymer matrix increased in the presence of radical initiator such as organic peroxide. Hence, it facilitates strong adhesion at the interface of natural fibre and polymer material [86]. Acid number can be measured through titration to study the grafting effectiveness of maleic anhydride on natural fibre composites.

Table 2-16 summarised various maleic coupling agents used for improving properties of natural fibre reinforced composites. Maleic anhydride grafted polypropylene (MAPP) and maleic anhydride grafted polyethylene (MAPE) are extensively used in polyethylene and polypropylene matrices composites.

Mohamad Jani et al. studied the effects of maleic anhydride and Epolene 43 on the mechanical properties of OPF / PP composites and kenaf core / PP composites. They realised that tensile strength, tensile modulus, tensile toughness and dimensional stability of MAPP-treated composites are better than untreated polypropylene composites [87] [88]. Similar result was obtained by R Ramli et al. They found that addition of 3 wt. % of MAPP into oil palm fibre reinforced polypropylene composites will enhance their thermal properties,

tensile properties and flexural properties. Moreover, the optimum fibre loading is 30 wt. %. Overloading may lead to fibre agglomeration [11].

Table 2-16: Maleic coupling agents used in natural fibre reinforced composites

Name of maleated coupling agent	Concentration of coupling agents	Type of Fibre	Polymer Matrix	Ref.
MAPP / Epolene-43	5%	Oil Palm Fibre	Polypropylene	[87]
MAPP / Epolene-43	3%	Oil Palm Fibre	Polypropylene	[11]
MAPP / Epolene-43	2.5%	Sawdust, rice husk	Polypropylene	[89]
MAPP / Epolene-43	1-5%	Kenaf Core	Polypropylene	[88]
MAPP	5%	Coir	Polypropylene	[90]
MAPP	5%	Corn Chaff	Polypropylene	[90]
MAPP / Epolene	3-5%	Flax, jute	Polypropylene	[86]
MAPE	3%	Wood flour	High Density Polyethylene	[86]
MAPP	5%	Kenaf / rice hull	Polypropylene	[91]
Maleic anhydride graft PLA	5%	Kenaf & rice Hull	Poly(lactic acid)	[91]
MAPP	3wt %	Rice husk flour & wood flour	Polypropylene	[92]
MAPE	0-10 %	Thermomechanical pulp (TMP) fibre	High Density Polyethylene	[93]
MAPP	2 wt. %	Luffa fibre	polypropylene	[94]
Maleic anhydride	2 %	Banana, hemp and sisal	polystyrene	[95]
Maleic anhydride	1:10 MA : wheat straw fibre	Wheat straw fibre	polypropylene	[96]
Maleic anhydride	5 wt. %	Hemp fibre	polypropylene	[61]

2.7.3 Silane Treatment

Bonding Mechanism

The chemical structure and FT-Raman Spectra of 3-(Trimethoxysilyl)propyl methacrylate was shown in Figure 2-15 and Figure 2-16 respectively.

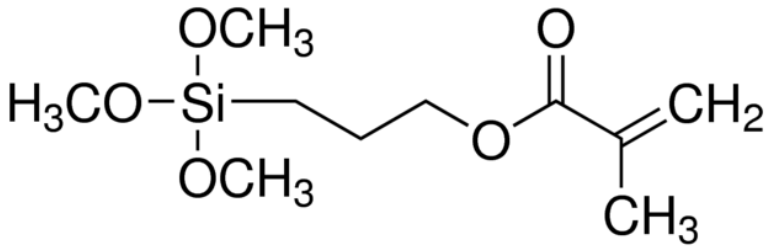

Figure 2-15: Chemical structure of 3-(Trimethoxysilyl)propyl methacrylate

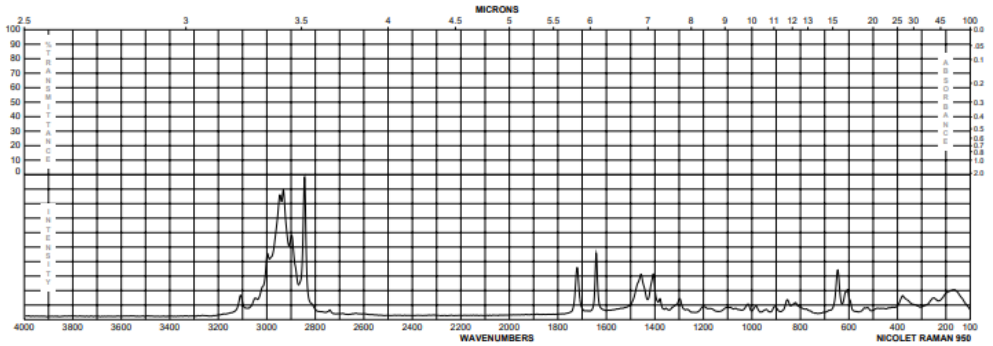

Figure 2-16: FT-Raman spectra of 3-(Trimethoxysilyl)propyl methacrylate [97]

To effectively couple the natural fibres and polymer matrices, the silane molecule should have bifunctional groups, which may react with the natural fibre and polymer matrix respectively and thereby forming a bridge in between them.

Trialkoxysilanes are amongst the most established silanes used for natural fibre composites. The alkoxy (OR) groups of silanes are hydrolysable groups such as methoxy, ethoxyl or acetoxy groups. Si-OR bonds hydrolyse readily with water. These silanol groups can then condense with each other to form polymeric structures with very stable siloxane Si-O-Si bonds. The hydrogen bonds between silanols and hydroxyl (OH) groups of natural fibre may convert to covalent bonds by heating. Silanol groups can also condense with metal hydroxyl groups on the surface of glass, minerals or metal. This allows inorganic and organic materials having very dissimilar surfaces to be coupled chemically.

The organofunctionalities (X) of silanes are generally amino, mercapto, glycidoxy, vinyl, or methacryloxy groups. The organofunctionalitity of the silane interacts with the polymer matrices with their interaction modes depending on the functionality's reactivity or compatibility towards the polymer [98].

Refer to Figure 2-17 (a), the silane monomers are hydrolysed in the presence of water and catalyst to generate reactive silanol groups. To fully hydrolyse one mole of trialkoxysilane, at least three moles of water is needed. It was found that γ–methacryloxypropyltrimethoxy silane (MPS) hydrolyses

much slower and requires the use of an amine as catalyst in the water/solvent solution.

As seen in Figure 2-17 (b), self-condensation of silanols also start during hydrolysis. The condensation should be kept at minimum level at this stage so that the silanols are free from being adsorbed to the hydroxyl groups in the natural fibres. Optimum conditions of hydrolysis are essential to accelerate hydrolysis while inhibiting condensation. Generally, under acid-catalyzed conditions, the hydrolysis rate of silanes forming silanol groups is greater than the condensation rate of the ensuing silanols forming siloxane bonds. In an acidic solution, the hydrolysis rate of MPS was accelerated and the self-condensation rate was reduced compared to those in the alkaline solution.

Refer to Figure 2-17 (c), absorption process starts to take place. Hydroxyl groups (OH) of natural fibres adsorbed reactive silanol monomers or oligomers by hydrogen bonding. In order to fully modify the cell wall of natural fibres, the molecular size of the silanols should be small enough to penetrate into interior of cell walls. On the other hand, the free silanols also adsorb and react with each other thereby forming a rigid polysiloxane structures linked with a stable –Si–O–Si– bond during this stage.

As shown in Figure 2-17 (d), the hydrogen bonds between the silanols and the hydroxyl groups of fibres can be converted into the covalent –Si–O–C– bonds under heating. The residual silanol groups in the fibres also further condense with each other [98][99] [100].

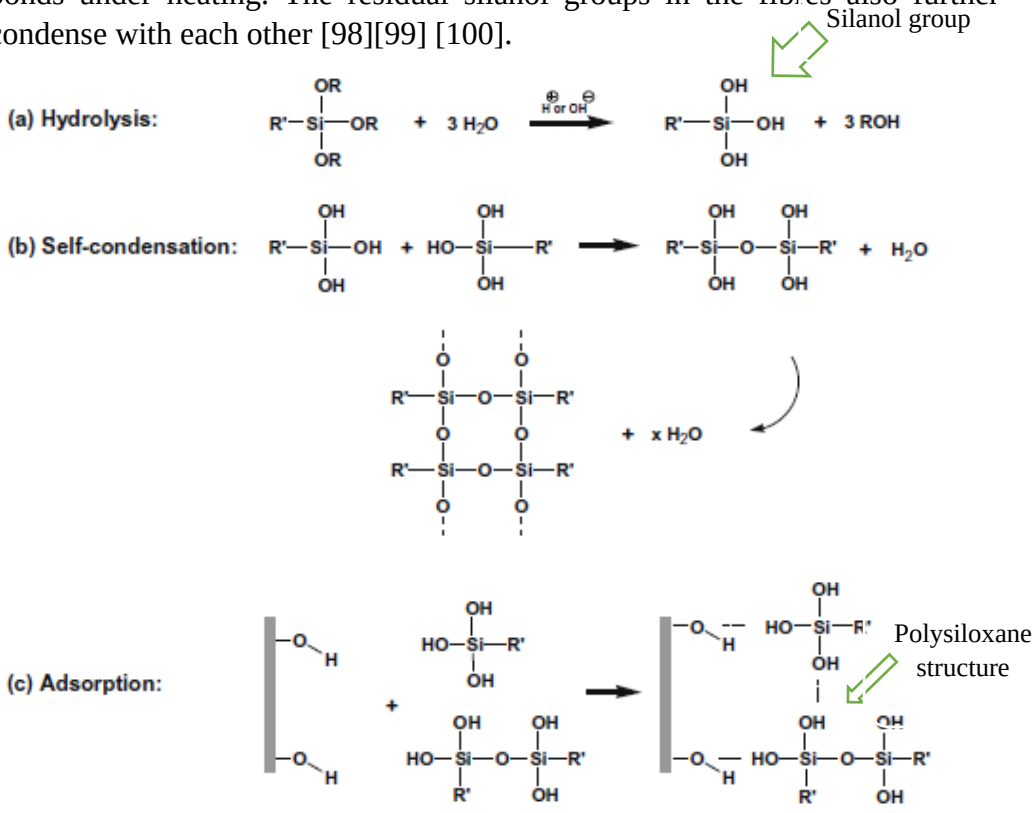

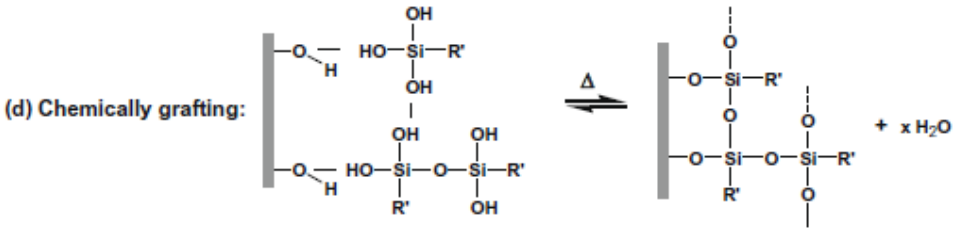

Figure 2-17: Reaction of silane and natural fibres under hydrolysis process [98][99] [100]

Table 2-17 provide a summary of various silane treatment used for improving properties of natural fibre reinforced polymer composites by other researchers.

Table 2-17: Silane treatments used in fibre reinforced composites

Name of Silanes	Concentration of coupling agents	Type of Fibre	Polymer Matrix	Ref.
3-Methacryloxypropyl trimethoxy silane	1 wt. %	wood saw dust	ABS	[101]
N-2(aminoethyl)3-aminopropyl trimethoxy silane	0.5 wt. %	wood saw dust	ABS	[101]
3-aminopropyl trimethoxysilane (3-APE)	2 %	short glass fibre	Poly(butylene terephthalate)	[102]
γ-aminopropyl trimethoxy silane	1wt. %	Pineapple leaf	Polycarbonate	[81]
γ-methacryloxy propyl trimethoxy silane	1wt. %	Pineapple leaf	Polycarbonate	[81]
γ-methacryloxypropyl trimethoxy silane (MPS)	0.65 (v/v)	tremolite	polyamide	[103]
3-aminopropyl)-triethoxysilane	2.5 wt. %	Luffa fibre	polypropylene	[94]
3-(trimethoxysilyl)-1-propanethiol	2.5 wt. %	Luffa fibre	polypropylene	[94]
γ -aminopropyl triethoxy silane	10 wt. %	Wood flour	PVC	[104]
N-2(aminoethyl)3 aminopropylmethyl dimethoxysilane (KBM602)	0.5 – 2 wt. % of sawdust	Sawdust	Poly(vinyl chloride)	[105]
N-2(aminoethyl)3-aminopropyl trimethoxysilane (KBM603)	0.5 – 2 wt. % of sawdust	Sawdust	Poly(vinyl chloride)	[105]

N-2(aminoethyl) 3-aminopropyl triethoxysilane (KBE603)	0.5 – 2 wt. % of sawdust	Sawdust	Poly(vinyl chloride)	[105]

2.7.4 Other Chemical Treatment

(I) Peroxide Treatment

Organic peroxide such as dicumyl peroxide (DCP) and benzoyl peroxide (BP) could initiate free radicals (RO·) to react with the hydroxyl group (OH) of the fibre matrix and thus improve the interfacial bonding between natural fibre and polymer matrix. The reaction between free radicals and cellulose is showed in Figure 2-18. It could be used with other coupling agents for better grafting efficiency.

RO. + Cellulose – H ➔ R – OH + Cellulose

Figure 2-18: Reaction between free radicals and cellulose

The concentration of peroxide is crucial. Excessive amount of peroxide could damage the properties of natural fibre composites. M.A Gunning et al. added MA and DCP into natural fibre filled PLA composites. The result showed that the tensile strength of the hemp fibre/PLA composites and jute fibre/PLA composites improved by 36% and 27.7% respectively. [106] Moreover, peroxide treatment could help to reduce moisture absorption of natural fibre composites [83] [107][108]. DCP is preferred as compared to BP due to its better thermal stability and longer half-life at high temperature [107]. Table 2-18 showed the summary of other coupling agents used in fibre reinforced composites by researchers.

Table 2-18: Other coupling agents used in fibre reinforced composites

Name of Coupling Agents	Concentration of coupling agents	Type of Fibre	Polymer Matrix	Ref.
Dicumyl Peroxide	0.006 wt. %	Flax	High density polyethylene	[109]
Dicumyl Peroxide	0.03 – 0.09 wt. %	Hemp, flax	PLA	[106]
Dicumyl Peroxide	0.003 - 0.006 wt.%	Wood flour	LLDPE	[107]
Benzoyl peroxide	0.005 - 0.01 wt. %	Wood flour	LLDPE	[107]
Dicumyl Peroxide	0.1 - 0.2 phr	n/a	Poly(L-lactic acid)	[110]
Hexamethylene Diisocyanate (HMDI)	1 wt. %	Rayon, tyre cord yarn	PLA, Polyhydroxybutyrate (PHB)	[111]
Epoxy	30-50 wt. % relative to fibre	Kenaf fibre	ABS	[112]

2-hydroxyethyl methacrylate (HEMA)	3%	Jute	PC	[113]
Polyethylenimine (PEI)	1.5%	Bleached eucalyptus kraft pulp	polypropylene	[114]

2.8 Overview of Nanocellulose

Nanocellulose is defined as cellulose nanoparticles with at least one dimension between 1 and 100 nanometres. The size, content, and properties of nanocellulose are greatly affected by the manufacturing process. Nanocellulose is generally categorized into three different types, which are cellulose nanocrystals (CNCs), cellulose nanofibrils (CNFs) and bacteria nanocellulose (BNCs) as shown in Figure 2-19 [115] [116] [117].

Long, thread like cellulose nanofibrils (CNF) can also be known as cellulose nanofibers or nanofibrillar cellulose (NFC), its width is approximately 3-50 nm while its length varying from 0.5 – 5.0 μm. It has coarser dimension than CNC. CNFs are made from wood-derived fibre by breaking up the hierarchical fibre matrix. Preparation of CNFs can be using mechanical grinding or homogenizing sometimes in combination with enzymatic or chemical pre-treatments [118][119]. CNFs have higher surface area, length to diameter ratio and flexibility as compared to CNCs. CNFs also ease for surface modifications due to high amount of hydroxyl groups [120].

Cellulose nanocrystal (CNC) can be described as rod like nanoparticle with the width of 3 to 20 nm and the length is ranging from 50 to 1000 nm. The crystallinity size of CNCs are affected by the type of cellulose and the extraction methods. Acid hydrolysis is being used for the extraction of CNC from native cellulose by removing of amorphous regions and preservation of highly-crystalline structure [121]. Sulphuric acid (H_2SO_4) or hydrochloric acid (HCl) are normally used during acid hydrolysis. However, H_2SO_4 requires lower treatment temperature, lower acid to cellulose ratio and lesser process time [122]. Concentrated H_2SO_4 will introduce sulphate group onto CNCs surface and hence create a more stable suspension due to the electrostatic repulsion. Furthermore, the sulphate-stabilized CNCs spontaneously form chiral nematic liquid crystal phases in aqueous suspensions which contribute to unique optical properties of CNCs.

Bacterial nanocellulose (BNC) is produced by specific bacteria during fermentation process. Its width is around 20 to 100 nm and its length is about 1.0 to 5.0 μm. Compare to CNCS, and CNFs, BNCs produce greater purity, degree of polymerization, crystallinity, water content and also mechanical stability. It is attributed to the absent of intensive processing during removal of the unwanted impurities or contaminants such as lignin, pectin and hemicellulose [121][122]. However, complicate procedures of removing the bacteria from the nanocellulose limit BNC for large scale production [122][123][124].

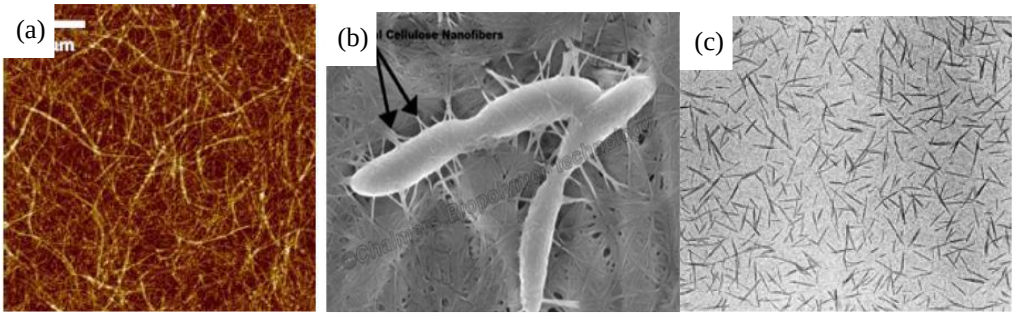

Figure 2-19: Cellulose nanofibrils (a), bacterial cellulose (b) and cellulose nanocrystals (c)

2.8.1 Properties of Nanocellulose

Nanocelluloses are lightweight, abundant and environmentally-friendly biomass material. Their distinctive mechanical and physical properties such as high strength, high crystallinity, large specific surface area, low thermal expansion and excellent gas barrier properties make them as promising material for use in various applications including nanocomposite materials, automotive part, filter material, gas barrier films, electronic devices and etc. Due to that, nanocellulose have attracted significant attention from both research scientists and industrialists [122] [125]. The properties of nanocellulose are affected by various factors. Source materials, the relative degree of crystallinity, geometrical aspect ratio (*l*/d) and acid hydrolysis parameters are important factors to control the properties of nanocellulose materials.

As one of the strongest and stiff materials available, nanocellulose exhibits remarkable properties such as high tensile strength (7500 MPa), high stiffness (Young's modulus of 100-140 GPa), high aspect ratio, large surface area (150-250 m^2/ g) and other fascinating electrical and optical properties. The theoretical value of Young's modulus along the chain axis for crystalline cellulose is estimated to be 167.5 GPa, which is even theoretically stronger than steel and similar to Kevlar, while elastic modulus of native nanocellulose from cotton and tunicate reach up to 105 and 143 GPa respectively; while non-crystalline regions provide the fibrils with flexibility [126] [127][128].

Furthermore, nanocellulose can undergo different types of surface modification due to high concentration of hydroxyl groups at the surface of nanocellulose. It can be modified with various chemical groups to accomplish expected surface modification such as esterification, etherification, oxidation, silylation, or polymer grafting. Surface modification can successfully functionalize the nanocellulose and facilitate the incorporation and dispersion of nanocellulose into different polymer matrices. Besides that, surface modification of nanocellulose can be done according to the need of applications [129].

The abundant hydroxyl groups on the surface of nanocellulose may function as active sites for chemical bonding with polymer matrices. Together with high aspect ratio and tangling effect of nanocellulose, effective stress

transfer between matrix and filler can be achieved. Enhanced matrix maximum shear stress improves tensile properties of polymer nanocomposites [124].

Moreover, nanocellulose is thermally and dimensionally stable. Sulphuric acid generates abundance of charged sulphate groups on CNC surface and forms stable colloidal dispersion during acid hydrolysis. The antiparallel arrangement of chains in CNF yields more hydrogen bonds and leads to more stable structure [129]. Another property that exhibited by nanocellulose are gas permeability. The ability of nanocellulose to form hydrogen bonds results in strong and more complex network. Thus, it increases the tortuosity and diffusion path of permeating molecules within the nanocellulose films. Furthermore, due to its superior nucleation ability, the highly crystalline structure within the nanocellulose also contributes to the gas barrier properties of nanocellulose films [124].

Nanocellulose such as CNC exhibits excellent optical properties. It is attributed to CNC will self-assemble to form a helical chiral nematic ordering when it reaches a critical value of concentration in aqueous suspension. Thus, CNCs are able to absorb visible light and the reflected light emits different colours which are depending on the wavelength of the pitch gap. Therefore, different coloured CNC film can be seen if the films are sufficiently thin.

2.8.2 Synthesis of Nanocellulose

Isolation of nanocellulose by using chemical treatment generally involved 3 stages: delignification, alkaline treatment, and acid hydrolysis. The first stage is delignification or purification of the source material. Delignification (also known as bleaching) process is conducted to remove lignin and other impurities that appear at the outermost layer from the natural fibres without changing the crystallinity or polymorphism of the cellulose.

Table 2-19 summarises delignification process parameters used by other researchers. Researchers used different delignification agents, treatment temperature and treatment duration to treat various types of natural fibres. Owing to different chemical composition of natural fibres, optimum process parameters such as concentration of chemicals used, treatment temperature and time need to be justified through experiments to achieve the highest effectiveness of delignification process [130].

After removing lignin and minerals, the output should be holocelluloses. White cellulose with increased ageing resistance is obtained after the delignification procedure. Delignification is necessary in the production of purified cellulose fibres because lignin behaves as a cementing domain for cellulose fibres and hemicellulose molecules, thus preventing separation of wood and plants in their constituent fibres. Common delignification agents used are sodium chlorite ($NaClO_2$), acetic acid, sodium hydroxide (NaOH) and hydrogen peroxide [131]. When sodium chlorite ($NaClO_2$) is added in an acidic buffer solution, it decomposes into chlorine dioxide (ClO_2) in the presence of buffer salts. This will aid in the liberation of chlorine dioxide from sodium

chlorite during the delignification process. The loss of lignin could cause the alkali-treated fibre to fibrillate even more as ClO_2 can oxidise lignin that has been left in the fibres by destroying the aromatic ring of the lignin. The white colour of bleached material implies that a considerable amount of lignin has been removed and thus, showing that the delignification has been successful and completed. Insufficient lignin removal during delignification may affect the effectiveness of the subsequent acid hydrolysis. The acid would be unable to impart significant morphological changes if significant amount of lignin is still remained in treated fibres. Purity, yielding and thermal stability of CNC after acid hydrolysis will be varied as well.

Table 2-19: Process parameters of delignification

Natural Fibre	Chemical Solution	Temp (°C)	Time	Ratio	Ref.
Empty fruit bunch fibres	Acetic acid was added to 0.7 % (w/v) $NaClO_2$ until pH reached 4.	70 - 80ºC	2h	Fibre:$NaClO_2$ 1:50	[64]
Agave tequilana bagasse	0.2 wt.% of acetic acid + 0.27 wt. % of $NaClO_2$ + 0.7 wt.% sodium hydroxide	70ºC	1.5h	-	[132]
Agave angustifolia fibres	1.7 wt.% $NaClO_2$	70 - 80ºC	4h	Fibre:Liquor 1:25	[62]
Corncobs	27g NaOH + 75 mL glacial acetic acid, diluted to 1 L of distilled water + 1.7 wt.% $NaClO_2$ in water	80ºC	6h	-	[65]
Cocoa pod husk	1.7 wt.% $NaClO_2$	80	2h	Fibre:liquor 100 : 5	[133]
Coconut fibre	5% (w/w) H_2O_2 + 3.8% (w/w) NaOH.	50	1.5h	Fibre:$NaClO_2$ 1 : 20	[134]
Tomato plant residue	27 g NaOH + 75 mL glacial acetic acid, diluted to 1 L of distilled water + 1.7 wt.% $NaClO_2$ in water	80	2h	Fibre:liquor 1 : 20	[135]
Oil palm leaves	0.06 mL acetic acid + 0.30g $NaClO_2$ + 30 mL distilled water	85	5h	Fibre : $NaClO_2$ 1: 0.3	[136]

Second stage is alkaline treatment. Alkaline treatment is the procedure of removing partial short-length crystallites by treating ground cellulose fibre chips to the highly concentrated strong base solution such as aqueous potassium hydroxide (KOH) or sodium hydroxide (NaOH) solution. The alkali treatment removes the hemicellulose and breaks the bonds between cellulose, hemicellulose and lignin. The intermolecular ester link between lignin and hemicelluloses undergoes saponification during the alkali treatment. Alkali treatment can enhance the amount of cellulose exposed on a fibre by reducing the outer non-cellulosic layer, which is made up of hemicelluloses, lignin, pectin, wax, oils, and other impurities found in raw fibre. Swelling of the cellulose occurs as a result of the alkali treatment, resulting in larger surface area and lower crystallinity [131].

Hemicellulose removal is critical because hemicellulose is undesirable for reinforcing purposes and the early degradation of cellulosic components occurs mostly attributed to hemicellulose. e justified through experiment.

Table 2-20 tabulated process parameter of alkaline treatment proposed by other researchers. Sodium hydroxide is commonly used to aid the removal of most of the non-cellulose components in the biomass include lignin, hemicellulose, fats and waxes, proteins, and inorganic contaminants. Optimum process parameters need to be justified through experiment.

Table 2-20: Process parameters of alkaline treatment

Natural Fibre	Chemical Solution	Temp (°C)	Time	Ratio	Ref.
Empty fruit bunch fibres	17.5 % (w/v) NaOH	-	2h	-	[64]
Agave tequilana bagasse	17.5 wt.% NaOH	-	0.5h	-	[132]
Agave angustifolia fibres	4% NaOH	70 - 80	2h	Fibre: Liquor 1:25 (g/ml)	[62]
Corncobs	2% (w/w) NaOH	100	4h	-	[65]
Cocoa pod husk	4% (w/v) NaOH	80	2h	Fibre: liquor 100:5	[133]
Corn cob	3% (w/w) NaOH	100	3h	-	[137]
Sugarcane bagasse	4 wt.% NaOH	80	2h	-	[138]
Oil palm empty fruit bunch	17 % (w/v) NaOH	160	1h	Fibre: liquor 1:4	[139]

Tomato plant residue	4 wt.% NaOH	80	2h	-	[135]

The third stage is acid hydrolysis. Harsh acid treatment will turn cellulose fibres into nanocellulose by preferentially breaking the disordered amorphous regions of the cellulose microfibrils while the crystalline regions are remained as they have better acid resistance. Table 2-21 summarized the process parameters of acid hydrolysis used by other researchers. Sulphuric acid (H_2SO_4) and hydrochloric acid (HCI) are often use in acid hydrolysis. Most researchers prefer sulphuric acid instead of hydrochloric acid with the intention that sulphuric acid solution induced sulfate ester groups on the surface of CNC and this help to create a more stable aqueous suspension. Mechanical stirring is often used during acid hydrolysis process to increase homogeneity of fibre in acid solution.

Table 2-21: Process parameters of acid hydrolysis

No.	Source materials	Acid Hydrolysis					Ref.
		Media	Stirring method	Temp / °C	Time / minute	fibre : acid ratio	
1	Empty fruit bunch fibres	64 wt.% H_2SO_4	Agitation	45	45	-	[64]
2	Agave tequilana bagasse	65 wt.% H_2SO_4	mechanical stirring	50	60	-	[132]
3	Barley	65 wt.% H_2SO_4	mechanical stirring	50	60	-	[132]
4	Agave angustifolia Fibre	60 wt.% H_2SO_4	-	45	45	1:20 (wt. %)	[62]
5	Corncobs	9.17 M solution of H_2SO_4	mechanical stirring	45	30 – 90	1 gram:15 ml	[65]
6	MCC	63 wt.% H_2SO_4	mechanical stirring	50	35	1 gram:10 ml	[140]
7	Sugarcane baggasse	60 wt.% H_2SO_4	mechanical stirring	45	60	1:10 (wt %)	[141]
8	Cocoa pod husk	64 wt.% H_2SO_4	-	45	60	-	[133]

9	Coconut husk	64 wt.% H_2SO_4	-	45	30	15:1	[142]
10	Corn husk	64 wt.% H_2SO_4	-	45	90	20:1 v/w	[143]
11	Eggplant plant residue	64 wt.% H_2SO_4	-	50	30	-	[144]
12	Oil palm empty fruit bunch	58 wt.% H_2SO_4	-	45	45	-	[145]
13	Oil palm frond	64 wt.% H_2SO_4	-	45	1h	10:1 v/w	[146]
14	Rice straw	58 wt.% H_2SO_4	-	45	3h	-	[147]
15	Sugarcane bagasse	64 wt.% H_2SO_4	-	50	30	-	[138]
16	Tomato plant residue	64 wt.% H_2SO_4	-	50	30	-	[135]

Apart from acid hydrolysis (chemical method), nanocellulose can also be produced by using mechanical refining process. High shear forces were applied to cellulose materials to separate crystalline and amorphous region of cellulosic materials. The process is relatively simple and low cost. However, it leads to high energy consumption during production and broad distribution in size of nanocellulose [148]. Figure 2-20 illustrated the synthesis of nanocellulose by using different methods and Figure 2-21 showed micrographs of Transmission Electron Microscope (TEM) of cellulose nanocrystals derived from cotton and avicel through acid hydrolysis.

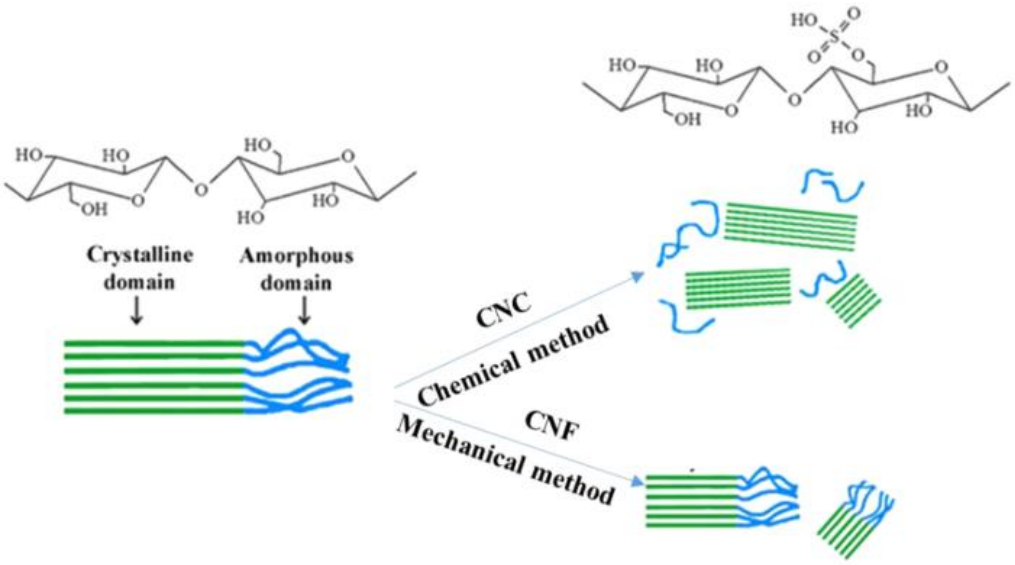

Figure 2-20: Synthesis of nanocellulose [141]

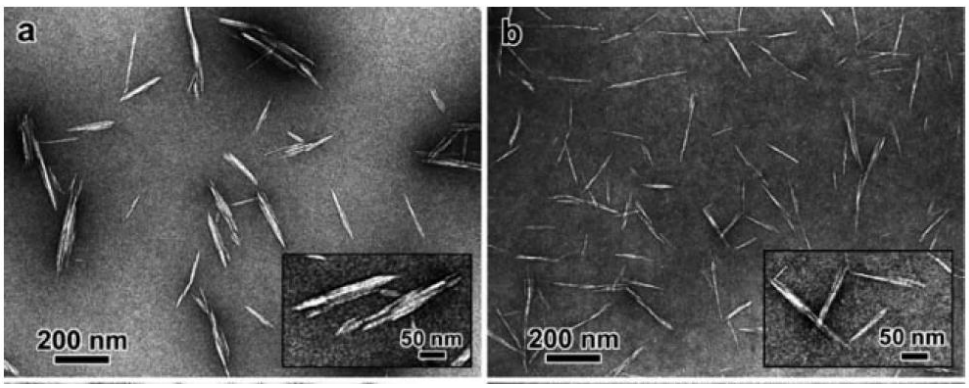

Figure 2-21: TEM micrographs of CNC of cotton (a) and avicel (b) [126]

After acid hydrolysis, cold distilled water is often used to dilute the acid solution and stop the chemical reaction. The objective of centrifugation is to separate acid solution and nanocellulose. The function of dialysis is remove unwanted precipitates and stabilize the PH value of nanocellulose suspension. Dialysis also applied to improve thermostability of CNC due to acid hydrolysis. The characterisation and testing result from different researchers showed that source materials, concentration of acid solution and process parameters could affect the morphological properties, crystallinity index and yielding of nanocellulose.

2.8.3 Potential application of Nanocellulose

Nanocellulose can be used in a variety of applications, including nanocomposite materials, barrier / separation membranes, electronic devices, food packaging, food coatings, biomedical products, wood adhesives, batteries, super capacitors, electronic component templates, electroactive polymers, catalytic supports, continuous fibres and textiles and antimicrobial agents, as shown in Figure 2-22 [125].

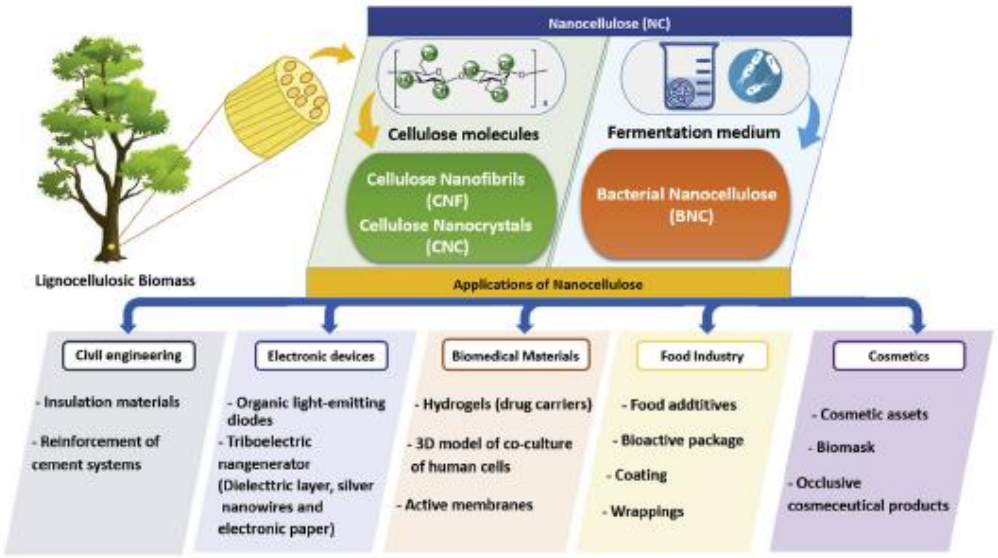

Figure 2-22: Applications of nanocellulose [118]

Nanocellulose as a promising renewable green material can be used as reinforcing agent in high performance polymer nanocomposites. Many new nanocomposite materials with attractive properties such as superior mechanical strength and thermal properties, as well as being lightweight and transparent were obtained by physical incorporation of nanocellulose into either natural or synthetic polymer matrix. The mechanisms and aspects of properties enhancement in polymer composites by introducing nanocellulose as reinforcement materials embrace aspect ratio, homogeneous dispersion of reinforcements, formation of entanglement by cellulose nanofibrils, better bonding, and minimization of surface defects.

The geometrical aspect ratio, defined as the length-to-diameter (L/d) ratio, is a major factor that controls the mechanical properties of nanocomposites and determines the percolation threshold value. In other words, fillers with a high aspect ratio give the best reinforcing effect [126]. This phenomenon, as aforementioned, can be exemplified with the case of cellulose nanofibrils, in which their lengths are in micrometre and widths in nanometre scale. When the diameter of the cellulose reduces to nanometre, aspect ratio increases as aspect ratio is inversely proportional to the diameter of the materials [149]. Homogeneous dispersion of nanocellulose in polymer matrix becomes critical factor when incorporation of nanocellulose acts as reinforcing agents in polymer composites. It is suggested that simple chemical modification on nanocellulose surface holds the potential to improve its dispersibility in different solvents and expands its utilization in nano-related applications, namely drug delivery, protein mobilization, and inorganic reaction templates[126].

Cellulose nanofibrils are also addressed to generate tangling effect among themselves and with the polymer matrix due to their length. In the event that the length of cellulose nanofibrils is in micrometre while diameter is

reduced to nanometre, a flexible and hirsute cellulose nanofibrils is observed [150].

Meanwhile, some of the researchers claimed that the reinforcing effect of nanocellulose fillers occurs most probably from the cellulose hydrogen bonding network within the polymer matrix. Cellulose nanofibrils reinforced polymer composite showed greater improvements in mechanical and thermal behaviour as compared to cellulose nanocrystals due to its morphology.

In fact, fillers often fracture because of surface imperfections, inclusions, and defects. By making the diameter of the fillers as small as possible, provides the filler less surface area and, consequently, fewer flaws that might propagate during processing or under a loading condition. Hence, it is envisaged that incorporating nanocellulose into polymer matrix will produce better performance polymer nanocomposites [151] [152] [153][154] [155].

Moreover, nanocellulose can be used in electronic applications such as nanocellulose paper which has optically clear, high transparency, printability, functionality and thermal stability with outstanding mechanical properties. Nanocellulose transparent papers can substitute conventional papers, plastic or glass substrate in electronic devices such as sensors, electrodes and actuators, flexible displays and circuits, as well as solar cells [123] [156].

Nanocellulose is suitable to be utilised in the food industries owing to its aspect ratio, large surface area, rheological properties, non-genotoxic and non-cytotoxic features. Nanocellulose is widely used as an essential food element, food stabiliser and food packaging. Nanocellulose based films have exceptional air and oxygen barriers, hence protecting the food from undesirable entities. Nano-based films also have properties that are comparable to commercial poly bags [157].

Nanocellulose has the potential to be utilised in biomedical research because of its unique properties, which include biocompatibility, sustainability, accessibility, high strength, high surface area to volume, environmental friendly and low production costs. In biomedical applications, nanocrystals and nanocellulose fibre derived from plant resources differ from bacterial cellulose derived from bacteria. For example, nanocellulose membranes had a high water storing feature, conformability, and extreme flexibility, making them an ideal material for wound dressing [121][123] [158].

2.9 Flame retardants

The flammability resistance of polymeric materials may be enhanced by additives called flame retardants. Flame retardants (FR) refers to a variety of substances that are incorporated into combustible materials as well as commercial and consumer products in area such as furnishing, electronic and electrical devices, building and construction materials, transportation interiors, etc [159].

Flame retardants are substances that can be chemically inserted into the polymer molecule or be physically blended in polymers after polymerization to suppress, reduce, delay or modify the propagation of a flame. The retardants may function by interfering with the combustion process through the gas phase, or by initiating a different combustion reaction that generate less heat, thereby reducing the temperature and this cause a slowing or cessation of burning [159].

To prevent combustion, it becomes necessary to design a thermally stable polymer that has a lesser probability of decomposing into combustible gases under heat stress. However, thermally stable polymers may exhibit performance limitations and are often too expensive and difficult to process. Therefore, manufacturers add various flame retardants to impart flame retardancy to a plastic. Flame Retardants (FR) play important role in making fire proof plastics. In many cases, use of flame retardants in polymer for particular application is required to pass a specific flammability test. The subsection below discusses flame retardants species shortlisted to be introduced in this work to improve flame resistance of OPF filled ABS composites.

2.9.1 Mechanism of Flame retardation

Flame retardants can be classified into 5 main categories: halogenated flame retardants, inorganic flame retardants, nitrogen flame retardants, phosphorus containing flame retardants and intumescent flame retardants. However, all types of flame retardants take effects by using either one or both of three mechanism of flame retardants action. Namely gas phase flame retardancy, endothermic flame retardants, and char forming flame retardants [160].

Gas phase retardancy, also known as vapour phase inhibition, are commonly used with halogenated and phosphorous flame retardants, in which heat released from combustion is reduce during gas phase of the combustion by scavenging free radicals. Endothermic flame retardants will undergo an endothermic decomposition in condense phase and gas phase by liberating non-combustible gases such as CO_2 and H_2O in the presence of fire. This leaves behind ceramic-like residue, protecting the underlying materials due to the result of fuel dilution and cooling of polymer through endothermic decomposition of the FR additives. Char-forming flame retardants function in the condensed phase. It reacts and form a carbonaceous layer (char) surrounding the surface to provide thermal insulation for underlying polymer.

Apart from effective flame retardancy, other favorite properties of FR include colorless, ease of process, no detrimental effect on mechanical properties of materials, long term effectiveness, excellent environmental resistance, low smoke emission and toxicological effects.

2.9.2 Alumina Trihydrate (ATH)

Alumina trihydrate (ATH) is also known as hydrated alumina, aluminium hydroxide and aluminium trihydroxide.[161] Alumina trihydrate is inorganic flame retardants which often associated with its role as a non-halogen

flame retardant and smoke suppressant. Non-halogen compounds do not release toxic smoke when burned. Under normal conditions of use, it is not a health hazard, nor expected to be hazardous to the environment [161] [162]. Inorganic flame retardants could also serve as catalyst and synergist when combined with other flame retardants. Despite that, inorganic FRs often to be used in higher concentration to provide adequate flame retardant performance.

Alumina trihydrate is in the form of white powder normally and has a specific density of 2.42g/cm^3. It is a non-abrasive powder with a Mohs hardness between 2 to 3 which aids in the dispersion of the powder and is easy on the equipment. [161] Alumina trihydrate is chemically inert. Therefore, it improves weatherability, stain, scrub and water resistant of the polymer. However, it is still compatible with cationic or anionic systems, allowing complete flexibility in choosing polymers [161].

Alumina trihydrate decomposes at approximately 220 °C where three water molecules in ATH are released in an endothermic reaction. The released water molecules quench the surface of the surrounding materials by forming of a protective layer of aluminium oxide, thus providing flame retardance and smoke suppression. Lastly, the resulting aluminium oxide from the reaction forms a layer of char which insulates the polymer from the oxygen and high temperature. These reactions take place all together when alumina trihydrate is subjected to temperature above 220°C which allows it to act as an effective flame retardant [161] [162] [163].

2.9.3 Ammonium Polyphospate (APP)

Ammonium polyphosphate (APP), also known as ammonium pyrophosphate is an effective non-halogen flame retardant. It does not generate additional amount of smokes during burning and it is environmentally useful when compared to other halogen-containing flame retardants [164]. Phoshorous-based FRs also possible to combine with different FRs for better fire resistance.

Ammonium polyphosphate appear in white powder form. It has two types of crystal phase, Crystal phase I (APP I) and Crystal phase II (APP II). Crystal phase I is characterized by a variable linear chain length whereas Crystal phase II is cross-linked or branched. Therefore, APP II has higher molecular weight and thermal stability than APP I while water solubility of APP II is lower than APP I. Flame retardants are commonly made from APP II [165][166].

APP II is able to function as flame retardant in the condensed or polymer phase through intumescence. During intumescence, a material swells when it is exposed to heat or fire to form a porous carbonaceous foam which acts as an effective barrier to prevent heat, air and pyrolysis product from entering the material surface. When material containing APP II are subjected to fire, APP II will first decompose into polyphosphoric acid and ammonia at around 275°C. The polyphosphoric acid would react with hydroxyl group to form a non-stable phosphate ester. Upon dehydration of phosphate ester, charring would occur

which involves the formation of carbon foam, a viscous molten layer or surface glass can also be obtained on the polymeric surface which protects the polymeric materials from heat and oxygen. Therefore, slowing down the propagation of the flame [164] [165][166][167].

2.9.4 Zinc Borate

Zinc borate (ZB) is one of the non-halogen flame retardants which its physical appearance is in white powder form with the molecular formula $B_2O_6Zn_3$. ZB has a molecular weight of 313.754 g / mol, melting point at 980°C, density of 3.64g/cm^3 and have no odour. ZB is soluble in dilute acids and slightly soluble in water [168].

ZB is an anti-dripping and char-promoting agent. It can suppress the glow by forming char on the surface of the material to stop fire propagation. In non-halogen flame retardant, ZB can use together with alumina trihydrate (ATH), magnesium hydroxide (MDH) or ammonium polyphosphate (APP), which induce a synergy effect of fire resistance. Furthermore, ZB is effective in both solid state and gaseous state, it is also a strong smoke suppressing agent which helps to increase the time of rescue in case of fire [169].

ZB will help to promote the formation of char which can reduce the formation of smoke and toxic during fire. It cools down the front of the flames and take the energy and subtract to the fire. ZB will dehydrated at temperature above 290°C. Moreover, ZB improves resistance against electrical degradation such as high anti-arcing and anti-tracking indexes. It is an afterglow suppressant because it forms char on the layer and hence prevent the oxygen to take place in the burning area [170].

2.9.5 Expandable Graphite

Expandable graphite (EG) or expandable flake graphite, also known as intumescent flake graphite, is a graphite intercalation compound (GIC), made of crystalline graphite flake, which composed of layering of carbon atoms planes, and intercalant material. The intercalant materials such as halogens, alkali metals, sulphate, nitrate, various organic acids, aluminium chloride, ferric chloride, other metal halides, arsenic sulphide, thallium sulphide, etc. are inserted between the graphene layers of a graphite crystal or particle to form GIC. Expandable graphite (EG) is one of the intumescent flame retardants that has a density of 2.2 g/cm^3 approximately. Intumescent fire retardant additives undergo a thermal degradation process while heating, which will produce a stable residue called char. Intumescent char can stick on the surface layer of polymeric material, providing an insulation effect to the underlying materials during fire [171].

EG can expand up to 100 times of its original size when it is exposed to heat or flame. The graphite layer planes are forced apart by the gas and then expands. The expanded graphite is a low-density, non-burnable, thermal insulation compound that can reflect up to 50% of radiant heat. The expanded graphite has a ‘worm’ shape physical appearance and twisted. When the EG

expands, it can prevent the protected substrate from burning and help to increase the total heat flux by blocking of oxygen from entering into the burning site. EG have many advantages when used as a flame retardant such as increase the time to ignite the substance, reduce heat release and mass loss during fire, reduce smoke produced and flame spread can be slowed down [172] [173].

In short, EG is halogen-free FR which demonstrate excellent fire inhibition and suitable for wide range of application. In spite of that, EG is high cost and not environmental friendly. EG also does not provide uniform flame resistance in all direction [172] [173].

2.9.6 Flame Retardancy of Natural Fibre Composites

The flammability of natural fibre composites is greatly affected by various factors such as properties of matrix and fillers, manufacturing process and effectiveness of flame retardants. From the aspect of materials, it is believed that higher cellulose crystallinity index will lead to higher ignition temperature. Moreover, different chemical components of plant fibres have different thermal properties and thus affect the onset degradation temperature. Matrix materials is the continuous phase that dominant the degradation properties of composites. Thermosets generally have better fire resistance than thermoplastics and the properties of matrix polymer such as limiting oxygen index directly affect the flammability of polymer composites [44][45] [174].

Various approaches were proposed to improve the flame retardancy of natural fibre composites. Addition of various flame retardants (FR) are widely used as it is the most effective way to enhance the fire resistance. Reactive flame retardants which used mainly in thermosets (epoxy resin, UP, polyurethane) are chemically bound to the polymer; Additive FRs which used primarily in thermoplastics such as ABS, PC/ABS, HIPS, EPS, PP, PE, PA, PC, PBT are physically mixed with the resin during or after polymerisation. Table 2-22 tabulates the flame retardants and fillers used in natural fibre composites for improving fire resistance. A number of researches showed that natural fibre as fillers, able to improve fire resistance of composites. Flame retardants such as alumina trihydrate (ATH), zinc borate (ZB), ammonium polyphosphate (APP), expandable graphite (EG), magnesium hydroxide are commonly used in thermoset composites. The improvement in fire resistance of natural fibre composites is significant. Some researchers reported that combination of different FRs in natural fibre composites can yield the attractive synergistic effects in flame retardancy. However, limited research has been reported on the flammability of natural fibre filled thermoplastic composites, particularly acrylonitrile butadiene styrene (ABS) composites.

Hence, it is envisaged that addition of flame retardants such as ATH, APP, ZB and EG into oil palm fiber filled ABS composites could improve their fire resistance and possibly meet the stringent flame, smoke and toxicity (FST) requirement. The effects of combination of different FRs into oil palm fiber filled ABS composites will be studied.

Table 2-22: Flame retardants and fillers used in natural fibre composites

No.	Flame retardants (FRs)	Compo. of FRs	Fillers	Polymer matrix	Flame retardant properties	Ref.
1.	Zinc Borate (ZB) / Ammonium polyphosphate (APP)	5 % - 15 %	Empty fruit bunch (20 %)	epoxy	Composite with the hybrid of 10 wt. % APP and 5 wt. % ZB revealed the best fire retardancy with 0 sec drip flame time and 0 sec total flame time as attained from 12 sec and 60 sec vertical Bunsen burner tests.	[7]
2.	Expandable Graphite (EG)	1 % - 5 %	Empty fruit bunch (20 %)	epoxy	EG 5% samples showed the shortest burn length with 0 sec drip flame time and 0 sec total flame time.	[8]
3.	Intumescent flame retardant (IFR) consists of APP, pentaerythritol (PER), and melamine (MEL)	35 – 40 %	Chicken eggshell (1 – 5%)	epoxy	Addition of IFR with 3% chicken eggshell increased LOI value and help to pass UL 94 Test. Addition of IFR with 3% chicken eggshell greatly decrease the heat release and smoke production.	[175]
4.	Magnesium hydroxide	5%	Empty fruit bunches (20 – 50%) and PET yarn (5%)	epoxy	Addition of oil palm empty fruit bunches reduced burning rate but greatly reduce tensile strength.	[176]
5.	Alumina Trihydrate (ATH) / Zinc Borate (ZB) /Ammonium polyphosphate (APP)	5%	Empty fruit bunch (18%)	epoxy	APP, ZB and ATH, were able to enhance the fire retardancy of EFB epoxy composite without significantly deteriorating the mechanical behaviours.	[177]
6.	Expandable Graphite (EG)	3 – 7%	Empty fruit bunch (20%)	epoxy	Addition of 3 – 7% expandable Graphite into natural fibre composites help to achieve 0 sec drip flame time and 0 sec total flame time in vertical Bunsen burner test	[178]
7.	Alumina Trihydrate (ATH) / Zinc Borate (ZB) / Ammonium polyphosphate (APP)	5 % - 15 %	Empty fruit bunch (18%) mat	epoxy	Mix 5% ATH and 10% APP into natural fibre reinforced epoxy composite help to achieve 0 sec drip flame time and 0.5 sec total flame time in vertical bunsen burner test as well as reduced gross heat from calorimetry test	[6]
8.	Alumina Trihydrate (ATH)		Empty fruit	epoxy	Adding ZB, APP and ATH improved the flame retardancy	[179]

	/ Zinc Borate (ZB) / Ammonium polyphosphate (APP) /Expandable Graphite (EG)		bunch (18%)		whereas it was found to reduce the mechanical properties. Zero drip flame time was recorded for both APP and ZB containing composites. Significant reduction in GH was observed with the inclusion of 15% of ATH or ZB.	
9.	Ammonium polyphosphate (APP) / ATH	5 % - 15 %	Empty fruit bunch (18%)	epoxy	The hybrid of 10 wt.% APP and 5 wt.% ATH was the formulation which could meet the aircraft interior FAR requirements in terms of vertical Bunsen burner test.	[180]
10.	phosphorus-containing reactive amine		Carbon fibre (40%)	epoxy	Inclusion of carbon fibres and reactive flame retardant into the resin resulted in significant increase LOI value and time to ignition.	[181]
11.	Nanoclays	1 % - 3%	Kenaf (10 – 50%)	Acrylonitrile butadiene styrene (ABS)	Kenaf fibre increased LOI value. Addition of 50% of kenaf fibre and nanoclay decreased burning rate.	[182]
12.	bisphenol-A bis (diphenyl phosphate) (BDP) and 9, 10-Dihydro-9-oxa-10-phosphaphenanthrene-10-oxide (DOPO)	10% - 20%	Pineapple leaf fibres (10%)	Acrylonitrile butadiene styrene (ABS)	Addition of phosphate derivative flame retardant into PALF/ABS composites increase LOI value of PALF/ABS composites.	[183]
13.	Expandable graphite (EG)	5% - 20%	N/A	Acrylonitrile-butadiene-styrene (ABS)	20% EG inclusions lead to decrease in heat release rate and increase in LOI value of unfilled ABS.	[184]
14.	Nanozirconia and Polytetrafluoroethylene (PTFE)	1.25 % - 3%	N/A	Acrylonitrile-butadiene –styrene (ABS)	TGA results show addition of zirconia and PTFE improves the thermal stability of the composites. The peak degradation temperature gets shifted to higher values.	[185]
15.	Reactive polymeric intumescent flame retardant (PDSPB)	20% - 30%	N/A	Acrylonitrile-butadiene –styrene (ABS)	The addition of PDSPB can effectively reduce the flammability including peak heat release rate, total heat release and average mass loss rate. The LOI value was also greatly improved.	[186]

16.	Ammonium polyphosphate (APP)	20% - 30%	natural zeolite (1 – 10%)	Polypropylene (PP)	The LOI values increased approximately 8% for the MS treated composite containing 5 wt.% zeolite.	[187]
17	Magnesium hydroxide and rice husk ash	5% - 10%	Sponge gourd fibre (10 – 20 %)	High-density polyethylene (HDPE)	The composites with 80% HDPE + 5% Magnesium hydroxide and 5% rice husk ash + 10% sponge gourd fibre and 90% HDPE +10% magnesium hydroxide showed better flammability properties.	[188]
18	Magnesium hydroxide	5% - 25%	Sawdust / rice husk (25 – 50 %)	Polypropylene (PP)	Addition of 25% Magnesium hydroxide decreased burning rate.	[89]
19	Ammonium polyphosphate (APP)	10 – 20%	Thermomechanical pulp (TMP) / calcium carbonate	High-Density Polyethylene (HDPE)	Addition of APP increased LOI value.	[189]

Chapter 3: Research Methodology

3.1 Materials

Injection molding grade acrylonitrile butadiene styrene (ABS) used in this study was manufactured by BASF with the trade name of Terluran® GP-22. Its specific gravity is 1.04. The empty fruit bunch (EFB) fibre was supplied by Kah Hwa Industries Sdn. Bhd. The EFB fibre were pulverised into 3 – 5 mm long with diameter of 200 – 400 μm.

Hydral® PGA-SD Alumina Trihydrate, $Al(OH)_3$ was provided by J.M Huber Corporation, Malaysia. It has density of 2.41 $g \cdot cm^{-3}$ and average particle size of 1.5 μm. It starts to decompose at temperature of 220 °C and its LOI value is 34.5%. Exolit® AP 422 ammonium polyphosphate, $(NH_3PO_4)n$ (APP) was provided by Clariant (Singapore) Pte Ltd. It has density of 1.9 $g \cdot cm^{-3}$ and contains 31-32% of phosphorus. It starts to decompose at temperature of 275 °C.

Zinc borate (ZB), Firebrake® 400 grade ($2ZnO.3B_2O_3.3.5H_2O$) was provided by J. M. Huber Corporation, Malaysia. It has a density of 2.76 $g \cdot cm^{-3}$ and with average particle size of 7 – 9 μm. It starts to decompose and release its water of hydration at temperature of 290 °C. ZB consists of 37 – 40% of zinc oxide (ZnO), 47 – 49% borate oxide (B_2O_3) and 13 – 15.5% of water (H_2O). Expandable graphite (EG) was obtained from QingDao LIANYOU Graphite Products Co., Ltd. (Shan Dong, China). Sulphuric acid was used as intercalant and has a pH value of 6 – 8.

0.5 grams of EG (supplied by QingDao LIANYOU Graphite Products Co., Ltd.) was put into Thermconcept Laboratory chamber furnace (Model: KL 09/13) for 30 minutes at temperature of 150 °C, 200 °C, 250 °C and 300°C respectively to observe its staring expansion temperature. Figure 3-1 showed the SEM images of expandable graphite after heating in furnace at temperature of 150 °C, 200 °C, 225 °C and 250 °C for 30 minutes. It can be observed that expandable graphite starts to expand after 200 °C. Figure 3-1 (c) and (d) showed that EG was exfoliated and turn into worm-like structure at temperature of 225 °C and 250 °C. If the expansion of EG is initiated at a temperature similar to the processing temperature of natural fibre composites, it could potentially impact the effectiveness of EG as a flame retardant. This is because expandable graphite, which is designed to form an intumescent layer when exposed to high temperatures during a fire, may lose its ability to do so if it expands prematurely. During the manufacturing process, if the temperature reaches the point where EG begins to expand, the material might already be in an expanded state before encountering actual fire conditions. As a result, it will not form the protective, foam-like intumescent layer that insulates and protects the underlying material from the heat and flames. This premature expansion could significantly reduce the flame retardant properties of the EG, thereby compromising the safety and fire resistance of the natural fibre composites in which it is used.

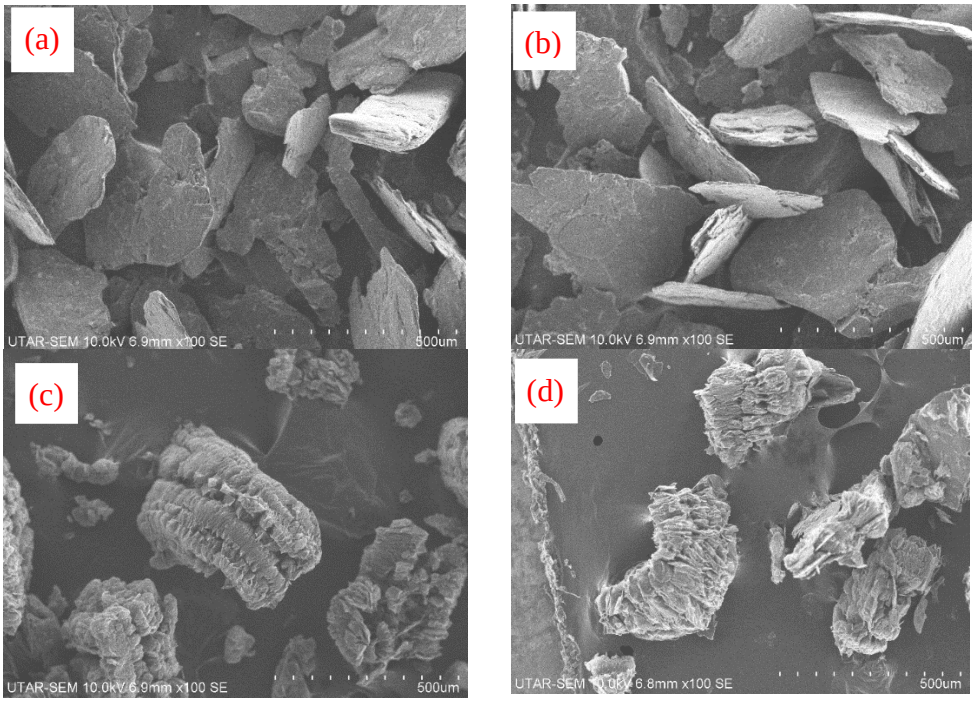

Figure 3-1: SEM image of expandable graphite after heating at temperature of (a) 150 °C, (b) 200 °C, (c) 225 °C and (d) 250 °C for 30 minutes

Coupling agents used in this study are maleic anhydride ($C_4H_2O_3$) and silane (3-(trimethoxysilyl) - propyl methacrylate). Maleic anhydride, 95 % assay with specific density of 1.32 g·cm^{-3} and molecular weight of 98.06 g·mol^{-1} was obtained from Merck Sdn. Bhd. Silane, 98 % assay with density of 1.045 g·cm^{-3} and molecular weight of 248.35 g·mol^{-1} was supplied by Sigma-Aldrich Pte Ltd.

For nanocellulose extraction process, sodium hydroxide (99 % assay), acetic acid, (99.85% assay), acetone, (99.9% assay) were supplied by Wataka Trading. Sodium hypochlorite (industrial grade) was supplied by Staren Watech (M) Sdn. Bhd. Microcrystalline cellulose powder (MCC) was supplied by Sigma-Aldrich. Its particle size is approximately 18 – 22 um with a bulk density of 0.5 g·cm^{-3}. Commercial cellulose nanocrystals (NCC_B) were purchased from CelluForce. It is a white, odourless powder with a density of 1.5 g·cm^{-3}.

3.2 Fibre Preparation

Refer to Figure 3-2, the long EFB fibre was first rinsed, and washed with clean tap water to remove contaminants. The cleaned OPF is then dried in the oven at the temperature of 80 °C for 5 hours to remove the excessive moisture content. After that, the dried oil palm fibre (OPF) was manually cut into fibre length of 3 mm to 5 mm by using scissor.

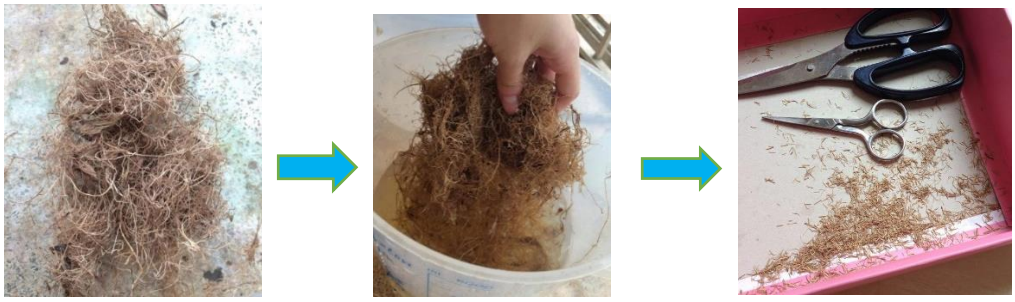

(I) Dry long OPF (II) Rinse and Wash OPF (III) Short OPF cut into 3-5mm length

Figure 3-2 Fibre cutting process

100 pieces of trimmed fibre is then being selected randomly to calculate the average length of OPF by using profile projector (MITUTOYO PJ3000). Refer to the Table 3-1, the average fibre length is around 3.38 mm.

Table 3-1: Oil palm fibre length distribution

Dimension (mm)	Quantity	Calculation
0-1	-	-
1-2	7	1.5 x 7 = 10.5
2-3	36	2.5 x 36 = 90
3-4	24	3.5 x 24 = 84
4-5	28	4.5 x 28 = 126
5-6	5	5.5 x 5 = 27.5
	Total:	338
	Average:	338/100= 3.38

3.2.1 Oil Palm Fibre Surface Pre-treatment

Surface treatment was conducted to modify the fibre surface of oil palm fibre. Alkali treatment was applied to improve the adhesion strength between the surface interface of hygroscopic EFB fibre with hydrophobic polymeric species. The alkali treatment was slightly modified according to method described in ASTM D1103.

4 g of 3 mm – 5 mm long oil palm fibre was added into 20 ml of 17.5 wt.% sodium hydroxide solution and was soaked into ultrasonic bath at room temperature for 5 minutes. An additional 10 ml of 17.5 wt.% sodium hydroxide solution was poured into the 250 ml glass beaker. This step was repeated every 5 min until a total of 50 ml sodium hydroxide solution was reached in the glass beaker. The mixture was soaked in ultrasonic bath for another 30 minutes. Subsequently, 66 ml of distilled water was added into the mixture. The mixture was stirred thoroughly with glass rod and continued to be soaked in ultrasonic bath for 60 minutes. The mixture was then filtered to remove excess sodium hydroxide solution. 1 – 2 ml of 10 wt.% acetic acids was subsequently added

into the mixture to neutralise the pH. After 3 minutes of soaking times, the alkali-treated oil palm fibre (aOPF) was repeatedly washed with distilled water until a pH of 7 was attained. The alkali-treated oil palm fibre was dried in oven at temperature of 80 °C for 5 hours and stored in desiccator. Figure 3-3 displays apparatus used in alkali treatment.

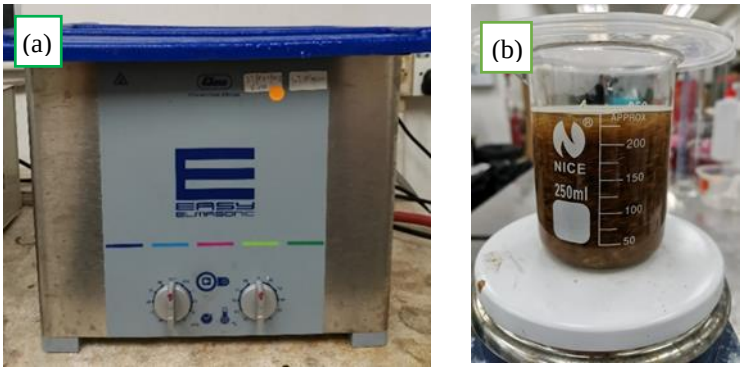

Figure 3-3: (a) Ultrasonic bath and (b) OPF / sodium hydroxide solution

3.2.2 Maleic Anhydride Treatment

10 wt.%, 20 wt.% and 30 wt.% maleic anhydride solutions were prepared by adding maleic anhydride powder into acetone solution. Then, 10 g of alkali-treated oil palm fibre (fibre-solvent ratio 1:10) was added into maleic anhydride solutions separately at 50 °C for 3 hours to coat a bonding layer on the surface of the EFB fibre. The treated oil palm fibre (10maOPF, 20maOPF and 30maOPF) was then washed with distilled water to remove excessive chemicals. Next, the treated EFB fibre was dried in oven at temperature of 80 °C for 5 hours and stored in desiccator.

3.2.3 Silane Treatment

Ethanol/distilled water solution was prepared according to ratio 80:20 by weight. 1 wt.%, 3 wt.% and 5 wt.% of silane solution were prepared by adding 0.1 g, 0.3 g and 0.5 g of and silane into the ethanol/distilled water solution for hydrolysis. 10 g of alkali-treated oil palm fibre was added into silane solution (silane – fibre ratio 1:100) and the solution was then stirred continuously for 1 hour. The oil palm fibre was soaked in silane solution for another 3 hours at ambient temperature. Then, the treated oil palm fibre (1saOPF, 3saOPF and 5saOPF) were dried in oven maintained at 80 °C for 5 hours and stored in desiccator.

3.2.4 Incorporation of Dicumyl Peroxide

Dicumyl Peroxide (DCP) was used as free radical initiator to improve grafting efficiency between maleic-treated OPF and ABS matrix. First, 0.04 grams (0.1 phr) of dicumyl peroxide was added into 40 grams of mixture (8 grams of OPF and 32 grams of ABS resin). Glass rod was used to stir the mixture for 1 minute. After dry mixing, the mixture was poured into Brabender Plastograph for melt compounding.

3.2.5 Extraction of Nanocellulose

Step 1: Delignification

The procedure of delignification process was slightly modified according to method described in ASTM D1104. Firstly, delignification process was carried out on 3 mm–5 mm oil palm fibre by adding 5 g of oil palm fibre, different concentration of acetic acid, sodium hypochlorite and distilled water were added into a 250ml Erlenmeyer flask. The mixture was heated in a water bath at a temperature of 70 °C for 60 minutes. Specific amount of acetic acid and sodium hypochlorite were added into the solution every hour. The chlorination process ended after 6 hours and water bath was switched off. Then, the sample was left in the water bath overnight. After 24 hours of reaction, the samples were cooled and the holocelluloses were filtered out. Drying of holocelluloses took place at 80 °C for 5 hours in an aging oven. Figure 3-4 displays apparatus used in delignification.

Figure 3-4: (a) Digital constant temperature tank and (b) Erlenmeyer flask

Step 2: Alkali Treatment

Subsequently, holocelluloses were subjected to alkali-treatment as stated in section 3.2.1. The output of this process is cellulose.

Step 3: Acid hydrolysis

During acid hydrolysis, 20 ml of 64 wt.% of sulphuric acid was used to treat 2 g of cellulose. The process was conducted on a hot plate stirrer at a temperature of 40 °C and a fixed speed of 750 min^{-1} as shown in Figure 3-5 (a). 200 ml of cold deionized water was added to the solution to stop the chemical reaction after 30 minutes, as illustrated in Figure 3-5 (b). The solution was then transferred into visking tubes for dialysis. Dialysis was done by changing deionized water daily for a period of 3 days until the pH value of deionized water became neutral. Nanocellulose were extracted from oil palm fibre and keep in solution, as indicated in Figure 3-5 (c) or in dry powder form through Freeze-drying process (Figure 3-5 (d)).

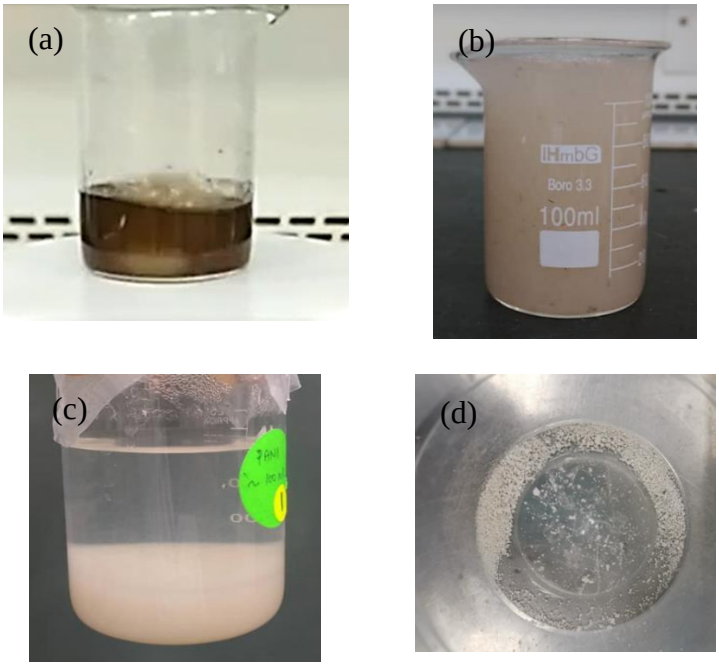

Figure 3-5: (a) and (b) is Acid hydrolysis and (c) and (d) is dialysis process

3.3 Compounding

Brabender Plastograph® EC as shown in Figure 3-6 was used to mix the sample materials thoroughly and study the process ability of oil palm fibre filled ABS composites. The process parameters were then optimised by referring to Plastogram® (torque and stock temperature vs. time graph). The optimized process setting as shown in Table 3-2 should enable compounds well mixed at shorter mixing time and lower temperature to avoid potential materials degradation. All NCC/ABS composites and OPF/ABS composites were melt-blended using same process setting. The detailed discussion about optimized process setting are discussed in *Section 4.1 Mixing Parameters of Melt* Compounding.

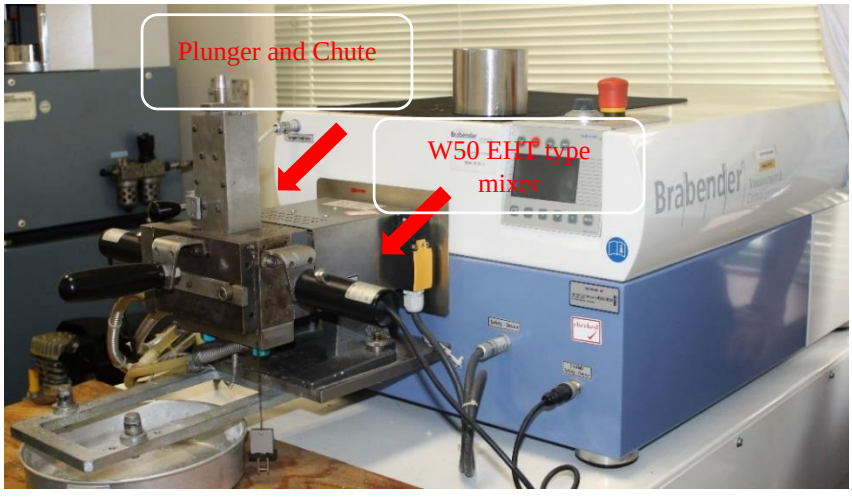

Figure 3-6: Brabender Plastograph ® EC

Table 3-2: Process setting of Brabender Plastograph® EC

Mixing Speed:	30 rpm
Mixer Temperature:	220°C
Mixing Time:	5 minutes
Total Sample Mass:	40 gram

3.4 Hot Compression

The melt blended compounds were hot-pressed into flat sheets with dimensions 20 cm x 15 cm x 2.5 mm (L x W x H) and tolerance of ± 0.5 mm in thickness using a Labtech hydraulic hot press as shown in Figure 3-7.

Table 3-3 summarised the process setting of hot compression process. A measured amount of mixed compounds was placed on the mould. Then the mould was transferred in between hot plates of compression machine. The preheating temperature of 230 °C and preheating time of 5 minutes was set to allow sufficient heat transferred from hot plates of compression machine to the mould so that the compounds became soften. Then, degassing was applied by controlling the mould plate up and down. This step will reduce the bubbles which might be trapped inside the mould during heating. Next, pressing temperature of 220 °C were applied on the mould for 2 minutes. After that, the mould was transferred to cool plate and water cooling system was used to cool down the sheets to room temperature. The cooling process was ended after 10 minutes.

Table 3-3: Hot compression process setting

Preheating Temperature:	230°C
Preheating time:	5 minutes
Pressing Temperature:	220°C
Pressing Time:	2 minutes
Cooling Time:	10 minutes
Pressure	2.1 MPa

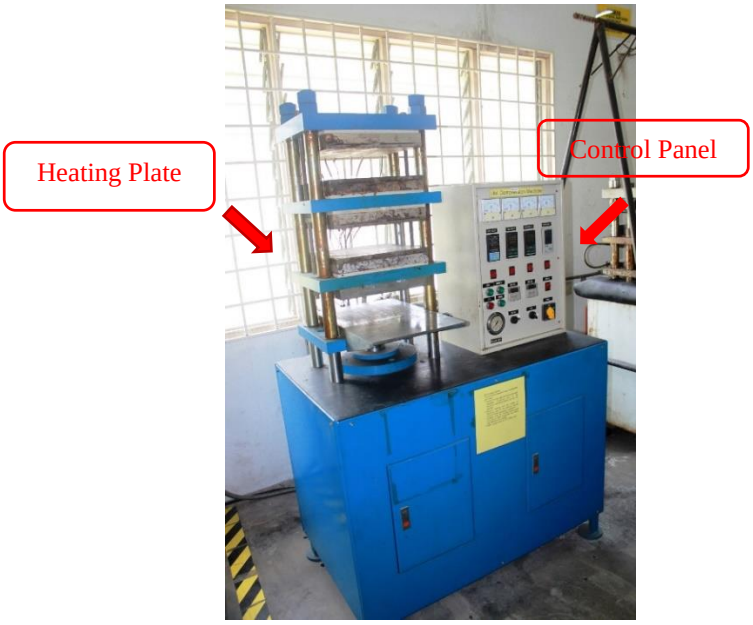

Figure 3-7*:* Hot compression machine

3.5 Nomenclature

After treated by various chemical treatments, OPF samples were classified and named as outlined in Table 3-4. In addition, various types of OPF and nanocellulose were melt blended with ABS resin to produce OPF-filled ABS composites and NCC/ABS composites respectively. These composite samples were categorized and named as shown in Table 3-5. The composition details of the various ABS composites are tabulated in Table 3-6, Table 3-7 and Table 3-8. The short form used in this study are shown as below.

r = raw
a = alkali-treated
m = maleic treatment
c = dicumyl peroxide
s = silane treatment
α = α-cellulose
OPF = oil palm fibre
GP = ABS resin
10m = treated in 10 wt. % maleic anhydride solution
20m = treated in 20 wt. % maleic anhydride solution
30m = treated in 30 wt. % maleic anhydride solution
1s = treated in 1 wt. % silane solution
3s = treated in 3 wt. % silane solution
5s = treated in 5 wt. % silane solution
APP = Ammonium polyphosphate
ATH = Alumina Trihydrate
ZB = Zinc Borate
EG = Expandable Graphite

Table 3-4: Description of different chemically treated OPF samples

Sample No.	Sample Name	Short Form	Description
1	Water-washed oil palm fibre	rOPF	OPF that washed with tap water only.
2	Delignified OPF	dOPF	OPF that treated by delignification only.
3	Alkali-treated OPF	aOPF	OPF that treated by alkali treatment only.
4	Maleic – treated OPF	maOPF	OPF that first treated by alkali treatment and then follow by maleic treatment.
5	Silane – treated OPF	saOPF	OPF that first treated by alkali treatment and then follow by silane treatment.
6	α-cellulose	αOPF	OPF that first treated by alkali treatment and then follow by maleic treatment.
7	Microcrystalline cellulose powder	MCC	Commercial cellulose powder that purchased from Sigma-Aldrich.
8	Nanocellulose	NCC_A	Nanocellulose isolated from oil palm fibre
9	Celluforce NCC	NCC_B	Commercial cellulose nanocrystals that purchased from CelluForce
10	Maleic – treated Celluforce NCC	mNCC	Commercial cellulose nanocrystals that treated by maleic treatment
11	Silane – treated Celluforce NCC	sNCC	Commercial cellulose nanocrystals that treated by silane treatment

Table 3-5: Description of different ABS composites

Sample No.	Short Form	Description
1	100GP / CONTROL	ABS resin with trade name of GP-22. Pure GP-22 compounded by Brabender Plastograph.
2	01NCC99GP	1 wt. % of Celluforce NCC mixed with 99 wt. % of GP-22
3	03NCC97GP	3 wt. % of Celluforce NCC mixed with 97 wt. % of GP-22
4	05NCC95GP	5 wt. % of Celluforce NCC mixed with 95 wt. % of GP-22
5	07NCC93GP	7 wt. % of Celluforce NCC mixed with 93 wt. % of GP-22
6	10NCC90GP	10 wt. % of Celluforce NCC mixed with 90 wt. % of GP-22
7	01mNCC99GP	1 wt. % of mNCC mixed with 99 wt. % of GP-22
8	03mNCC97GP	3 wt. % of mNCC mixed with 97 wt. % of GP-22
9	05mNCC95GP	5 wt. % of mNCC mixed with 95 wt. % of GP-22
10	07mNCC93GP	7 wt. % of mNCC mixed with 93 wt. % of GP-22

11	10mNCC90GP	10 wt. % of mNCC mixed with 90 wt. % of GP-22
12	01sNCC99GP	1 wt. % of sNCC mixed with 99 wt. % of GP-22
13	03sNCC97GP	3 wt. % of sNCC mixed with 97 wt. % of GP-22
14	05sNCC95GP	5 wt. % of sNCC mixed with 95 wt. % of GP-22
15	07sNCC93GP	7 wt. % of sNCC mixed with 93 wt. % of GP-22
16	10sNCC90GP	10 wt. % of sNCC mixed with 90 wt. % of GP-22
17	10OPF90GP	10 wt. % of oil palm fibre mixed with 90 wt. % of GP-22
18	20OPF80GP	20 wt. % of oil palm fibre mixed with 80 wt. % of GP-22
19	30OPF70GP	30 wt. % of oil palm fibre mixed with 70 wt. % of GP-22
20	20rOPFGP	20 wt. % of rOPF mixed with 80 wt. % of GP-22
21	20aOPFGP	20 wt. % of aOPF mixed with 80 wt. % of GP-22
22	10maOPFGP	20 wt. % of 10maOPF mixed with 80 wt. % of GP-22
23	20maOPFGP	20 wt. % of 20maOPF mixed with 80 wt. % of GP-22
24	30maOPFGP	20 wt. % of 30maOPF mixed with 80 wt. % of GP-22
25	10mcaOPFGP	20 wt. % of 10maOPF mixed with 80 wt. % of GP-22 and dicumyl peroxide.
26	1saOPFGP	20 wt. % of 1saOPF mixed with 80 wt. % of GP-22
27	3saOPFGP	20 wt. % of 3saOPF mixed with 80 wt. % of GP-22
28	5saOPFGP	20 wt. % of 5saOPF mixed with 80 wt. % of GP-22
29	05APP95GP	5 wt. % of ammonium polyphosphate mixed with 95 wt. % of GP-22
30	05ATH95GP	5 wt. % of alumina trihydrate mixed with 95 wt. % of GP-22
31	05ZB95GP	5 wt. % of zinc borate mixed with 95 wt. % of GP-22
32	05EG95GP	5 wt. % of expandable graphite mixed with 95 wt. % of GP-22

33	15EG85GP	15 wt. % of expandable graphite mixed with 85 wt. % of GP-22
34	15APP20OPF65GP	15 wt. % of ammonium polyphosphate mixed with 20 wt.% of oil palm fibre and 65 wt. % of GP-22
35	15ATH20OPF65GP	15 wt. % of alumina trihydrate mixed with 20 wt.% of oil palm fibre and 65 wt. % of GP-22
36	15ZB20OPF65GP	15 wt. % of zinc borate mixed with 20 wt.% of oil palm fibre and 65 wt. % of GP-22
37	05EG20OPF75GP	5 wt. % of expandable graphite mixed with 20 wt.% of oil palm fibre and 75 wt. % of GP-22
38	15EG20OPF65GP	15 wt. % of expandable graphite mixed with 20 wt.% of oil palm fibre and 65 wt. % of GP-22
39	20OPF80GP	20 wt. % of oil palm fibre mixed with 80 wt. % of GP-22
40	10APP05ATH20OPF65GP	10 wt. % of ammonium polyphosphate mixed with 5 wt. % of alumina trihydrate, 20 wt.% of oil palm fibre and 65 wt. % of GP-22
41	10APP05ZB20OPF65GP	10 wt. % of ammonium polyphosphate mixed with 5 wt. % of zinc borate, 20 wt.% of oil palm fibre and 65 wt. % of GP-22
42	05ATP10ATH20OPF65GP	5 wt. % of ammonium polyphosphate mixed with 10 wt. % of alumina trihydrate, 20 wt.% of oil palm fibre and 65 wt. % of GP-22
43	10ATH05ZB20OPF65GP	10 wt. % of alumina trihydrate mixed with 5 wt. % of zinc borate, 20 wt.% of oil palm fibre and 65 wt. % of GP-22
44	05APP10ZB20OPF65GP	5 wt. % of ammonium polyphosphate mixed with 10 wt. % of zinc borate, 20 wt.% of oil palm fibre and 65 wt. % of GP-22
45	05ATH10ZB20OPF65GP	5 wt. % of alumina trihydrate mixed with 10 wt. % of zinc borate, 20 wt.% of oil palm fibre and 65 wt. % of GP-22

Table 3-6: The composition of OPF/ABS composites

Sample No.	Short Form	ABS (%)	OPF (%)	Alkali treatment	Maleic treatment	Silane treatment
1	100GP	100	-	-	-	-
2	10OPF90GP	90	10	-	-	-
3	20OPF80GP	80	20	-	-	-
4	30OPF70GP	70	30	-	-	-
5	20rOPFGP	80	20	-	-	-
6	20aOPFGP	80	20	✓	-	-
7	10maOPFGP	80	20	✓	✓	-
8	20maOPFGP	80	20	✓	✓	-
9	30maOPFGP	80	20	✓	✓	-
10	1saOPFGP	80	20	✓	-	✓
11	3saOPFGP	80	20	✓	-	✓
12	5saOPFGP	80	20	✓	-	✓

Table 3-7: The composition of NCC/ABS composites

Sample No.	Short Form	ABS (%)	NCC (%)	Maleic Treatment	Silane treatment
1	100GP	100	-	-	-
2	01NCC99GP	99	1	-	-
3	03NCC97GP	97	3	-	-
4	05NCC95 GP	95	5	-	-
5	07NCC93 GP	93	7	-	-
6	10NCC90 GP	90	10	-	-
7	01mNCC99 GP	99	1	✓	-
8	03mNCC97 GP	97	3	✓	-
9	05mNCC95 GP	95	5	✓	-
10	07mNCC93 GP	93	7	✓	-
11	10mNCC90 GP	90	10	✓	-
12	01sNCC99 GP	99	1	-	✓
13	03sNCC97 GP	97	3	-	✓
14	05sNCC95 GP	95	5	-	✓
15	07sNCC93 GP	93	7	-	✓
16	10sNCC90 GP	90	10	-	✓

Table 3-8: The composition of each FR-contained ABS composites

Sample No.	Short Form	ABS (%)	OPF (%)	APP (%)	ATH (%)	ZB (%)	EG (%)
1	100GP	100	-	-	-	-	-
2	05APP95GP	95	-	5	-	-	-
3	05ATH95GP	95	-	-	5	-	-
4	05ZB95GP	95	-	-	-	5	-
5	05EG95GP	95	-	-	-	-	5
6	15EG85GP	85	-	-	-	-	15
7	15APP20OPF65GP	65	20	15	-	-	-
8	15ATH20OPF65GP	65	20	-	15	-	-
9	15ZB20OPF65GP	65	20	-	-	15	-
10	15EG20OPF65GP	65	20	-	-	-	15
11	25EG20OPF45GP	45	20	-	-	-	25
12	20OPF80GP	80	20	-	-	-	-
13	10APP05ATH20OPF65GP	65	20	10	5	-	-
14	10APP05ZB20OPF65GP	65	20	10	-	5	-
15	05ATP10ATH20OPF65GP	65	20	5	10	-	-
16	10ATH05ZB20OPF65GP	65	20	-	10	5	-
17	05APP10ZB20OPF65GP	65	20	5	-	10	-
18	05ATH10ZB20OPF65GP	65	20	-	5	10	-

3.6 Materials and Samples Characterisation

3.6.1 Fourier Transform Infrared Spectrometry (FTIR) Analysis

Fourier Transform Infrared Spectrometry (FTIR) analyses are conducted to identify molecular components, functional groups and structures of samples. As shown in Figure 3-8, the FTIR model used in this experiment was the Spectrum 65 FT-IR spectrometer supplied by PerkinElmer. The instrument was set to scan 16 times as opposed to the usual 4 times to reduce the noise in the results. The resolution set for the scan was 4 cm^{-1}, within the scanning range from 4000 cm^{-1} to 650 cm^{-1}. Each scan requires a background scan to filter out the noise, with adjustments made to the preview scan before obtaining the final scan.

Figure 3-8: Spectrum 65 FT-IR spectrometer

3.6.2 Scanning Electron Microscopy (SEM)

SEM was conducted to characterise the morphological properties of the samples. SEC Desktop Mini-SEM SNE-3000M from SEC Co. Ltd, Suwon, Korea (Figure 3-9) was used to investigate the materials morphology, untreated and treated oil palm fibre surface and fracture surface of the post polymer composites tensile test samples. The test samples were observed under different magnification at an accelerating voltage of 30 kV.

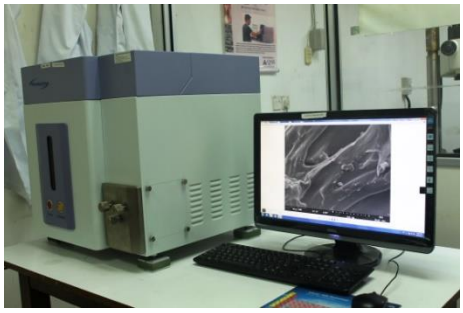

Figure 3-9: SEC Desktop Mini-SEM SNE-3000M

3.6.3 Particle Size Measurements

The particle size distribution was measured using a particle size analyser (Model: Litesizer 500 from Anton Paar) as shown in Figure 3-10. The equipment able to determine particle via dynamic light scattering (DLS) at three different measurement angles. The dynamic light scattering (DLS) is a non-invasive method to estimate the size distribution profile of nanoparticles in a colloidal solution. 0.05 % (w/v) nanocellulose suspension was prepared by adding 7.5 milligram of nanocellulose into 15 ml of deionised water. To ensure nanocellulose is well dispersed in the solution, 0.05 % (w/v) nanocellulose suspension are put into ultrasonic bath and sonicated for 30 minutes. 1 ml of NCC suspension was put into the plastic cuvette by 1 ml syringe with the aid of 0.45 μm PVDF filter.

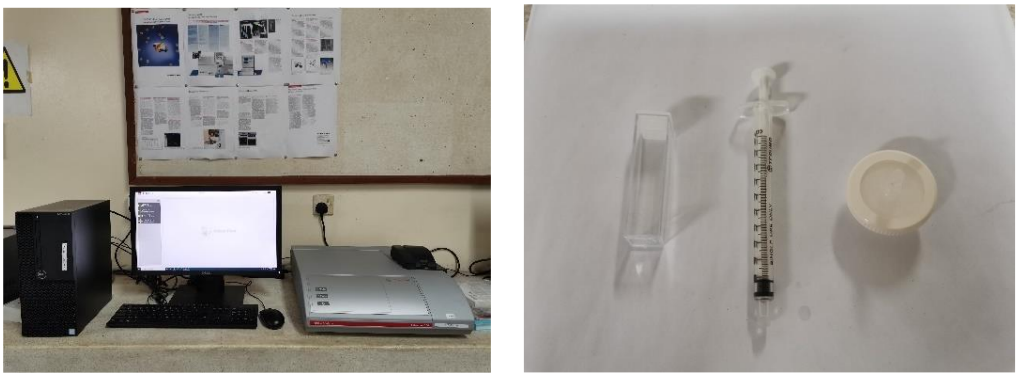

Figure 3-10: Litesizer 500 (left) and cuvette, 1ml syringe and 0.45 μm PVDF filter (right)

3.7 Tensile Test

GT-7016-HA hard plastic specimen cutting machine was used to shape the flat sheets into dumbbell shape tensile test specimens according to dimensions (Type I) specified in ASTM D638-02a. Tensile Test was conducted to determine the mechanical properties of OPF reinforced ABS composites. It was conducted according to ASTM D638-02a by using GT-TCS-2000 universal testing machine with a capacity of 20 kN load-cell as shown in Figure 3-11.

Table 3-9 summarised the tensile test setting. Force-displacement data was obtained from software U60 and these data were converted to the corresponding nominal stress-strain using constitutive formulations. The tensile properties of the materials were interpreted from the stress-strain curves and extensometer are used to determine maximum elongation of test samples.

Figure 3-11: GT-TCS-2000 computer system universal testing machine

Table 3-9: Tensile test setting

Testing speed:	5mm / min
Number of specimen tested:	5 pieces per sample

3.8 Thermal Properties Test

3.8.1 Thermal gravimetric Analysis (TGA)

TA Instruments SDT-Q600 as shown in Figure 3-12 was used to conduct thermal gravimetric analysis. The changes in mass loss of the sample was detected up to 0.1µg at a temperature sensitivity of 0.001°C. The TGA result could be affected by the sample preparation method, heating rate, controlled atmosphere and gas flow rate of the TGA. Higher heating rate during pyrolysis may shift chemical reaction steps of test samples to higher temperatures. Different atmosphere may lead to different pyrolysis behaviour. Table 3-10 indicates the TGA test setting with compliance to ASTM E1131. Approx. 10 mg to 30 mg of samples were placed on open alumina sample pan and were heated from 30 °C to 700 °C at heating rate of 20 °C per minute under inert (nitrogen) atmosphere at the flow rate of 100 ml/min. Two specimens from each formulation were analysed.

Table 3-10: Simultaneous TGA/DSC test setting

Temperature Range:	30 – 700 °C
Heating Rate:	20°C / minute
Gas flow rate:	100 ml / min
Gas type:	Nitrogen

The TGA test was performed on two test specimens from each sample preparation/formulation to verify the reproducibility of the result. The TGA and DTG curves were plotted with interpolation formula in Ms Excel using raw data exported from SDT software. The extrapolated onset decomposition

temperature is determined by the intersection of the first and second tangents of the DTG curve and the mass loss rate of chemical components were determined by identifying the signal peak in the DTG curves.

Figure 3-12: TA Instruments SDT-Q600

3.8.2 UL 94 Flammability Test

Yasuda No.252-UL-94 Plastic Flammability Tester is used to conduct horizontal burn test (94HB) and vertical burn test (VB) according to ASTM D635 and ASTM D3801 respectively. The flat sheets fabricated by hot compression were cut into test specimens according to dimensions of 125 mm ± 5 mm (L), 13 mm ± 0.5 mm (W) and 3 mm ± 0.5 mm (thickness). Five specimens per sample are required for the flammability test. They are conditioned at temperature of 23 ± 2 °C and humidity level of 50 ± 5 % for at least 48 hours. The equipment and the setup of vertical burn test are illustrated in Figure 3-13.

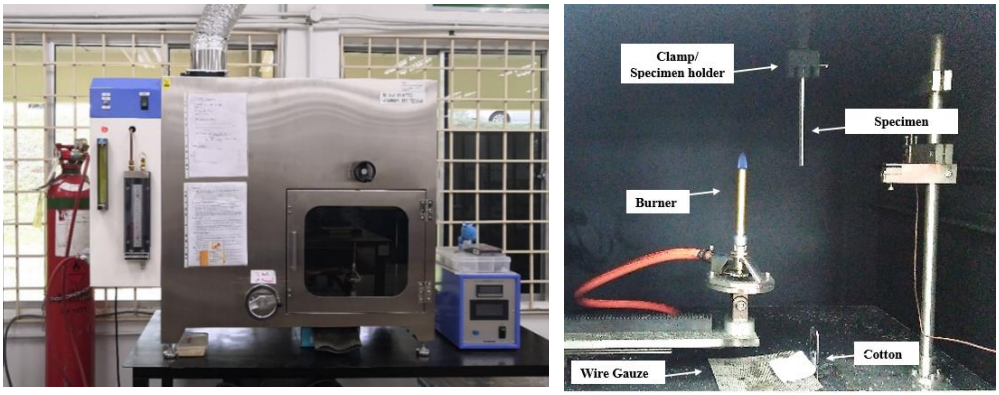

Figure 3-13: Yasuda No. 252 -UL-94 plastic flammability tester (left) and setup of UL-94 vertical burning test

3.8.3 Limiting Oxygen Index Test

Limiting Oxygen Index (LOI) of various OPF/ABS composites were measured to study the minimum oxygen concentration that required to sustain combustion. Oxygen is one of the key elements in fire triangle. The fire triangle is a simple model used to illustrate the three essential components (fuel, heat and oxygen) required for a fire to occur and sustain itself. The fire triangle concept is vital for understanding fire behaviour, prevention, and firefighting techniques. Without sufficient oxygen, fuel is unable to undergo a chemical

reaction that t releases energy in the form of heat and light. Hence, combustion will achieve self-extinguishing.

The FESTEC's LOI (Limited Oxygen Index tester) as shown in Figure 3-14 are used to determine the minimum percentage of oxygen needed to sustain flaming combustion. Limiting oxygen index test (LOI) was conducted in according to ASTM D2863 and it is a widely used method to assess burning capability or flammability of polymer. 15 test specimens per sample were prepared by cutting into 125 ± 5 mm (L), 6.5 ± 0.5 mm (W) and 3 ± 0.25 mm (*t*). These samples are conditioned at temperature of 23 ± 2 °C and humidity level of 50 ± 5 % for at least 48 hours.

Figure 3-14: Limiting oxygen index tester (left) and test samples (right)

Chapter 4: Results and Discussions

4.1 Mixing Parameters of Melt Compounding

Numerous technical challenges are encountered during melt compounding, i.e. restricted maximum processing temperature of natural fibres and plastic resins, proper wetting and dispersion of natural fibres in high melt viscosity polymer matrix often influence the processability of natural fibre filled thermoplastics. To determine optimum processing setting for oil palm fibre (OPF) filled acrylonitrile butadiene styrene (ABS) polymer composites, process parameters of Brabender Plastograph® such as mixer temperature, mixing time and rotor speed were studied. The resulting materials properties of the natural fibre filled ABS were analysed and their relations to the processing parameters were established to determine the optimum process setting.

4.1.1 Fusion Behaviour - Mixer Temperature

According to materials data sheet provided by supplier, the recommended processing temperature is ranging from 220 °C to 260 °C. The results of varying melt temperature of ABS are depicted in Table 3-3. As expected, the results reveal that higher mixer temperature reduced the melt viscosity of the compounds. Hence, maximum torque and energy consumption for driving rotor at speed of 30 rpm is reduced by 53 % and 63.71 % respectively. However, the cost saving with reduction of energy usage needs to be balanced with potential thermal degradation of the resin and the OPF. Prolonged exposure at higher processing temperature could potentially accelerate the thermal degradation of the OPF as well as the oxidative degradation of the ABS.

Based on the literature studies, the preferred processing temperature is 220 °C [190][191]. As demonstrated in Figure 4-1, it can be observed that ABS experienced thermal degradation when the material is processed at 260 °C for 10 minutes, as evidenced by its discoloration and yellowish physical appearance.

Table 4-1: Comparison of Plastogram® of neat ABS compounds at different mixer temperatures

Mixer Temperature / °C	220	260
Rotor Speed / rpm	30	30
Maximum Torque / Nm	43.8	20.6
Time to Reach Maximum Torque / Sec	27	14
Time to Reach Inflection Point / Sec	293	257
Fusion Time / Sec	266	243
Energy consumption during fusion / kJ	11.7	3.7
Total Energy consumption after 10 minutes / kJ	23.7	8.6
Stock Temperature at injection point / °C	218	252.2
Stock Temperature after 10 minutes / °C	220.7	257.2

Figure 4-1: Surface morphology of the neat GP-22 sample heated at 260 °C for 10 minutes at rotor speed of 30 rpm

4.1.2 Fusion Behaviour – Rotor Speed

Rotor speed is one of the key mixing parameters that affects the melting behaviour of OPF/ABS composites, with higher shear rate produces greater shear induced heating. In the current study, the mixer temperature was fixed at 220 °C. Three rotor speeds (10 rpm, 30 rpm and 50 rpm) were investigated to determine the optimum rotor speed and the results were shown in Table 4-2.

It can be observed that the maximum torque, fusion time and energy consumption increased with increasing rotor speed as shown in Table 4-2 and Figure 4-2. At excessively high rotor speed, i.e. at 50 rpm, the study revealed that the recorded bulk material temperature exceeded the pre-set temperature of 220 °C at inflection point and the temperature continue to increase until the end of compounding, attributed to excessive shear heating. As depicted in Table 4-3, the overheating became more serious when the formulation is loaded with OPF. Furthermore, higher rotor speed could lead to excessive fibre fragmentation [192].

High screw speed is frequently used to shorten plasticising time, thereby minimising the residence time and reduces the risk of thermal degradation as well as to aid fibre distribution within the polymer matrix. However, excessively high screw speed may result in trapped air within the molten plastic and shear induced thermal degradation, causing various moulding defects such as blisters, burn marks and splay [191].

Conversely, at lower rotor speed, i.e. at 10 rpm, it was observed that the stock temperature was unable to reach preset temperature after 10 minutes of mixing. This suggested that lower range of rotor speed could not generate sufficient shear heating to fully melt the materials and consequently some of the unmelted pellets entering into further downstream of the system, leading to inconsistency in product quality. It is thereby concluded from the current findings that 30 rpm rotor speed provides a balance and optimum output.

Table 4-2: Comparison of Plastogram® of Neat ABS compounds at different shear rate

Rotor Speed / rpm	10	30	50
Maximum Torque / Nm	26.4	43.8	88.6
Time to Reach Maximum Torque / Sec	16	27	40
Time to Reach Inflection Point / Sec	228	293	384
Fusion Time / Sec	212	266	344
Energy consumption during fusion / kJ	2	11.7	31.6
Total Energy consumption after 10 minutes / kJ	4.3	23.7	48.5
Stock Temperature at inflection point / °C	212.6	218	221.7
Stock Temperature after 10 minutes / °C	216	220.7	225.4

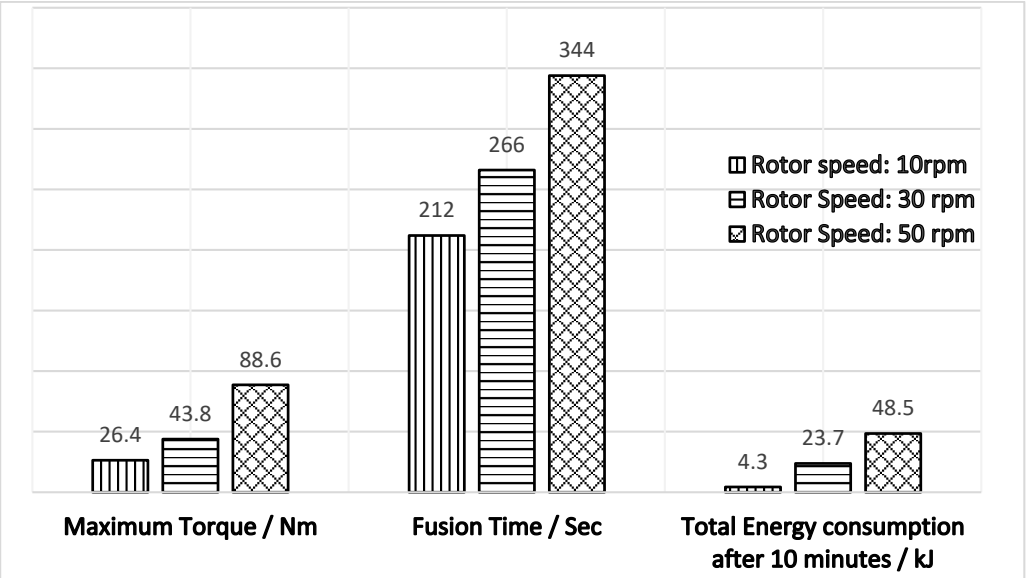

Figure 4-2: Maximum torque, fusion time and energy consumption as a function of rotor speed

Table 4-3: Plastogram® output as different OPF/GP loadings

	100GP	10OPF90GP	30OPF70GP
Mixer temperature / °C	220	220	220
Rotor Speed / rpm	50	50	50
Maximum Torque / Nm	88.6	51.6	47.4

Stock Temperature at inflection point / °C	221.7	225.4	226.7
Stock Temperature after 10 minutes / °C	225.4	226.5	228.1

4.1.3 Fusion Behaviour – Mixing Time

Mixing time affects the total process cycle time and residence time which in turn influence the tendency of material degradation during compounding. The optimum mixing time often depends on the total heat energy required to raise a material temperature to its melt processing range. H. Blom et al. reported that ABS tends to experience oxidative degradation when exposed to high temperature in particularly in environment with the presence of oxygen. When the duration of holding time increases, the extent of degradation may increase as oxygen is able to diffuse further into ABS [190]. Hence, the mixing time and mixing temperature should be kept low to avoid thermal degradation.

The process time necessary to reach inflection point in torque reflects the fusion time where the compounds achieve their molten stage. Fusion time is determined when mixing reached inflection point. The compounds are completely molten when the torque is consistent. Figure 4-3 showed the variation of torque with varying formulation of the compounds. Adding OPF into ABS compounds reduced maximum torque required for melt blending. Since the total load remains constant, a higher percentage of OPF results in lower ABS content. As the ABS concentration in the blend decreased, the mixture's viscosity reduced. This reduction leads to less energy and torque being required to thoroughly mix the compound. The result shown in Table 4-4 indicates that neat ABS (100GP) required 266 seconds to be fully molten. This fusion time decreases in samples loaded with OPF. Furthermore, reduction in mixing time significantly decreases energy consumption.

In addition, the collection of mixed compounds from Brabender chamber should finish as fast as possible as ABS compound exposed to elevated temperature in an open environment may tend to cause oxidative degradation. Figure 4-4 illustrates that the neat ABS (100GP) compounds started to turn yellowish after 10 minutes of mixing time. However, neat ABS (100GP) compounds are still broadly white in colour after 5 minutes of mixing time.

Mixing time in Brabender compounding is analogue to the residence time of injection moulding. Excessive residence time generate moulding defects such as black specks and discoloration due to material degradation. When materials get hotter, the melt viscosity drop and the increased flow characteristic could lead to flashing. Conversely, inadequate residence time could resulted in partially molten and unmelted mixture of plastic resins. Those unplasticised resin may lead to moulding defects such as flow lines, low gloss and warpages.

In order to avoid polymer degradation while ensuring melt uniformity, the current study reveals that an optimum compounding time of 300 seconds

could be established for ABS resin. Table 4-4 depicts the recorded fusion time along with other process parameters.

Table 4-4: Melting behaviour of OPF/ABS composites

	100GP	10OPF90GP	20OPF80GP	30OPF70GP
Mixer Temperature / °C	220	220	220	220
Rotor Speed / rpm	30	30	30	30
Time to Reach Maximum Torque / Sec	27	33	35	47
Time to Reach Inflection Point / Sec	293	284	262	213
Fusion Time / Sec	266	250	227	166
Energy consumption during fusion / KJ	11.7	9.6	9.2	7.6
Total Energy consumption after 10 minutes / KJ	23.7	19.7	20.1	21.6
Maximum Torque / Nm	43.8	40.4	40.3	32.6
Stock Temperature at inflection point / °C	218	217.2	218.1	217.2
Stock Temperature after 10 minutes / °C	220.8	220.3	221.7	221.5

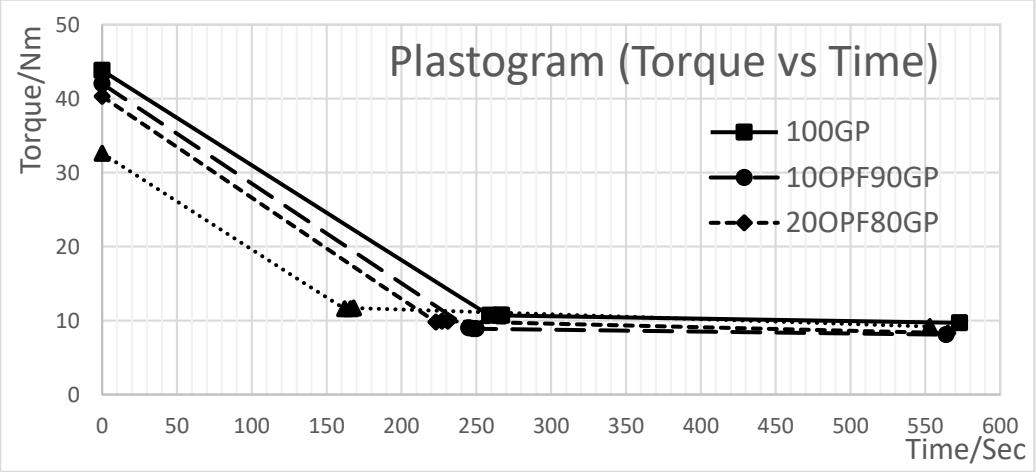

Figure 4-3: Fusion behaviour of neat ABS and varying composition of OPF/ABS composites

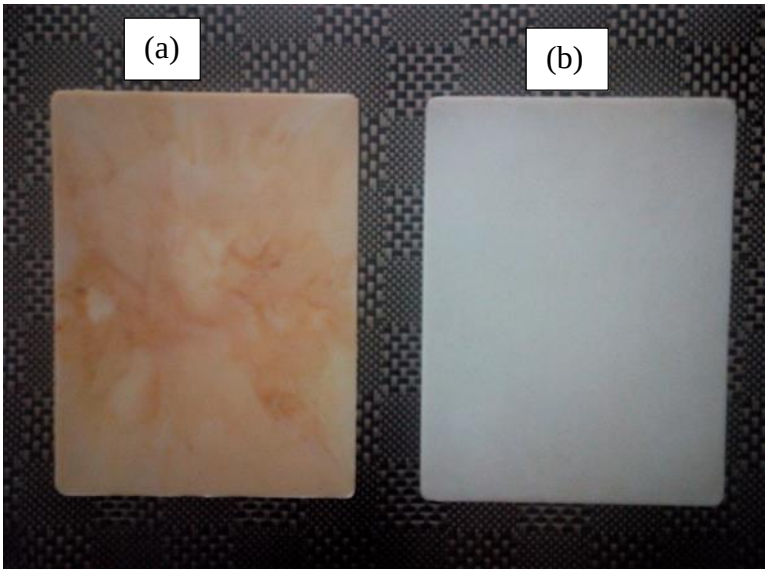

Figure 4-4: Physical appearance of compounded samples with different mixing time at (a) 10 minutes and (b) 5 minutes

4.1.4 Fusion Behaviour – Maximum Torque

Torque refers to the force that acts on the mixing screw and drive the screw rotation during compounding operation. Table 3-3, Table 4-2 and Table 4-4 showed that higher torque during mixing leads to higher energy consumption. However, the maximum torque required to mix the compounds decreased as the OPF loading increased. It follows that introducing OPF into ABS resin reduces both the maximum torque and total energy consumption, which could be related to the reduced volume of ABS resin with increasing OPF loading thereby lower the overall system energy requirement to raise the compound to its melting temperature.

Plasticising stage contributes a significant portion of power consumption in conventional plastic moulding processes. A process with low torque implies that the manufacture of short fibre thermoplastic composites through injection moulding or extrusion compounding does not consume extra production cost.

4.1.5 Effects of mixing time on the mechanical properties of ABS

The tensile properties and Izod notched impact strength of neat ABS with difference mixing time were tabulated in Table 4-5. The results clearly indicated that extended mixing time reduced both the tensile and impact strengths by ~20 % and ~30%, respectively. The observed phenomenon can be attributed to the effects of thermally induced degradation in the event of prolonged residence time, i.e. 10 minutes, leading to molten compound with shorter molecular chains, fiber length degradation and poor mechanical properties. Owing to the reduced elongation at break, degraded samples tend to be more brittle with greater elastic modulus. Within the molecular backbone of ABS, the butadiene phase provides superior impact resistance to ABS resin. However, it is susceptible to oxidative degradation in the presence of oxygen at

high temperature over a long period of time. Therefore, the impact resistance of ABS was greatly reduced [190][193][71].

Table 4-5: Tensile properties and impact strength of neat ABS as a function of mixing time

Mixing Time	5 minutes	10 minutes	Difference (%)
Ultimate Tensile Strength / MPa	31.48	25.13	-20.17
Tensile Elongation at break / %	2.53	2.37	-6.32
Yield Strength / MPa	28.00	22.80	-18.57
Elastic Modulus / GPa	2.43	3.10	27.68
Energy / width, J/m	193.98	134.83	-30.49

4.1.6 Summary

The result reveals that introducing pulverised natural fibres (OPF) into thermoplastic (ABS) reduces energy consumption during the compounding operation. The compounding of OPF and temperature sensitive ABS could be optimised by controlling the process parameters whereby the optimised mixing parameters of Brabender Plastograph® were found at 220 °C (mixer temperature), 30 rpm (rotor speed) and 5 minutes mixing time. The underlying principles determining the relationship of process parameter, material properties and formulation are demonstrated with the aid of counter rotating twin screw Brabender mixer in the current study and provides a valuable guideline for moulding of natural fibre filled ABS composites.

4.2 Isolation of Nanocellulose

4.2.1 Process parameters of Delignification and Alkali Treatment

Delignification of oil palm fibre (OPF) with different ratios of chemicals were carried out with the intention to obtain optimum concentrations of chemicals to fully delignify OPF while maintain higher yield. The initial weight of OPF in each sample were identical (5 grams) and the holocellulose content after filtration were weighed accordingly. The initial weight, final weight and their difference were recorded in the Table 4-6. It is believed that volume of distilled water used for delignification did not affect the remaining amount of holocelluloses significantly. All samples were having approximately 20 – 30% of weight loss due to dissolution of lignin content. The FTIR result summarised in Table 4-10 verified that the loss of fibre content is mainly lignin as all the peaks in the FTIR spectra of dignified OPF (dOPF) that related to lignin were disappeared.

Table 4-6: Delignification of OPF in different ratios of chemicals

Sample No.	Deionized water (ml)	NaClO : Acetic Acid (ml)	Final Weight (g)	Weight Loss (g)	Percentage of Remaining (%)
1	160	8 : 4	3.60	1.40	72.0
2	160	12 : 6	4.00	1.00	80.0
3	160	16 : 8	3.50	1.50	70.0
4	80	16 : 8	3.70	1.30	74.0

The holocelluloses collected from delignification was then subjected to alkali treatment. The detailed procedure is stated in *Section 3.2.1*. The initial and final weight of samples were recorded in Table 4-7. The output is cellulose fibres. The FTIR result summarised in Table 4-10 confirmed that only eight peaks related to cellulose are still remained in the FTIR spectra of OPF which undergone delignification and alkali-treatment. Hence, it can be concluded that the output is cellulose fibres. Sample 4 has the highest percentage of remaining, which is 28.1%. Hence, the concentration of chemicals used for sample 4 is justified as optimum chemical concentration for cellulose extraction from oil palm fibre.

Table 4-7: Weight records for each sample after alkali treatment.

Sample No.	Initial Weight (g)	Final Weight (g)	Residue (g)	Weight Loss (g)	Percentage of Remaining (%)
1	3.60	0.36	1.70	1.54	10.0
2	4.00	0.75	1.10	2.15	18.8
3	3.50	0.76	0.94	1.80	21.7
4	3.70	1.04	0.60	2.06	28.1

4.2.2 Process parameters of Acid Hydrolysis and Dialysis

Acid hydrolysis was conducted in different conditions to justify the optimum process parameters to extract nanocellulose from OPF. As summarised in Table 4-8, the optimum process parameters for acid hydrolysis are treating the OPF / sulphuric acid solution on a hot plate stirrer at a temperature of 40 °C and a fixed speed of 750 rpm for 30 minutes. Refer to Figure 4-5 (a), higher treatment temperature (45 °C) and longer treatment time (45 minutes) resulted in a colour change of solution (black), which indicated side reactions such as dehydration. Furthermore, greater amount of impurities (black fibrils) was observed when acid hydrolysis was carried out at temperature of 45 °C for 45 minutes [129].

Table 4-8: Process parameters of acid hydrolysis

No.	OPF : Acid ratio (g:ml)	Treatment Temperature / °C	Treatment Time / minutes	Stirring Speed (rpm)	Initial Weight (g)	Final Weight (g)	Weight Loss (g)	Percentage of Remaining (%)
1	1:10	40	30	750	2.00	0.94	1.06	47.0
2	1:10	45	45	950	2.00	0.54	1.46	27.0

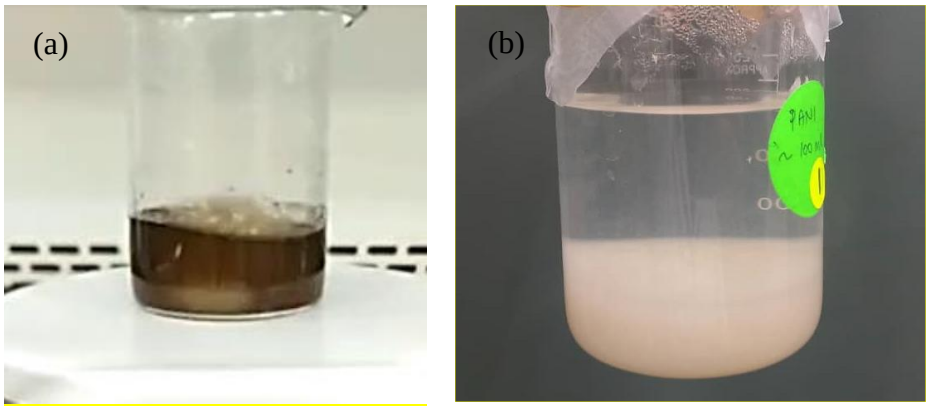

Figure 4-5: Cellulose solution after acid hydrolysis

To cease chemical reaction and neutralise the pH value of solution, 10-fold of cold water was added into solution. The solution looks cloudy due to the agglomeration of nanocellulose, as shown in Figure 4-5 (b). The dialysis was conducted in 2 types of water to study the effectiveness of dialysis process. The result showed in Table 4-9 indicates that dialysis process conducted by using deionized water has lower dialysis time as compared to distilled water. Freeze-drying process was used to turn nanocellulose into dry powder form. The nanocellulose solution was first kept at -21°C. Then the frozen nanocellulose was transferred to freeze dryer and the water vapour is suctioned out of the drying chamber with assisted by a vacuum pump.

Table 4-9: pH readings of dialysis process

	Day 1	**Day 2**	**Day 3**	**Day 4**
pH (Distilled water)	2	3	5	7
pH (Deionzed water)	2	5	7	7

4.2.3 Characterisation of nanocellulose

4.2.3.1 Scanning electron microscope (SEM) analysis

Field Emission Scanning Electron Microscopy (FESEM) observations were conducted to verify the effects of fibre surface treatment on the morphology of OPF samples. As illustrated in Figure 4-6 (a), the average thickness of water-washed OPF (rOPF) is approximately 279.8 µm. With reference to Figure 4-6 (b) and (c), it can be observed that a large quantity of

silica bodies were embedded in the water washed oil palm fibre. During delignification process, sodium hypochlorite reacts with acetic acid to release the hypochlorous acid (HClO). HClO is an oxidizer that can remove lignin from natural fibre. After the delignification process, some of these silica bodies were peeled off and left micropores on the surface of the oil palm fibre.

Figure 4-6 (d), and (e) indicated that the average fibre thickness after delignification process and alkali treatment, respectively. The average thickness of delignified OPF (dOPF) and cellulose are about 152.76 µm and 10.38 µm, respectively. Lignin holds cellulose and hemicellulose together. It is well knowing that once lignin and hemicellulose leached out after fibre surface treatment, the fibre thickness reduces.

Figure 4-6 (f) indicated the nanocellulose isolated from oil palm fibre through acid hydrolysis. Due to high reactivity of the sample and FESEM sample preparation method (air-dried method), NCC showed tendency of agglomeration. Small spherical particles which intend to gather and form a larger particle was observed. In spite of this, an average of dimension measuring about 365.7 nm was defined in Figure 4-6 (f). In short, FESEM analysis verified that isolation of nanocellulose from OPF is feasible through delignification, alkali treatment and acid hydrolysis.

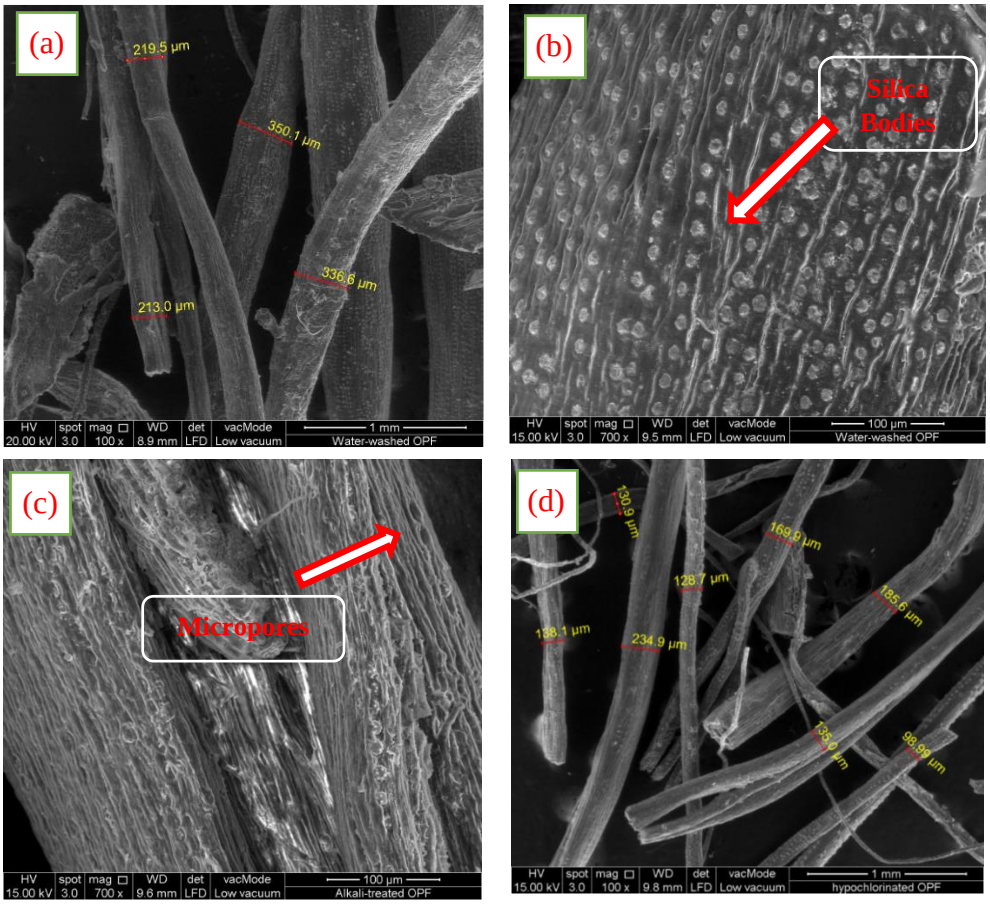

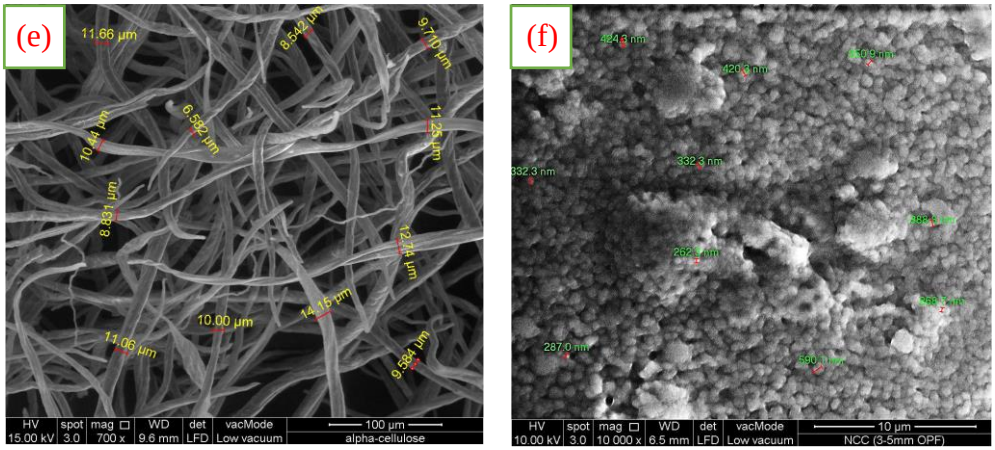

Figure 4-6: Field emission scanning electron microscopy (FESEM) images of (a) & (b) water-washed oil palm fibre, (c) & (d) delignified OPF, (e) cellulose and (f) nanocellulose

4.2.3.2 Fourier Transform Infrared Spectrometer (FTIR)

Characteristic bands of the FTIR spectra of various OPF samples were tabulated into Table 4-10, respectively. FTIR spectra of water-washed OPF (rOPF) was shown in the Figure 4-7. It illustrates that water-washed OPF consists of 13 peaks, which indicates the existence of different components in natural fibre.

Eight peaks indicated in the FTIR spectra are found to be related to cellulose of OPF. The peak at 3335.77 cm^{-1} and 2915.75 cm^{-1} in the broad band region of 3300 - 3400 cm^{-1} and 2850 - 2970 cm^{-1} corresponded to free O-H stretching vibration of the hydroxyl (OH) group and C-H stretching vibration in cellulose molecules, respectively. A weak peak at 1425.63 cm^{-1} is corresponding to $–CH_2$ scissoring of cellulose. The peak of 1370.7 cm^{-1} detected in the wavenumber of 1360 - 1375 cm^{-1} is attributed to C-H asymmetric deformation in the polysaccharide aromatic rings in cellulose and the peak found at 1320.46 cm^{-1} indicates –OH bending vibration of cellulose. Furthermore, the weak peak at 1160 cm^{-1} could be assigned to C-O antisymmetric bridge stretching of cellulose. The sharp peaks at 1032.46 cm^{-1} and 897.34 cm^{-1} are associated with the C-O stretching and the C-H rocking vibrations of the cellulose respectively.

There are five peaks that could be attributed to hemicellulose or lignin. A weak band at 1720.5 cm^{-1} is assigned mainly to the C=O stretching vibration of the carbonyl and acetyl groups in the xylan component of hemicelluloses and in the lignin. The weak band at 1603.33 cm^{-1} was attributed to C=C stretching of lignin. Another weak peak detected at 1506 cm^{-1} was corresponding to C=C stretching of the aromatic ring of lignin. The maximum at 1457.2 cm^{-1} indicated C-H deformation in methyl, methylene and methoxyl groups of lignin. An intense peak at 1241.61 cm^{-1} may correspond to C-O-C stretching in hemicellulose and lignin. It is commonly observed when ether, ester, and phenol groups are present. Apart from that, a weak peak was detected at range of 1645

- 1650 cm^{-1}. It could be attributed to pectin content of OPF or water molecule of OPF.

As for the FTIR spectra of delignified OPF (dOPF), the peaks supposed appear at absorption bands in between 1600 - 1620 cm^{-1}, 1510 - 1560 cm^{-1} and 1430 - 1470 cm^{-1}, which related to lignin content of OPF were absent. Hence, it may prove that delignification process had successfully remove most of the lignin content from the OPF. The appearance of peaks at 1242.9 cm^{-1} and 1731.29 cm^{-1} in the range of 1240 - 1250 cm^{-1} and 1700 - 1740 cm^{-1} respectively indicated that some lignin and hemicellulose still remain on delignified OPF. Since most of the lignin was removed from OPF, this sample tends to have lower thermal degradation temperature as lignin is more thermally stable than holocellulose.

The FTIR spectra of the OPF sample that after chlorination process and alkali-treatment (daOPF) is shown in Figure 4-8. The results showed that all five peaks related to lignin and hemicellulose of natural fibres were successfully removed while the eight peaks related to cellulose are still remained. FTIR spectroscopy analysis was also conducted on commercial grade microcrystalline cellulose powder (MCC). The result showed that cellulose derived from OPF and commercial grade microcrystalline cellulose powder (MCC) have similar pattern on FTIR spectra. In short, delignification and alkali treatment able to remove lignin and hemicellulose of OPF whereby all eight peaks related to cellulose molecules of OPF are remained in all test samples. The intensity of peaks of OPF samples reduced after treated by fibre surface treatment. A better packing of cellulose chains can be made by removal of cementing substances like lignin and hemicellulose.

As shown in Table 4-10 and Figure 4-9, a comparison of the functional groups detected in FTIR analysis between commercial grade (Celluforce) cellulose nanocrystals (NCC_B) and nanocellulose isolated from OPF (NCC_A) was presented. It can be seen that all functional groups related to lignin and hemicellulose were absent for both nanocellulose samples. The broad bands around 3334.23 cm^{-1} and 3330.66 cm^{-1} detected in both NCC_A and NCC_Bsamples could be attributed to -OH group stretching. Both of the samples also showed bands at 2893.06 cm^{-1} and 2891.50 cm^{-1} which can be corresponded to the stretching of CH groups. The peak found at around 1417.80cm^{-1} and 1428.03cm^{-1} respectively indicate the CH_2 scissoring which usually can be found in cellulose compound.

The peaks detected in 1370.1cm^{-1} and 1369.19 cm^{-1} could be attributed to C-H asymmetric deformation of cellulose. Furthermore, OH bending vibration of cellulose was illustrated by the band of 1313.95cm^{-1} in NCC_A and 1315.65cm^{-1} in NCC_B. The peaks detected in the wavenumber range of 1155 – 1163 cm^{-1}, 1033 – 1060 cm^{-1} and 890 – 900 cm^{-1} are related to functional groups that attributed to cellulose of natural fibre.

In conclusion, the FTIR analysis showed that NCC derived from OPF had the similar spectra if compared to the Celluforce NCC sample. Acid hydrolysis does not incur any extra peaks in the FTIR spectra.

Table 4-10: Characteristic bands of FTIR spectra of all OPF samples [60][61] [62] [63][65][66][67] [64][68]

Functional Groups	Component	Wave Number Range (cm^{-1})	rOPF	dOPF	daOPF	MCC	NCC_A	NCC_B
O-H stretching	cellulose	3300-3400	3335.77	3332.89	3338.4	3337.17	3330.66	3334.23
C-H stretching vibrations	cellulose	2850-2970	2915.75	2917.15	2892.3	2895.2	2891.50	2893.06
C=O stretching of acetyl or carboxylic acid	hemicellulose	1700-1740	1720.5	1731.29	N/A	N/A	N/A	N/A
COO, C=C	pectin	1645-1650	1641.5	N/A	1650.5	1647.6	1647.67	1635.15
C=C stretching	lignin	1613	1603.33	N/A	N/A	N/A	N/A	N/A
C=C stretching of the aromatic ring	lignin	1510-1560	1506	N/A	N/A	N/A	N/A	N/A
$O\text{-}CH_3$, C-H asymmetric bending in CH_3	lignin	1430-1470	1457.2	N/A	N/A	N/A	N/A	N/A
$\text{-}CH_2$ scissoring	cellulose	1426-1430	1425.63	1430.2	1421.2	1427.2	1417.80	1428.03
C-H asymmetric deformation, O-H bending vibrations (in plane)	cellulose	1360-1375	1370.7	1371.13	1363.83	1367.6	1370.10	1369.19
CH_2 wagging, -OH bending vibration	cellulose	1317-1343	1320.46	1317	1314.96	1315.25	1313.95	1315.65
C-O-C stretching	Lignin / hemicellulose	1240-1250	1241.61	1242.9	N/A	N/A	N/A	N/A
C-O antisymmetric bridge stretching	cellulose	1155-1163	1160	1161.13	1157.09	1160.09, 1105.05	1161.58	1158.42

C-O stretching and C-O deformation	cellulose	1033-1060	1024	1032.56	1023.72	1054, 1030.6	1047.81	1055.78
C-H stretching, asymmetric, out of phase ring stretching	cellulose	890-900	897.34	897.16	895.36	897	894.88	897.88

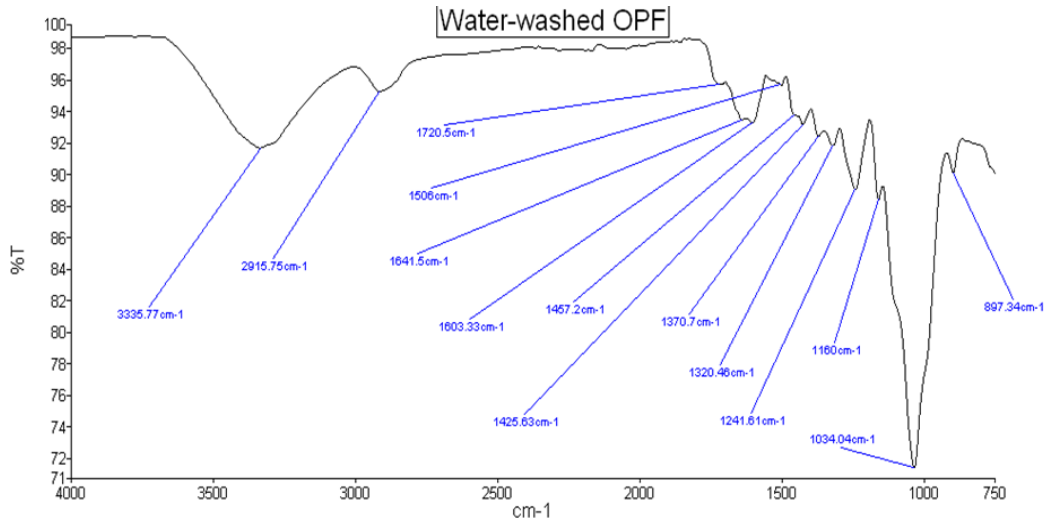

Figure 4-7: FTIR spectra of water-washed OPF

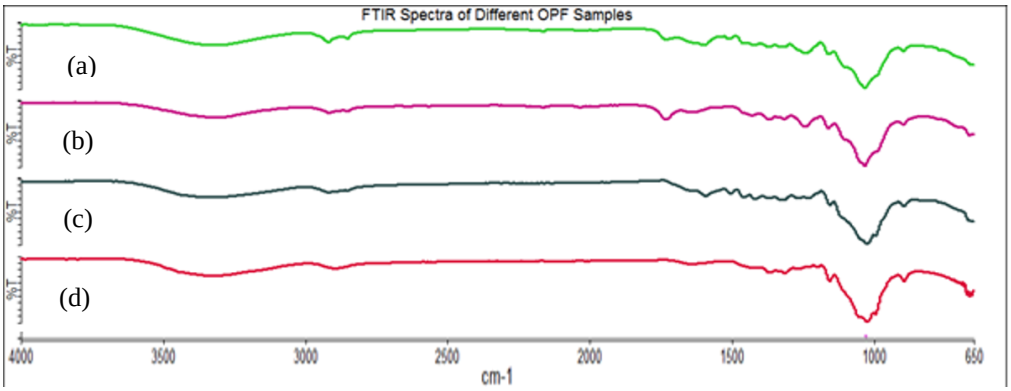

Figure 4-8: FTIR spectra of (a) rOPF, (b) dOPF, (c) daOPF, and (d) MCC

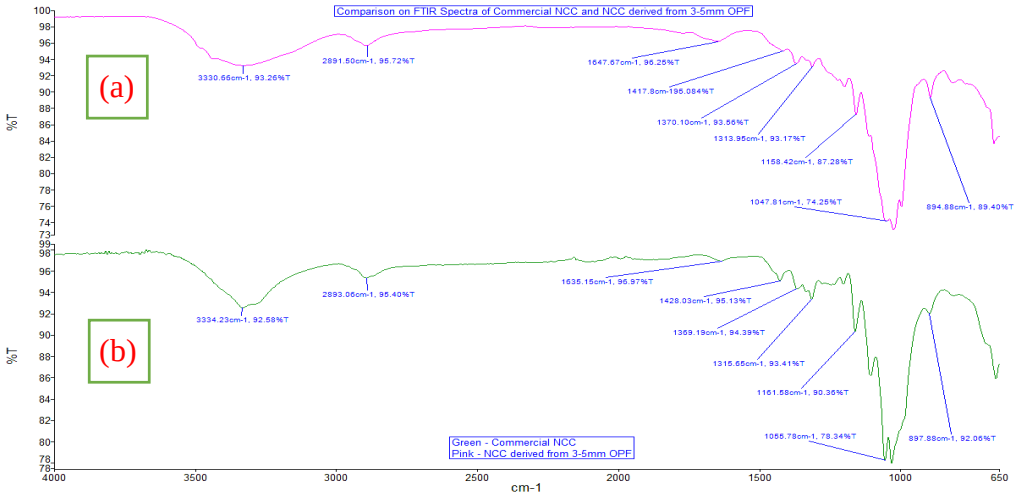

Figure 4-9: FTIR spectra of (a) commercial grade NCC and (b) NCC from OPF

4.2.3.3 Particle Size Measurement

Zeta particle size test is used to determine the particle size of NCC_A and NCC_B. The results were depicted in Figure 4-10, Figure 4-11 and Table 4-11. There is only one peak observed in each sample. It implies that 100% of particles is within the range of 10 – 500 nm. The average particle size of nanocellulose extracted from OPF (NCC_A) is 175.19 nm with standard deviation of 108.03 nm and the average particle size of Celluforce NCC (NCC_B) is 125.42 nm with standard deviation of 50.06 nm. NCC_A has a slightly larger particle size and standard deviation as compared to NCC_B. The particle size measurement could be affected by the direction of diffusion of particles. Stokes-Einstein law for diffusion in solution mentioned that while NCC diffuses horizontally across the aqueous medium against the light source, smaller size interpretation will be reported due to faster detection. Vice versa, bigger size interpretation was found when NCC diffuses vertically across the aqueous medium against the light source, as illustrated in Figure 4-12 [12]. In spite of that, nanocellulose extracted from OPF is still classified as nanomaterials. This finding is tally with the conclusion stated in SEM observation [194].

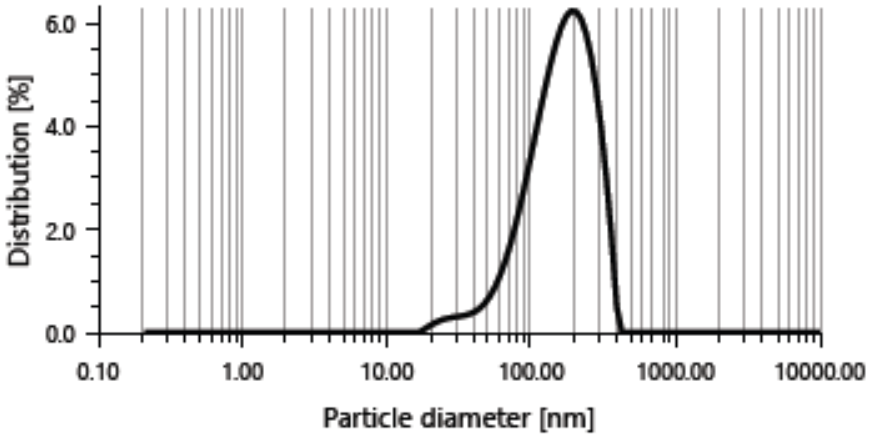

Figure 4-10: Particle size distribution of nanocellulose (NCC_A)

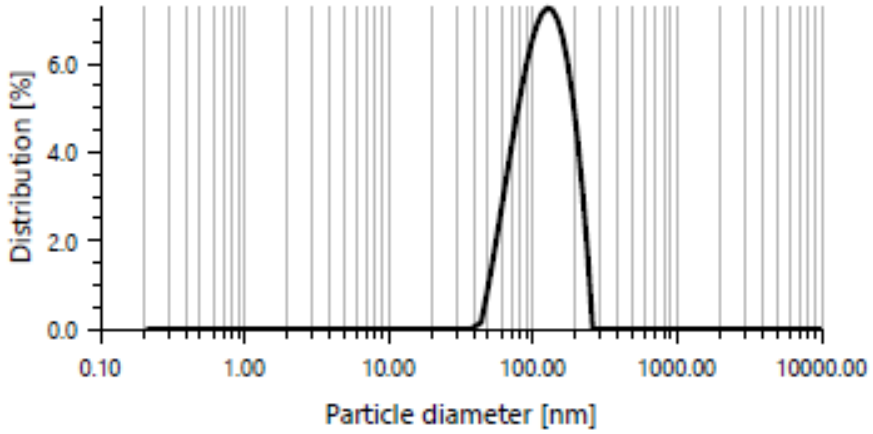

Figure 4-11: Particle size distribution of Celluforce NCC (NCC_B)

Table 4-11: Particle size distribution of nanocellulose samples

Peak name	Size (nm)	Area (%)	Standard deviation (nm)
NCC_A	175.19	100.00	108.03
NCC_B	125.42	100.00	50.06

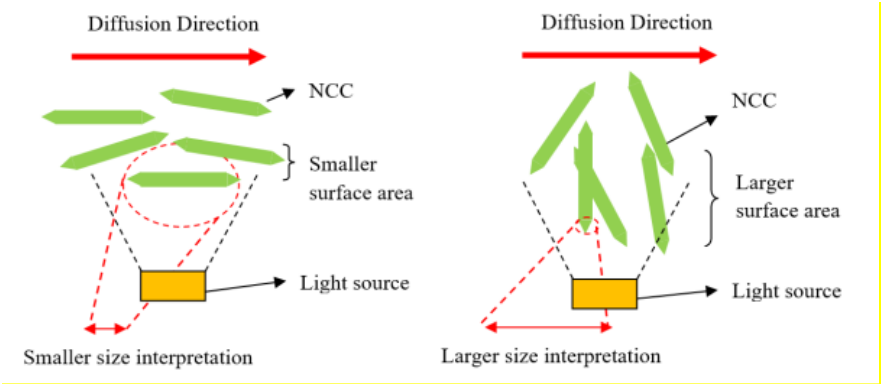

Figure 4-12 Effect of surface area in the direction of diffusion for interpretation of the size [195]

4.2.4 Summary

Nanocellulose was successfully extracted from oil palm fibre. Sodium hypochlorite (NaClO) was used to replace sodium chlorite ($NaClO_2$) due to cost saving and potential industrial application.

According to literature review in *Section 2.5*, OPF should contain 41 – 65% of cellulose, 17.1 – 33.9 % of hemicellulose and 13.2 – 25.31% of lignin theoretically [10][48][49][50]. However, through the actual practices in this research, it was found that only 20.8% of OPF (cellulose) was remained after delignification and alkali treatment. The remaining of OPF (nanocellulose) further decrease to approximately 10% after acid hydrolysis and dialysis processes. It indicates that 1 gram of NCC can be derived from 10 grams of raw OPF by using optimum process parameters. The low yield could be attributed

to filtration system and tools. Some of the nanocellulose are lost during filtration process.

Fourier Transform Infrared Spectrometry (FTIR) analysis, Scanning Electron Microscopy (SEM) and particle size measurements verified the morphological properties and chemical composition of nanocellulose extracted from OPF. The properties of nanocellulose extracted from OPF is similar to the commercial grade cellulose nanocrystals (Celluforce NCC).

Even though the synthesis cost of nanocellulose was reduced, the isolation of nanocellulose from OPF is still time-consuming. It took 5 working days to synthesize 3 grams of NCC in lab and hence it is not practical to synthesize nanocellulose for fabrication of ABS composites. Hence, it was suggested that the commercial grade Celluforce NCC could be used for fabricating NCC/ABS composites.

4.3 Tensile Test

4.3.1 The effect of chemically treated oil palm fibre on the tensile properties of ABS Composites

Various types of chemically treated oil palm fibre were incorporated into ABS in order to enhance the tensile properties of ABS composites. The amount of OPF was set at 20 wt.% as an excessive content of fillers can tend to have counterproductive outcomes.

A comparison between ultimate tensile strength (UTS) of different oil palm fibres filled acrylonitrile butadiene styrene composites was shown in Figure 4-13 and Table 4-12. The ultimate tensile strength of neat acrylonitrile butadiene styrene (CONTROL) is 33.24 MPa. After adding 20 wt.% of water-washed oil palm fibre (rOPF) into acrylonitrile butadiene styrene matrix, the ultimate tensile strength of water-washed oil palm fibres filled acrylonitrile butadiene styrene composites (20rOPFGP) is reduced to 21.92 MPa. The properties reduction is 34% as compared to CONTROL sample. It showed that water-washed OPF mainly act as filler and unable to reinforce ABS without any chemical treatment or coupling agents. It could be attributed to weak interfacial bonding between water-washed OPF and ABS resin.

Oil Palm Fibre Surface Pre-treatment was used enhance the adhesion strength between the surface interface of hygroscopic OPF with hydrophobic ABS matrix. The detailed procedure was described in *Section 3.2.1*. The tensile test result showed that alkali-treated OPF (aOPF) able to improve tensile properties of OPF/ABS composites as compared to water-washed oil palm fibres. The alkali treatment helps to improve interfacial bonding between oil palm fibres and acrylonitrile butadiene styrene. The ultimate tensile strength of 20aOPFGP was measured at 25.97 MPa, an increase of 4 MPa compared to 20rOPFGP. Alkali treatment capable of removing portion of hemicellulose and lignin from oil palm fibre, hence it increases the tensile strength of oil palm fibre as cellulose has much higher strength compared to hemicellulose and lignin.

Furthermore, alkali treatment makes the fibre surface rougher, which facilitated the interfacial bonding between natural fibre and matrix.

The study employed two primary types of coupling agents: maleic anhydride and silane (3-(trimethoxysilyl) - propyl methacrylate). Detailed explanations of maleic treatment and silane treatment can be found in *Section 3.2.2 and 3.2.3*, respectively.

The ultimate tensile strength (UTS) of maleic-treated OPF/ABS composites (10maOPFGP, 20maOPFGP, and 30maOPFGP) exhibited an elevation to around 33 – 34 MPa, showcasing a close similarity to the UTS of the control sample. Furthermore, this represents an increase of approximately 27.53% to 31% when compared to the alkali-treated OPF/ABS composite (20aOPFGP). The ultimate tensile strengths (UTS) of 10maOPFGP, 20maOPFGP, and 30maOPFGP exhibit similarity. This suggests that augmenting the concentration of maleic anhydride solution does not yield additional enhancements in the tensile strength of ABS composites. It can be inferred that a concentration of 20 wt. % maleic solutions is satisfactory for treating OPF.

Dicumyl peroxide (DCP) was expected to function as a free radical initiator, enhancing the bonding between maleic-treated OPF and the ABS matrix. Nevertheless, the introduction of dicumyl peroxide (DCP) into OPF/ABS compounds resulted in an unforeseen detrimental outcome. The tensile strength of 10mcaOPFGP reduced to 22.77 MPa. his decline could be attributed to an excessive amount of DCP, which appears to have compromised the properties of the OPF/ABS composites [83][107][108].

On the other hand, the outcomes of the tensile tests for 1saOPFGP, 3saOPFGP and 5saOPFGP indicated that 3-(trimethoxysilyl)-propyl methacrylate (MPS) capable of further enhancing the UTS of alkali-treated OPF/ABS composites. The alkali-treated OPF that was subsequently treated with a 3 wt.% silane solution exhibited the highest tensile strength among all silane-treated OPF/ABS composites. The ultimate tensile strength (UTS) of 3saOPFGP measures 33.58 MPa, demonstrating a resemblance to the control sample [10][51].

The SEM images illustrated in Figure 4-14 showed that clearer location of voids (red circle) left after tensile test. It could be attributed to the consequence of fibre pull-out during tensile test. This failure is consequence of weak bonding between OPF and ABS. hence affecting the tensile properties of the composites. The existence of clearance between oil palm fibres (green circle) and acrylonitrile butadiene styrene signifies reduced reinforcement efficiency. In order to ensure effective stress transfer from polymer matrix to oil palm fibres, such gap / void should be eliminated to enhance interfacial bonding of oil palm fibres and polymer. As illustrated in Figure 4-14 (d) and (e), application of coupling agents able to minimise the gaps existed at the interface of OPF and ABS.

In short, the tensile test results show that chemically treated oil palm fibre filled acrylonitrile butadiene styrene composites attained enhancement in tensile strength as compared to untreated counterpart. Maleic-treated OPF and silane-treated OPF are capable of marginally improving the mechanical properties of the composites. The optimum concentration of maleic anhydride treatment and silane treatment were justified.

Table 4-12: Tensile properties of various OPF/ABS composites

Sample No.	Short Form	Ultimate Tensile Strength / MPa	Elongation / %	Elastic Modulus / GPa
1	CONTROL	33.24	1.73	2.09
2	20rOPFGP	21.92	1.85	2.51
3	20aOPFGP	25.97	1.76	2.14
4	10maOPFGP	33.12	1.45	3.2
5	20maOPFGP	34.03	2.2	1.93
6	30maOPFGP	33.67	4.84	1.08
7	10mcaOPFGP	22.77	1.22	2.55
8	1saOPFGP	30.3	1.57	2.69
9	3saOPFGP	33.58	5.18	1.08
10	5saOPFGP	32.16	4.83	1.06

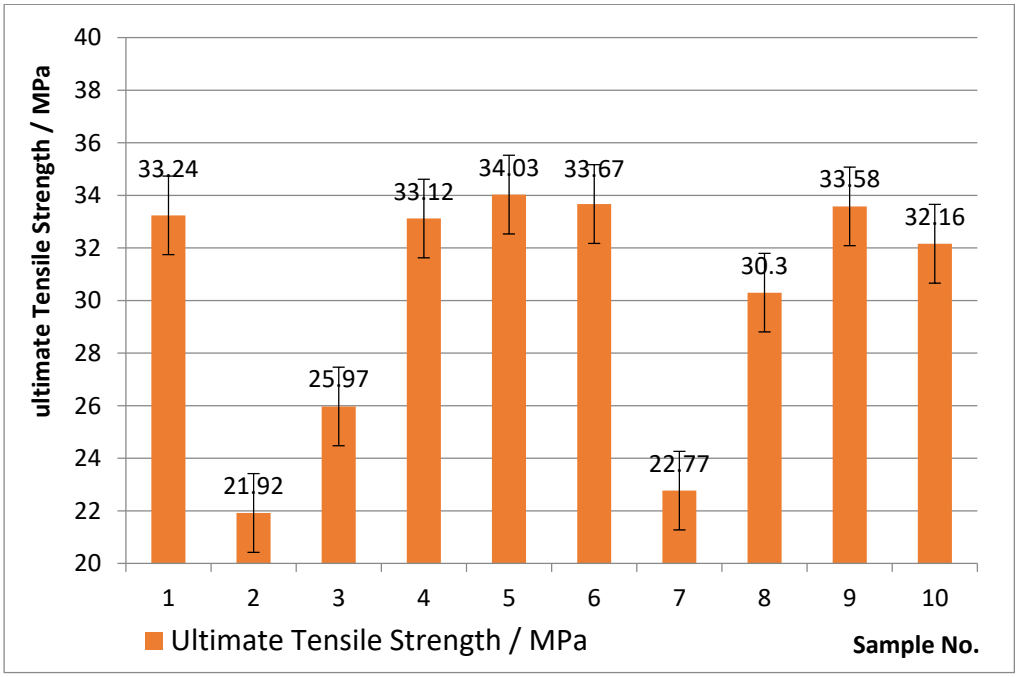

Figure 4-13: Ultimate tensile strength of different OPF/ABS composites

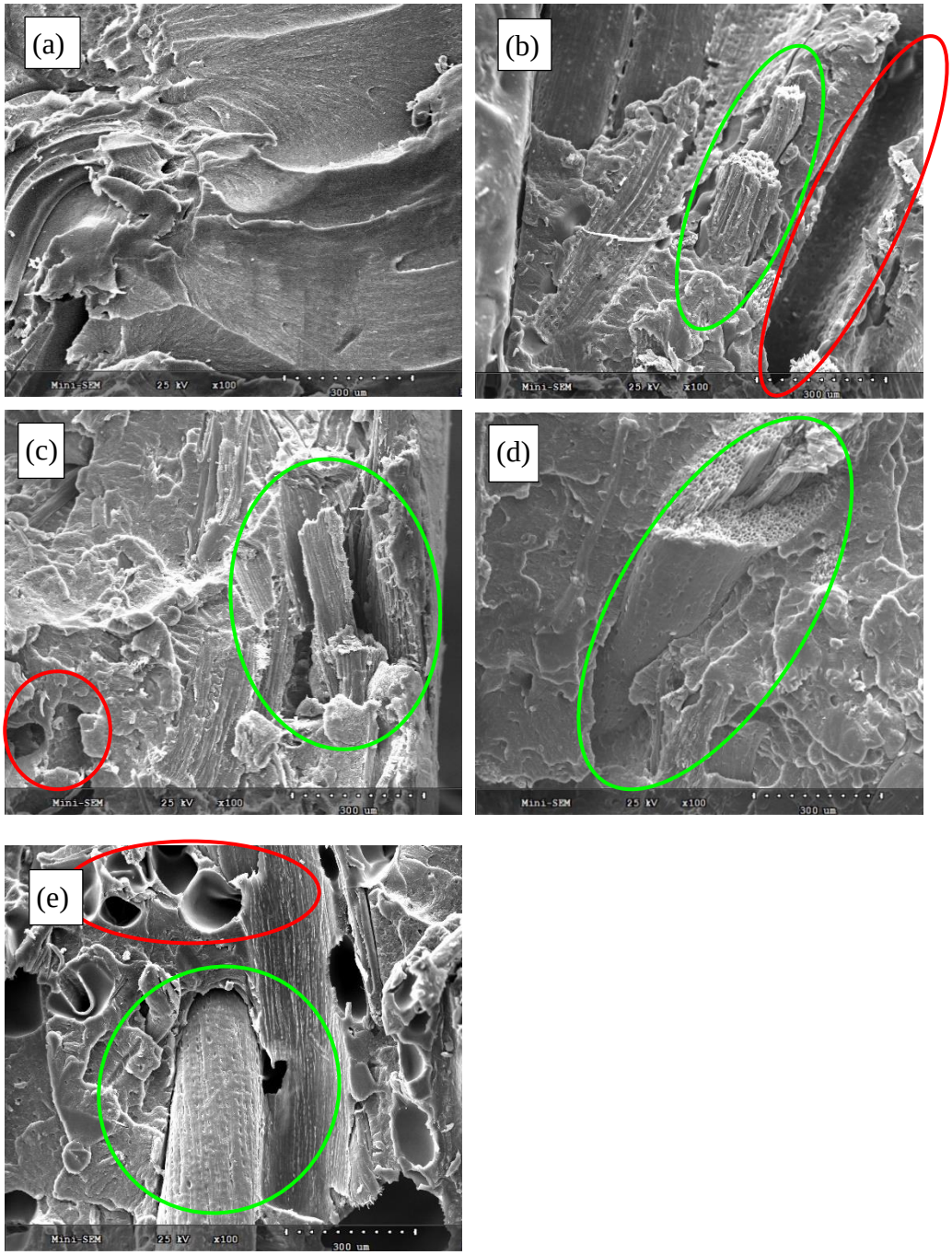

Figure 4-14: SEM images of fracture surface of (a) CONTROL, (b) 20rOPFGP, (c) 20aOPFGP, (d) 20maOPFGP and (e) 3saOPFGP at magnification of 100X

4.3.2 The effect of nanocellulose on the tensile properties of ABS Composites

1 wt. % to 10 wt. % of various NCC were melt-blended into ABS matrix to study the effects of nanocellouse and coupling agents (maleic anhydride and silane) on the tensile properties of NCC/ABS Composites. The tensile test result was tabulated in Table 4-13. It was observed that the incorporation of 3 wt. %

of untreated NCC into ABS composites led to a 6.53% improvement in the Ultimate Tensile Strength (UTS) of NCC/ABS composites. Increasing the filler loading beyond this amount did not result in any further increase in the UTS value. Conversely, excess amount of NCC loading led to adverse effects. Addition of 5 wt. %, 7 wt. % and 10 wt. % of NCC into ABS composites could deteriorate UTS by 2.59 %, 8.66 % and 17.33% respectively. As depicted in Figure 4-15, NCC particles were evenly dispersed and aligned within ABS matrix, it acted as reinforcing agent due to its exceptional properties. Furthermore, the even distribution of NCC throughout the matrix contributed to the more efficient distribution of applied loads, thereby preventing premature failure [126][127][128][196][197].

The results of the tensile test also provided evidence that coupling agents have the capability to further improve the tensile properties of NCC/ABS composites. Addition of 5 wt. % maleic-treated NCC into ABS matrix resulted in a recorded UTS value of 36.62 MPa. This implied that maleic anhydride able to facilitate stronger adhesion at the interface between NCC and ABS by promoting chemical bonds with polar functional groups on the surface of both fillers and matrix. Coupling agent also helps to avoid NCC particles agglomeration by increasing wettability of NCC. On the other hand, with reference to the TGA analysis result stated in *section 4.4.1*, maleic-treated NCC contains approximately 20 – 25 % maleic anhydride. Consequently, the effective NCC content in the NCC_B sample accounts for roughly 75 – 80 % of total weight of NCC_B. The optimum NCC loading of NCC is 3.75 wt. – 4 wt.%.

The tensile test result in this study revealed that silane treatment has the potential to further improve UTS of NCC/ABS Composites. Among all the test samples, the addition of 3 wt. % silane-treated NCC into the ABS matrix yielded the most significant improvement in Ultimate Tensile Strength (UTS). The test sample which labelled as 03saNCC97ABS achieved a UTS value of 37.22 MPa, representing an 11.97% improvement compared to pure ABS. Silane is unique in that it possesses both hydrophobic and hydrophilic functional groups. This dual nature enables silane to establish chemical bonds with both the hydrophilic NCC and hydrophobic ABS and consequently improving interfacial strength and reinforcing efficiency [98].

In summary, tensile test result showed that NCC able to improve tensile properties of acrylonitrile butadiene styrene composites. The optimum filler loading is 3 wt.%. An excessive amount of NCC loading resulted in adverse effects.

Table 4-13: Tensile properties of various NCC/ABS composites

Sample No.	Short Form	Ultimate Tensile Strength / MPa	Increment in UTS (%)
1	100GP	31.38	-
2	01NCC99GP	35	5.29

3	03NCC97GP	35.41	6.53
4	05NCC95 GP	32.38	-2.59
5	07NCC93GP	30.36	-8.66
6	10NCC90 GP	27.48	-17.33
7	01mNCC99 GP	32.65	-1.77
8	03mNCC97 GP	34.91	5.02
9	05mNCC95 GP	36.62	10.17
10	07mNCC93 GP	33.59	1.05
11	10mNCC90 GP	31.53	-5.14
12	01sNCC99 GP	33.83	1.77
13	03sNCC97 GP	37.22	11.97
14	05sNCC95 GP	36.02	8.36
15	07sNCC93 GP	33.82	1.74
16	10sNCC90 GP	32.72	-1.56

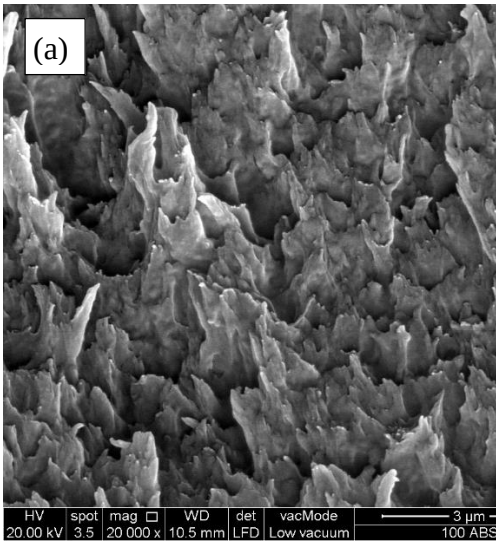

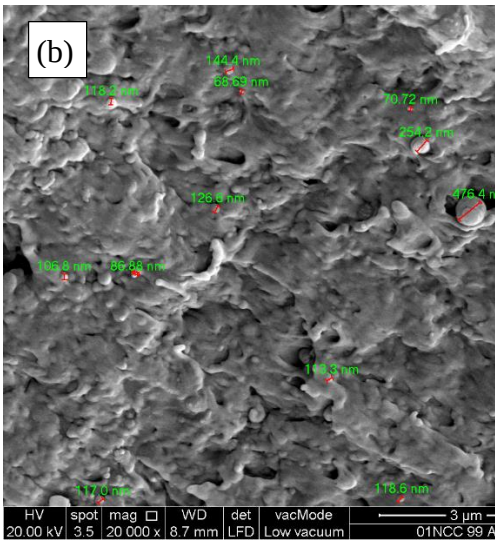

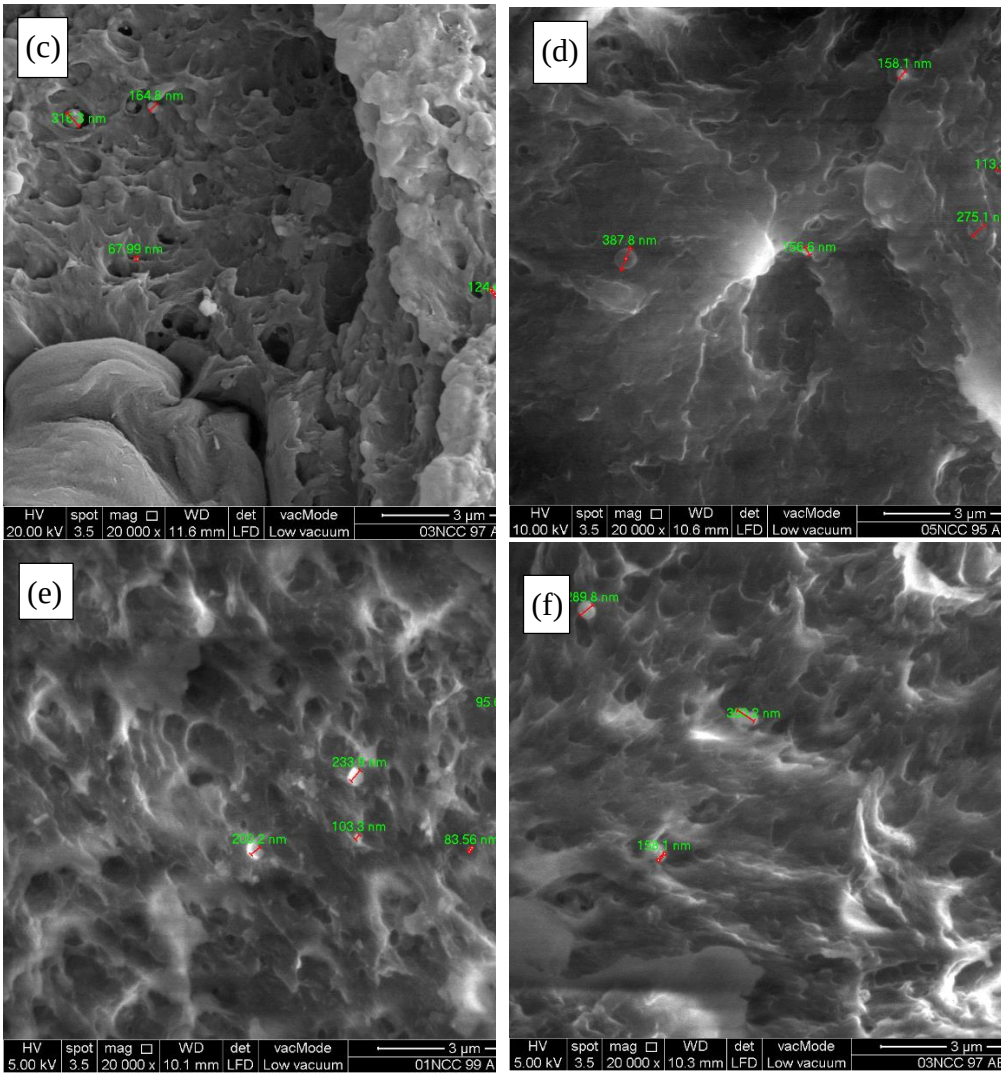

Figure 4-15: SEM images of fracture surface of (a) CONTROL, (b) 01NCC99GP, (c) 03NCC97GP, (d) 05NCC95GP, (e) 07NCC93GP and (f) 10NCC90GP at magnification of 20000X

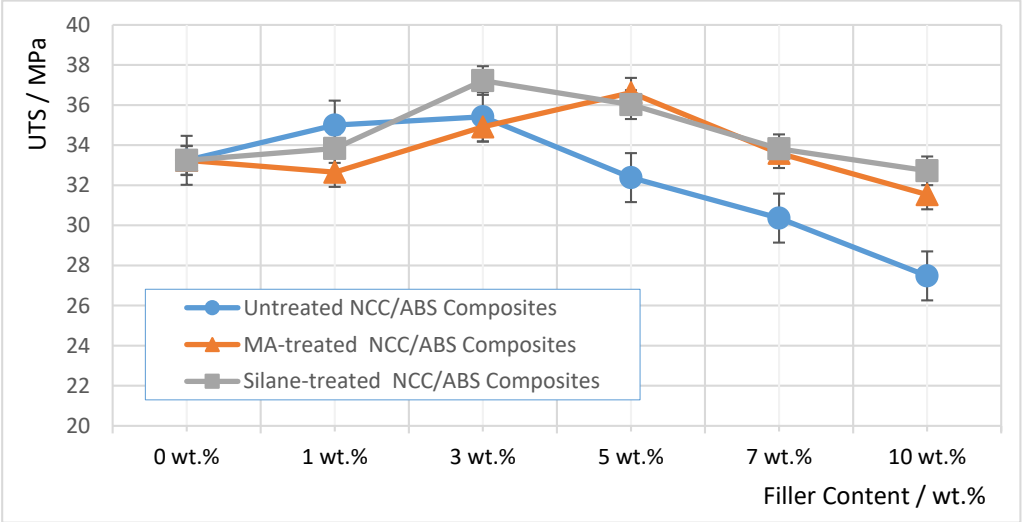

Figure 4-16: Ultimate tensile strength of different NCC/ABS composites

4.3.3 The effect of flame retardants on the tensile properties of ABS Composites

15 wt.% of flame retardants were incorporated into OPF/ABS composites and their effects on the tensile properties of OPF/ABS composites were studied. As summarised in Table 4-14 and Figure 4-17, The ultimate tensile strength of OPF/ABS composite (20OPF80GP) is 24.90 MPa. It can be noted that the tensile properties of OPF/ABS composites were further reduced to approximately 19.91 MPa – 23.39 MPa after adding 15 wt.% of flame retardants. The properties reduction is unrelated to the varieties of flame retardants. The applied tensile load did not transfer from the matrix to the fillers, causing the flame retardants to act as stress concentration points and making them prone to micro-crack formation [177][178][6] [185].

As depicted in Figure 4-18 (a), the fracture surface of neat ABS (100GP) is smooth, as no fillers were incorporated into ABS. However, when OPF and flame retardants were added to ABS composites, the fracture surface became rough, displaying visible folds and irregularities. Fibre pull-out (green circle) and voids left due to particle pull-out (red circle) were observed in OPF/ABS samples. It indicated that the tensile properties of test samples were damaged due to weak interfacial bonding between fillers (OPF and flame retardants) and matrix (ABS). Even though the OPF and flame retardants are well dispersed within ABS matrix, the fillers are unable to reinforce ABS composites but could deteriorate the properties of ABS composites [185].

In conclusion, the tensile properties of OPF/ABS composites are compromised after adding 15 wt.% flame retardants into OPF/ABS composites. The UTS of samples were reduced by 6 – 20%. SEM images of test samples exhibits the failure mechanism of the OPF/ABS composites

Table 4-14: Tensile properties of various OPF/ABS composites containing 15wt.% flame retardants

Sample No.	Short Form	Ultimate Tensile Strength / MPa	Changes in UTS as compared to 100GP (%)	Changes in UTS as compared to 20aOPFGP (%)
1.	100GP	33.24	-	-
2.	20aOPFGP	24.90	-25.09	-
3.	15APP20OPF65GP	18.98	-42.90	-23.78
4.	15ATH20OPF65GP	19.92	-40.07	-20.00
5.	15ZB20OPF65GP	20.94	-37.00	-15.90

6.	10APP05ATH20OPF65GP	21.13	-36.43	-15.14
7.	10APP05ZB20OPF65GP	22.19	-33.24	-10.88
8.	05APP10ATH20OPF65GP	23.39	-29.63	-6.06
9.	10ATH05ZB20OPF65GP	20.74	-37.61	-16.71
10.	05APP10ZB20OPF65GP	19.91	-40.10	-20.04
11.	05ATH10ZB20OPF65GP	23.20	-30.20	-6.83

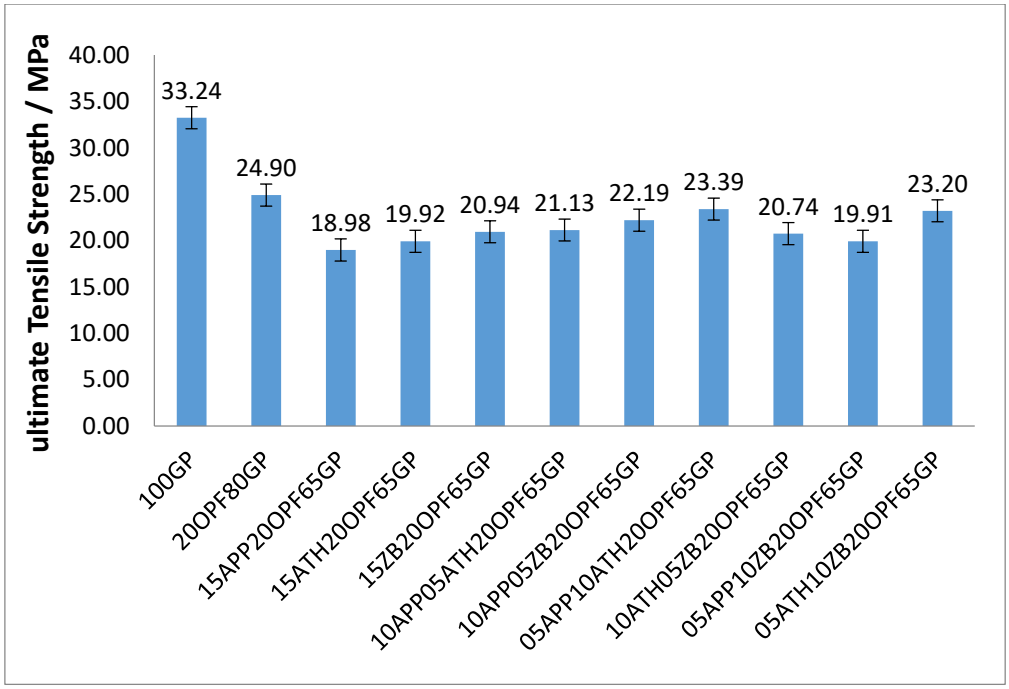

Figure 4-17: Ultimate tensile strength of different OPF/ABS composites containing 15wt. % flame retardants

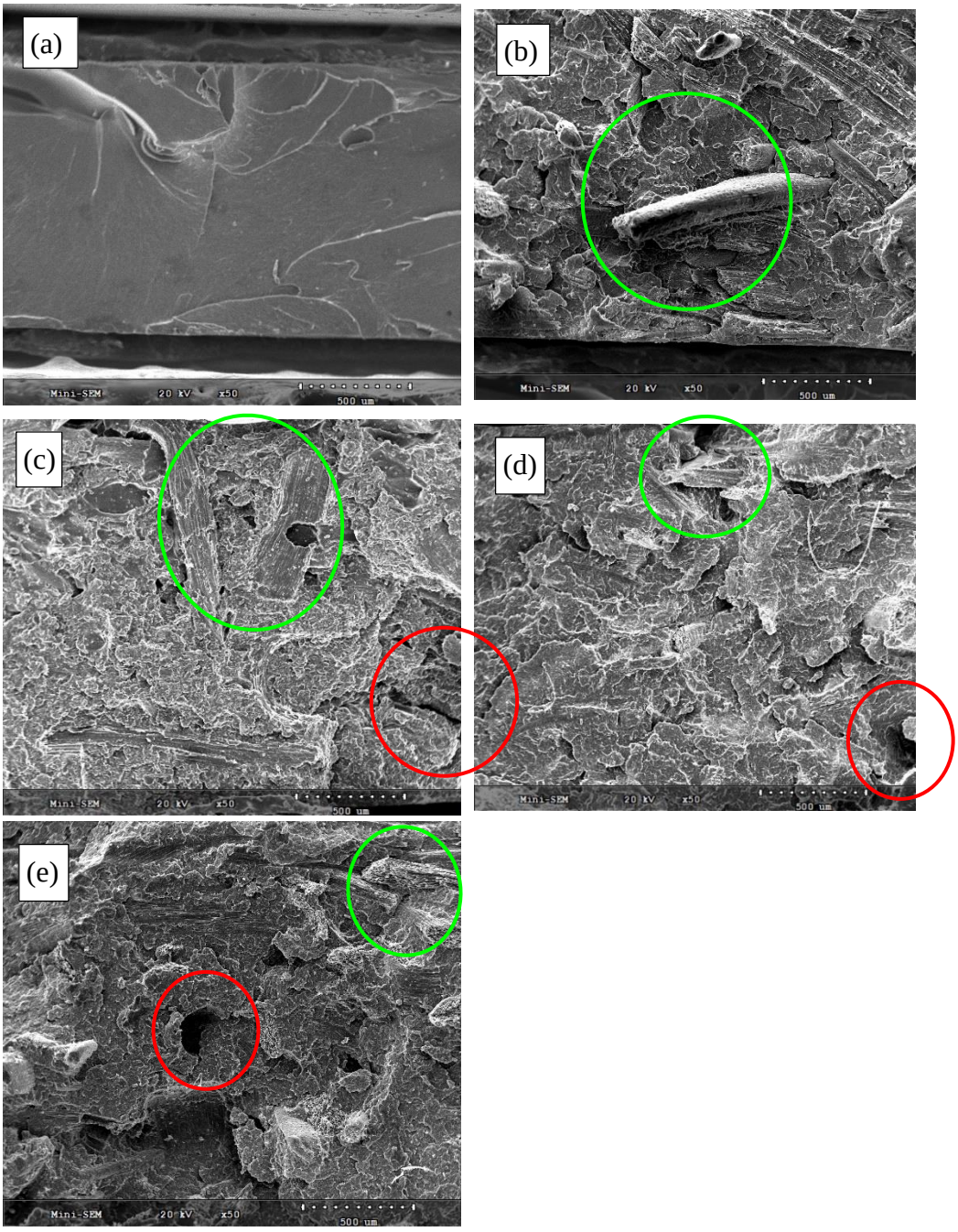

Figure 4-18: SEM Images of Fracture Surface of (a) 100GP, (b) 20OPF80GP, (c)15APP20OPF65GP, (d) 15ATH20OPF65GP and (e) 15ZB20OPF65GP at magnification of 50X

4.4 Thermal gravimetric Analysis (TGA)

4.4.1 TGA/DTG Analysis of Treated Oil Palm Fibres

Thermogravimetric analysis was conducted to determine the thermal degradation temperature of various test samples. The TGA result could be affected by the sample preparation method, heating rate, controlled atmosphere and gas flow rate of the TGA. Higher heating rate during pyrolysis may shift chemical reaction steps of test samples to higher temperatures. Different atmosphere may lead to different pyrolysis behaviour.

The thermogravimetric analysis (TGA) and differential thermogravimetry (DTG) result of various chemically treated OPF samples were summarised in Table 4-15. Thermogravimetric Curves and differentiate thermogravimetric (DTG) curves of various chemically treated OPF Samples were exhibited in Figure 4-19 and Figure 4-20 respectively.

Figure 4-20 exhibited differentiate thermogravimetric (DTG) curves of various OPF samples. As seen in Figure 4-20, the first peak was observed in all samples at the temperature range of 35 – 130 °C in DTG curves. Approximately 2 - 7 % of weight loss were detected and it can be attributed to moisture evaporation. The maximum mass loss rate in this stage mainly occurred at temperature range between 60 – 75 °C.

A shoulder peak had been found in the DTG curves of rOPF, dOPF, aOPF, maOPF and saOPF at the temperature range of 170 – 320 °C, where this region represents thermal decomposition of hemicellulose. The onset decomposition temperatures of hemicellulose were tabulated in Table 4-15. Water-washed oil palm fibre (rOPF) has onset degradation temperature of 260°C. A weight loss of approximately 25.27 % was observed in temperature range 220 - 330°C. The high onset degradation temperature of rOPF was attributed to lignin content. The complex and highly cross-linked structure of lignin makes it more resistant to thermal decomposition than holocelluloses. Holocelluloses contain polysaccharides that are more susceptible to degradation at elevated temperatures [53][54].

Delignified OPF (dOPF) was found having the lowest onset temperature (180 °C) among all OPF samples, with 22.1 % weight loss in the temperature range of 170 – 300 °C. The removal of lignin could be considered as the contributing factor for the decrement of onset decomposition temperature. Attributed to various oxygen functional groups in its structure, lignin is more thermally stable compared to hemicellulose and cellulose and hence it could help to increase the decomposition temperature of natural fibres. Without the protection of lignin, OPF tend to degrade at lower temperature [53][54][56].

In addition, it can be observed that the onset degradation temperature of alkali-treated OPF (aOPF) took place around 250°C with approximately 22.96 %weight loss in the temperature range of 220 – 320 °C. The slight difference in onset degradation temperature as compared to untreated OPF showed that alkali treatment did not impose signification influence towards the thermal properties of OPF. This implicated that alkali treatment is less effective in the removal of lignin and hemicellulose from untreated OPF.

Moreover, alkali-treated OPFs were then treated by maleic anhydride treatment and silane treatment respectively. The OPF samples denoted as maOPF and saOPF. Both maOPF and saOPF have similar onset degradation temperature as compared to aOPF. It indicated that maleic anhydride and silane did not significantly affect the thermal properties of OPF. However, a shoulder peak was found at temperature range of 185 – 225 °C in the DTG curve of maOPF and resulted in a weight loss of 2.36 %. It is believed that vaporisation

of maleic anhydride occurred in this range. As compared with untreated NCC sample (NCC_B), a distinct peak was found at the DTG curves of sample (maNCC) at temperature of 152.27 °C, the maleic-treated NCC experienced 22.16 % of weight loss at the temperature range of 130 – 200 °C. it could be attributed to the decomposition of maleic anhydride.

The DTG curves of rOPF, dOPF, aOPF, maOPF, saOPF and NCC_B, maNCC and saNCC also exhibited a distinct peak at temperature range between 300 – 400 °C and recorded weight loss ranging from of 41 – 64 %. It is attributed to the high thermal decomposition rate of cellulose within this narrow temperature range.

The TGA and DTG result are unsuitable for determination of the decomposition temperature for lignin as lignin decomposes over a wide temperature range and often overlapped with the decomposition temperature range of hemicellulose and cellulose. However, it is generally agreed that the gently sloping tail after 400°C, as shown in Figure 4-19 and Figure 4-20 can be attributed to the decomposition of lignin [60].

In conclusion, NCC samples showed the highest onset decomposition temperature among all samples due to the absence of hemicellulose. Hemicellulose is a complex, branched and heterogeneous polymeric network. It has lower degree of polymerization compared to α-cellulose. Hemicellulose is highly hydrophilic and susceptible to biological and thermal degradation. It can be hydrolysed by dilute acids and bases easily. Hemicelluloses start to degrade at temperature range between 200-260 °C and evolve non-combustible gases and tar during pyrolysis. Therefore, the presence of hemicelluloses results in a lower onset temperature for decomposition. [11] [59].

OPF surface pre-treatment and use of coupling agents are ineffective in the removal of hemicellulose, hence the recorded onset decomposition temperature of the treated OPF was not much higher than the untreated OPF.

Table 4-15: Thermogravimetric analysis result of various chemically treated OPF samples

Sample Name	Onset Temp. / °C	Weight loss of hemicellulose / %	2^{nd} Distinct Peak / °C	Weight loss of cellulose / %	Residue @ 685 °C
rOPF	260	25.27	370	41.25	16.74
dOPF	180	22.1	340	43.23	18.36
aOPF	250	22.96	365	44.05	18.71
maOPF	240	16.26	345	41.9	24.16
saOPF	255	20.09	360	45.08	17.76
NCC_B	298.52	-	307.19	63.43	23.58

maNCC	293.98	-	305.16	46.98	16.39
saNCC	295.49	-	304.84	62	21.61

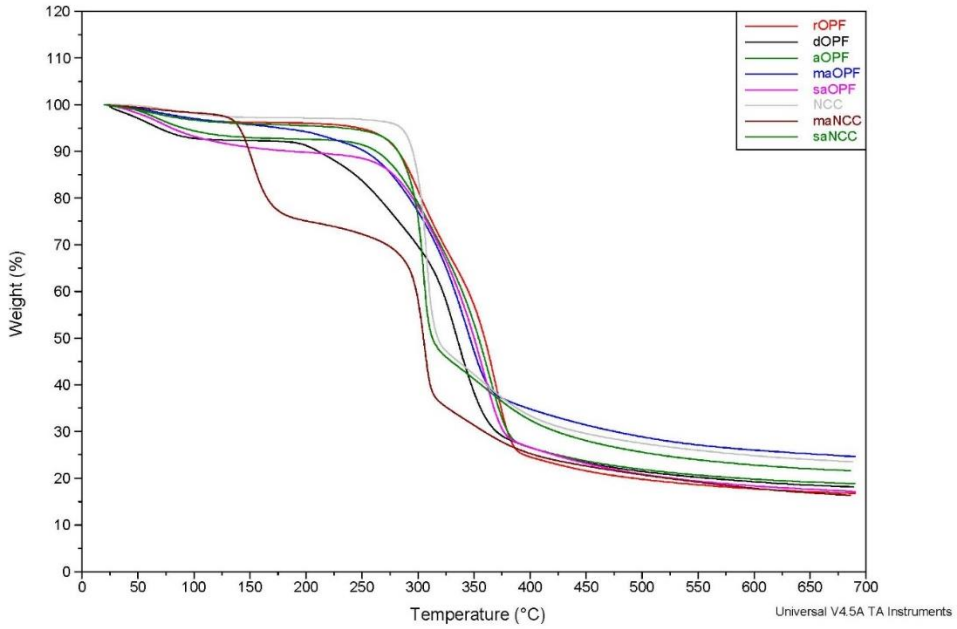

Figure 4-19: Thermogravimetric curves of various chemically treated OPF Samples

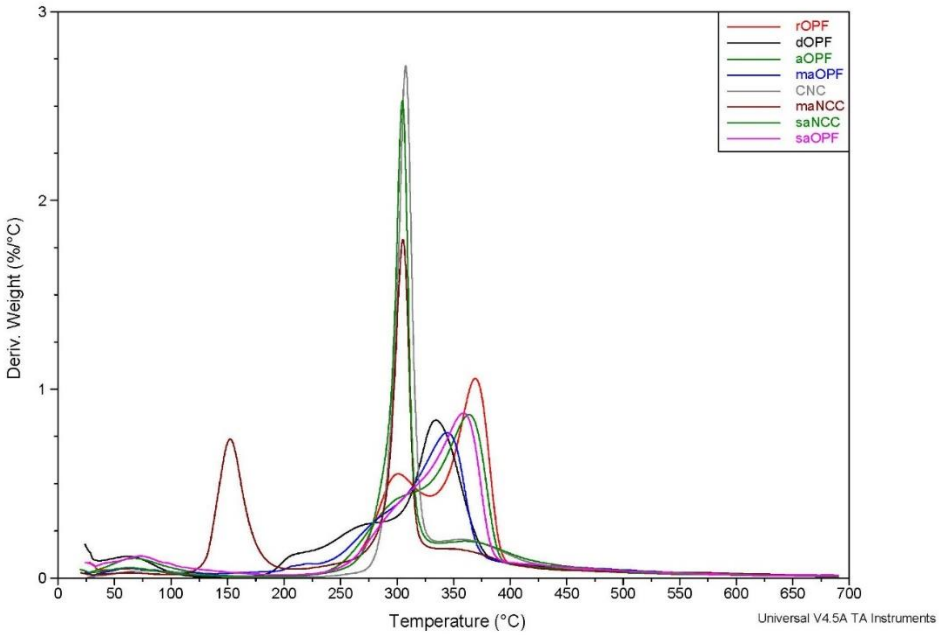

Figure 4-20: Differentiate thermogravimetric (DTG) of various chemically treated OPF samples

4.4.2 TGA/DTG Analysis of Flame Retardants

Thermal gravimetric analysis was conducted on the flame retardants (APP, ATH, ZB and EG) used in this study to evaluate the thermal stability of

FRs. The results are presented in Table 4-16 and illustrated in Figure 4-21 and Figure 4-22. The onset degradation temperature of APP is 336.58 °C. APP start to degrade into polyphosphoric acid, which can catalyse the dehydration reaction of polymers to yield char residues. The char layer will act as a protective barrier to prevent the further spread of flames and thus improve the fire resistance of the material. The maximum mass loss rate for APP occurred at 381.57 °C. it resulted a weight loss of approximately 15.13 %. At temperature of 685 °C, it was realised that 54.5 % of weight are remained as residue. The residue able to form char layer and contribute to fire resistance properties by surpressing the burning [164] [165][166][167][198].

TGA curve of alumina trihydrate (ATH) indicated that ATH begins to decompose gradually at temperature of approximately 258.11 °C. This decomposition involves the release of water molecules through an endothermic reaction. The release of water at a relatively lower temperature suggests that ATH acts as an effective hydrate flame retardant within the temperature range of 200 °C to 350 °C. Moreover, ATH left a significant amount (65.26 % residue) of aluminium oxide as protective layer [161] [162] [163].

TGA result indicated that EG initiates the expansion at 222.07 °C, and the maximum mass loss rate happened at 240.44 °C. These findings align with the heating experiment results presented in *Section 3.1*. This suggests that there is a possibility of expandable graphite (EG) beginning to expand during the melt compounding process of OPF/ABS composites. This phenomenon could potentially influence the effectiveness of EG as a flame retardant. It is noteworthy that EG loses approximately 67.27% of its mass when subjected to heating up to 400 °C. The observed noise in the DTG curve of expandable graphite may be attributed to the spontaneous expansion of EG during the heating process [171] [172] [173].

Refer to Figure 4-21, The TGA curves exhibits that ZB able to retain its hydration water up to 350 °C and the onset degradation temperature of ZB is 358.21 °C. This means that processing temperature (220 °C) of OPF/ABS composites does not adversely affect the effectiveness of ZB. The residue of ZB at 685 °C is 85.72 %. It showed that ZB able to form char layer to supress the combustion [168][169][199].

In summary, ammonium polyphosphate (APP) and zinc borate (ZB) are relatively stable during melt compounding of OPF/ABS composites as their flame-retardant mechanisms start to become active at higher temperatures (300 °C). Alumina trihydrate (ATH) and expandable graphite (EG) have low onset decomposition temperature, typically within the range of 220 °C to 260 °C. This means that there is a possibility that they may start to decompose during melt blending of OPF/ABS composites and subsequently affect their fire resistance during burn test.

Table 4-16: Thermogravimetric Analysis Result of Flame Retardants

Sample Name	Onset Temp. / °C	Weight loss / %	1st Distinct Peak / °C	Temperature range	Residue @ 685 °C
APP	336.58	15.13	381.57	200 - 450	54.5 %
ATH	258.11	34.58	286.08	100 - 685	65.26 %
ZB	358.21	12.47	367.88	200 - 450	85.72 %
EG	222.07	69.27	240.44	200 - 400	29.83 %

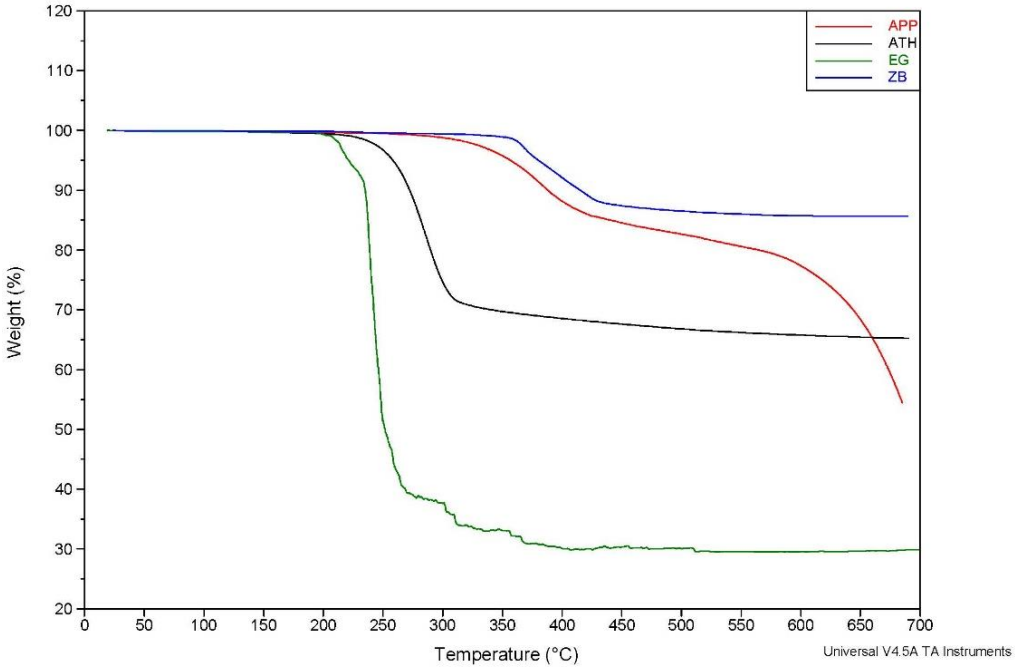

Figure 4-21: Thermogravimetric curves of various flame retardants

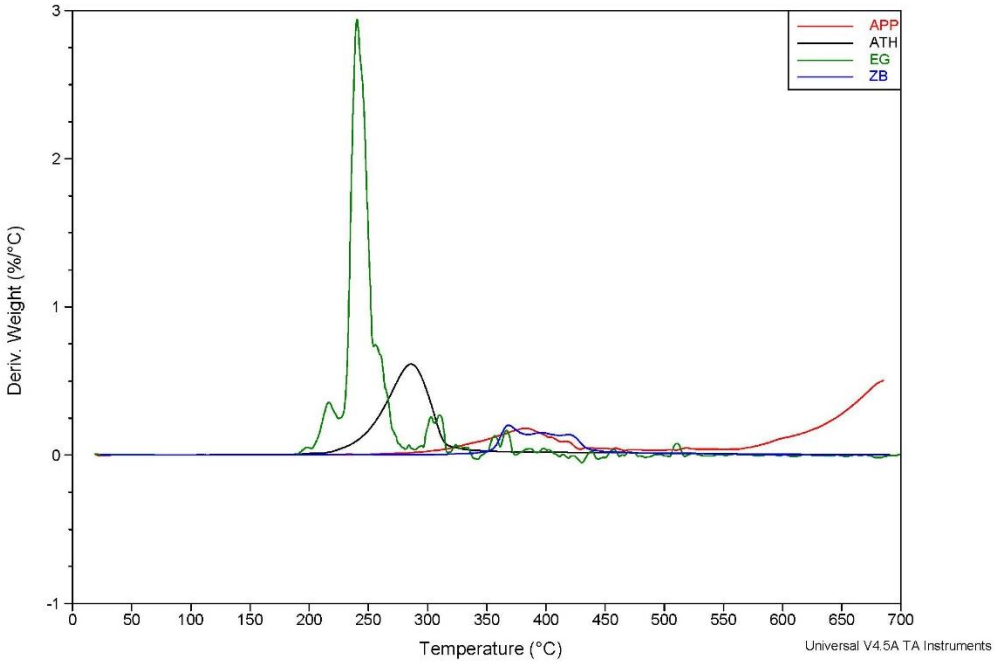

Figure 4-22: Differentiate thermogravimetric (DTG) of various flame retardants

4.4.3 TGA/DTG Analysis of ABS Composites

Thermal gravimetric analysis was conducted on the various flame retardants (FRs) filled Acrylonitrile Butadiene Styrene (ABS) composites. The results are tabulated in Table 4-17 and reveal distinct thermal degradation profiles and constituent phases for each sample.

The TGA data for the 100GP shows two primary stages of thermal degradation. The first stage occurs between 380 and 450 °C and results in a weight loss of 57.76 % with a peak temperature at 438.88 °C. This weight loss is attributed to the decomposition of Styrene Acrylonitrile (SAN). The second stage occurred between 450 and 500°C and exhibits a weight loss of 37.54 % with a peak at 455.74°C. This was corresponding to the breakdown of butadiene. [70][71]

A significant weight loss of 90.1 % is observed in 05APP95GP over the temperature range of 380 to 500°C with a peak temperature at 446.48°C. The 05ATH95GP shows a more complex degradation pattern, with three distinct stages. The first stage from 250 to 350 °C, results in a weight loss of 2.874 % with a peak at 320 °C indicating the presence of Alumina Trihydroxide (ATH). The second stage between 380 and 450°C shows a weight loss of 55.42 % with a peak at 438.45 °C corresponding to SAN decomposition. The third stage from 450 to 500 °C with a weight loss of 32.61% and a peak at 457.67 °C, is due to butadiene degradation. The peak decomposition temperature of ATH slightly increased from 286.08 °C to 320 °C. The TGA result of 05ZB95GP closely resembles that of the 100GP. It exhibits a weight loss of 57.05 % between 380 and 450 °C with a peak at 438.18 °C, due to ZB and SAN decomposition. The subsequent weight loss of 31.58% from 450 to 500°C, with a peak at 460.52°C corresponds to butadiene breakdown. This similarity indicates a comparable composition with SAN and butadiene being the primary constituents.

The TGA data of 05EG95GP shows two stages of weight loss. The first stage from 200 to 300 °C results in a minor weight loss of 1.678 % with a peak at 254.79°C indicating the presence of Expandable Graphite (EG). The second stage between 380 and 500 °C shows a significant weight loss of 89.31% with a peak at 438.97°C corresponding to ABS decomposition. The 15EG85GP shows a similar TGA result compared to 05EG95GP. The higher EG content in

15EG85GP results in a marginally higher weight loss at the lower temperature range (200 – 300 °C) compared to the 05EG95GP.

Table 4-17: Thermogravimetric Analysis Result of FR/ABS Composites

Sample Name	Temp. range (°C)	Weight loss / %	Peak / °C	Constituent
100GP	380 - 450	57.76	438.88	SAN
	450 - 500	37.54	455.74	butadiene
05APP95GP	380 - 500	90.1	446.48	APP and ABS
05ATH95GP	250 - 350	2.874	320	ATH
	380 - 450	55.42	438.45	SAN
	450 - 500	32.61	457.67	butadiene
05ZB95GP	380 - 450	57.05	438.18	SAN and ZB
	450 - 500	31.58	460.52	butadiene
05EG95GP	200 - 300	1.678	254.79	EG
	380 - 500	89.31	438.97	ABS
15EG85GP	200 - 300	2.407	253.14	EG
	380 - 500	80.89	435.77	ABS

Table 4-18 presents TGA result of various OPF/ABS Composites. It was noticed that OPF/ABS composites exhibited initial weight loss at lower temperature ranges (200 - 300°C and 300 - 380°C) due to the degradation of hemicellulose and cellulose. All OPF/ABS composites exhibited significant weight loss in the temperature range of 380 - 500°C, it indicated that the primary thermal degradation is attributed to ABS.

The TGA results showed that FRs degraded at their onset temperature. Therefore, inclusion of FRs did not affect the thermal degradation behaviours of OPF/ABS composites (15APP20OPF65GP, 15ATH20OPF65GP, 05ZB20OPF65GP, 05EG20OPF65GP and 15EG20OPF65GP). In short, the inclusion of natural fibres and flame retardants introduces additional degradation phases, which modify the thermal behaviour of the ABS composites.

Table 4-18: Thermogravimetric Analysis Result OPF/ABS Composites

Sample Name	Temp. range (°C)	Weight loss / %	Peak / °C	Constituent

100GP	380 - 450	57.76	438.88	SAN
	450 - 500	37.54	455.74	butadiene
20OPF80GP	200 -300	4.726	-	hemicellulose
	330-380	10.49	334.32	cellulose
	380 - 450	54.3	436.23	ABS
15APP20OPF65GP	200 - 300	4.9	287.62	APP, hemicellulose and cellulose
	300 - 380	8.293	346.44	
	380 - 500	65.18	440	ABS
15ATH20OPF65GP	200 - 300	4.559		hemicellulose
	300 - 340	6.741	324.59	ATH
	340 - 380	4.185	-	cellulose
	380 - 500	66.79	441.23	ABS
15ZB20OPF65GP	200 - 300	4.546	-	hemicellulose
	300 - 380	10.37	340.1	Cellulose and ZB
	380 - 500	65.04	437.91	ABS
15EG20OPF65GP	200 - 300	7.649	284.66	Hemicellulose and EG
	300 - 380	12.52	333.47	cellulose
	380 - 500	62.28	433.45	ABS
05EG20OPF65GP	200 - 300	5.44	293.26	Hemicellulose and EG
	300 - 380	10.96	337.53	cellulose
	380 - 500	70.99	436.38	ABS

4.5 UL 94 Burn Test

4.5.1 UL 94 50W (20mm) Vertical Burning Test (94V)

The vertical burning test (VB) was conducted to evaluate both the burning and afterglow times after repeated flame application and dripping of the burning test specimens. The results can be used to justify whether materials can be classified as V-0, V-1, or V-2. The detailed test criteria are described in Table 2-5, Section 2.4.2.

As summarised in Table 4-19, most of the test samples failed to cease the burning after applying 1st test flame for 10 seconds and the flame continues propagate up to holding clamp. It means that addition of 15 wt.% flame

retardants (FRs) such as ammonium polyphosphate (APP), alumina trihydrate (ATH), zinc borate (ZB) were unable to aid ABS composites to pass 94V test.

The test samples with 15 wt.% of expandable graphite addition (15EG85GP and 15EG20OPF65GP) able to stop the burning after first test flame application. However, 15EG85GP and 15EG20OPF65GP are unable to stop the burning after second flame application and the burning progress up to holding clamp. On the other hand, it can be seen that drips were detected by cotton indicator during burning.

The sample which able to rate as V-0 is 25EG20OPF65GP. 25 wt.% of expandable graphite mixed with 20 wt.% of OPF and 55 wt.% of ABS resin able to stop the burning after 2 times of test flame application. The burning immediately extinguished, and no drips was found. Hence, it can be concluded that higher amount (25 wt.%) of expandable graphite is needed for OPF/ABS composites to pass 94V criteria. Pooria et al. reported 3 % - 7 % of EG is sufficient to aid OPF/epoxy composites which passed 12-sec vertical bunsen burner test according to FAR 25.853 [178]. Cirmad et al. found that ABS composites required 15% - 20% of EG addition to achieve UL-94 rating of V1 [184]. Simionescu et al. also reported that adding 15 - 20 wt.% of APP into ABS composites able to help to reach UL-94 V-0 classification [200]. Generally, the testing result is tally with other researchers' work. Slightly higher amount of FRs (25 wt.%) is required in this study as compared with other researchers could be attributed to processing temperature of OPF/ABS composites used in this study. As reported in section 3.1, the starting expansion temperature of EG is around 200 – 225 °C and processing temperature of OPF/ABS composites are 220 °C. Hence, it may reduce the efficiency of EG as some of EG may expanded during sample preparation. On the other hand, thermoplastic (ABS) is more flammable than thermoset (epoxy). Relatively high amount of FRs is required to achieve similar fire retardancy.

Figure 4-23 shows test sample (25EG20OPF65GP) after vertical burning test (94V). It can be seen that expandable graphite expanded and formed an insulation layer to prevent further burning. SEM image illustrated that the burning surface of EG containing ABS composites were fully covered by the 'worm' shape expanded graphite and thus provide effective insulation barrier to cease burning.

Table 4-19: Vertical burning test (94V) result of different samples

Sample Name	Average 1st Burning Time (second)	Average 2nd Burning Time (second)	Average Glowing time after 2nd burning	Drips detection	Glowing or flaming combustion up to holding clamp	UL 94 flame classifications
100GP	≥ 120	N/A	N/A	Yes	Yes	Failed to meet test criteria

05APP95GP	≥ 120	N/A	N/A	Yes	Yes	Failed to meet test criteria
05ATH95GP	≥ 120	N/A	N/A	Yes	Yes	Failed to meet test criteria
05ZB95GP	≥ 120	N/A	N/A	Yes	Yes	Failed to meet test criteria
05EG95GP	≥ 120	N/A	N/A	Yes	Yes	Failed to meet test criteria
15EG85GP	0	≥ 120	N/A	Yes	Yes	Failed to meet test criteria
15APP20OPF65GP	≥ 120	N/A	N/A	Yes	Yes	Failed to meet test criteria
15ATH20OPF65GP	≥ 120	N/A	N/A	Yes	Yes	Failed to meet test criteria
15ZB20OPF65GP	≥ 120	N/A	N/A	Yes	Yes	Failed to meet test criteria
15EG20OPF65GP	0	≥ 120	N/A	Yes	Yes	Failed to meet test criteria
25EG20OPF45GP	0	0	N/A	No	No	V-0
20OPF80GP	≥ 120	N/A	N/A	Yes	Yes	Failed to meet test criteria
10APP05ATH20OPF65GP	≥ 120	N/A	N/A	Yes	Yes	Failed to meet test criteria
10APP05ZB20OPF65GP	≥ 120	N/A	N/A	Yes	Yes	Failed to meet test criteria
05ATP10ATH20OPF65GP	≥ 120	N/A	N/A	Yes	Yes	Failed to meet test criteria
10ATH05ZB20OPF65GP	≥ 120	N/A	N/A	Yes	Yes	Failed to meet test criteria
05APP10ZB20OPF65GP	≥ 120	N/A	N/A	Yes	Yes	Failed to meet test criteria
05ATH10ZB20OPF65GP	≥ 120	N/A	N/A	Yes	Yes	Failed to meet test criteria

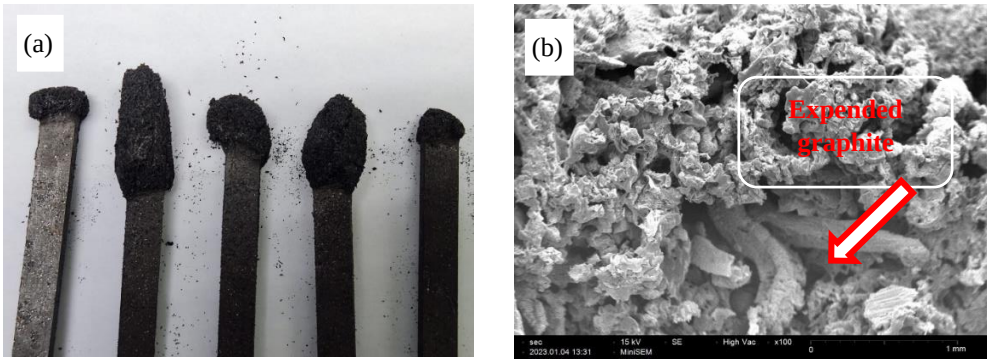

Figure 4-23: (a) The five test specimen (25EG20OPF65GP) after vertical burning test and (b) SEM image of burning surface at a magnification of 100X

4.5.2 UL 94 Horizontal Burning Test (HB)

UL 94 Horizontal Burning Test (HB) was conducted to determine the burning rate of material. The test flame is applied to the free end of the specimen for 30 seconds. The test results were used to justify whether materials can be classified as 94HB. Table 4-20 summarised UL 94 horizontal burning test (HB) result of different test samples. As seen in Figure 4-24, it can be noted that adding flame retardants (FRs) into ABS matrix was able to reduce horizontal burning rate of samples.

4 types of FRs were added into ABS matrix to study their performance on flame retardancy. When 5 wt.% of FRs were added into ABS matrix, it was found that the burning rate reduced by 10 – 38.5% as compared to neat ABS (100GP) sample. Expandable graphite (EG) provided better flame retardancy among the flame retardants used in the current study. It was found that the burning rate can be reduced up to 38.46 % after adding 5 wt. % of EG into ABS (05EG95GP). EG expanded and formed intumescent char layer during burning. This could insulate materials from fire and thus reduce the burning speed [200].

Other flame retardants such as APP, ATH and ZB also able to slow down the burning rate of ABS sample. Adding 5 wt. % of APP, ATH and ZB into ABS matrix separately manage to reduce the burning rate of samples by 24.31 %, 26.9 % and 10.04 % respectively. During burning analysis, APP formed a porous carbonaceous form and this protective char barrier resisted heat, air and pyrolysis product from entering the ABS surface. Thus, it was able to decelerate the burning rate of materials. ATH released water molecules through endothermic reaction ($2AI(OH_3) => AI_2O_3 + 3H_2O$) during burning, lowering the surface temperature of material and inhibit smoke generation. ZB able to promote char formation during burning and hence supress the release of smoke and toxic gas [6] [7] [180].

To improve the fire resistance of ABS matrix, 15 wt.% of EG was added into ABS matrix. it can be observed that 15EG85GP ceased the burning immediately after removing flame source. Hence, it could be concluded that

higher amount of EG addition able to further slowdown and even stop the burning of ABS composites. This result is tally with other researcher's finding. Hussam et al. also reported that adding higher loading of EG into ABS matrix can further improve its fire resistance performance. However, high loading of EG might reduce the impact strength of ABS [184].

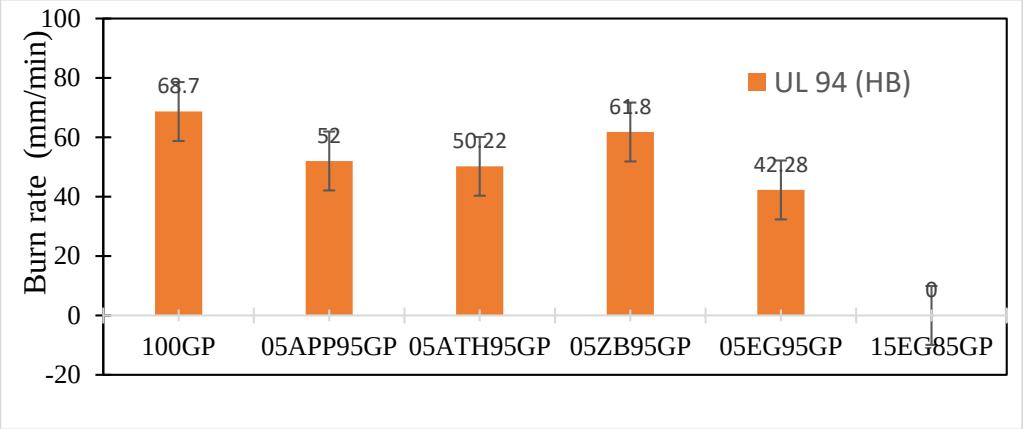

Figure 4-24: Horizontal burn rate of test samples with 5 wt.% FR

As shown in Figure 4-25, 20 wt.% of oil palm fibre (OPF) was incorporated into ABS matrix (20OPF80GP) to study the effect of natural fibre on the ABS based composites. It can be observed that the burning rate of OPF/ABS composites sample decreased to 44.86 mm min^{-1} and this value was about 34.7% slower than neat ABS sample. The result conforms to other similar work reported elsewhere. For instance, Karunakaran et al. and Poonsub et al. reported that adding 10% of natural fibres into ABS matrix could not improve fire resistance of ABS. Higher amount of natural fibres is required to ensure rapid formation of char layer to prevent heat and volatiles from penetrating the materials [183] [182]. The flammability of natural fibres are affected by their chemical composition. Natural fibre with high cellulose content and low silica content tend to increase flammability [174][44]. Hence, OPF that has high silica content was found able to retard the burning rate.

To further improve the flame retardancy of OPF/ABS composites, 15 wt.% of different FRs and 20 wt.% of OPF were mixed into ABS matrix. It was realised that the horizontal burning rate of the samples were further slowed down. 15EG20OPF65GP has similar burning behaviour to 15EG85GP. The burning stopped immediately after removing the flame. The improvement in fire resistance also can be seen in other test samples. The burning rate of 15APP20OPF65GP, 15ATH20OPF65GP and 15ZB20OPF65GP were recorded as 29.36 mm min^{-1}, 26.31 mm min^{-1} and 32.47 mm min^{-1} respectively. These values are about 52 – 62% reduction if compared to neat ABS sample (100GP).

Figure 4-26 illustrated SEM images of various 15 wt.% FR loading test samples after UL 94 horizontal burning test (HB). It can be seen that OPF were burnt and leaving honeycomb-like porous tubular structure on the burning surface of 20OPF85GP, as indicated in Figure 4-26 (a). Figure 4-26 (b)

demonstrated that a porous carbonaceous foam was formed on the burning surface of 15APP20OPF65GP due to decomposition of APP into polyphosphoric acid and ammonia [165][166][167]. This char layer slowed down the flame propagation. Figure 4-26 (c) exhibited that a protective layer of aluminium oxide was formed on the burning surface of 15ATH20OPF65GP. It indicated that ATH successfully protected the test specimens through endothermic reaction. Figure 4-26 (d) represented the burning surface of 15ZB20OPF65GP. It can be noticed that dense char layers were formed due to the presence of ZB.

In short, the most effective FR is EG, follow by ATH and APP. ZB was found to be the least effective FR in the current study.

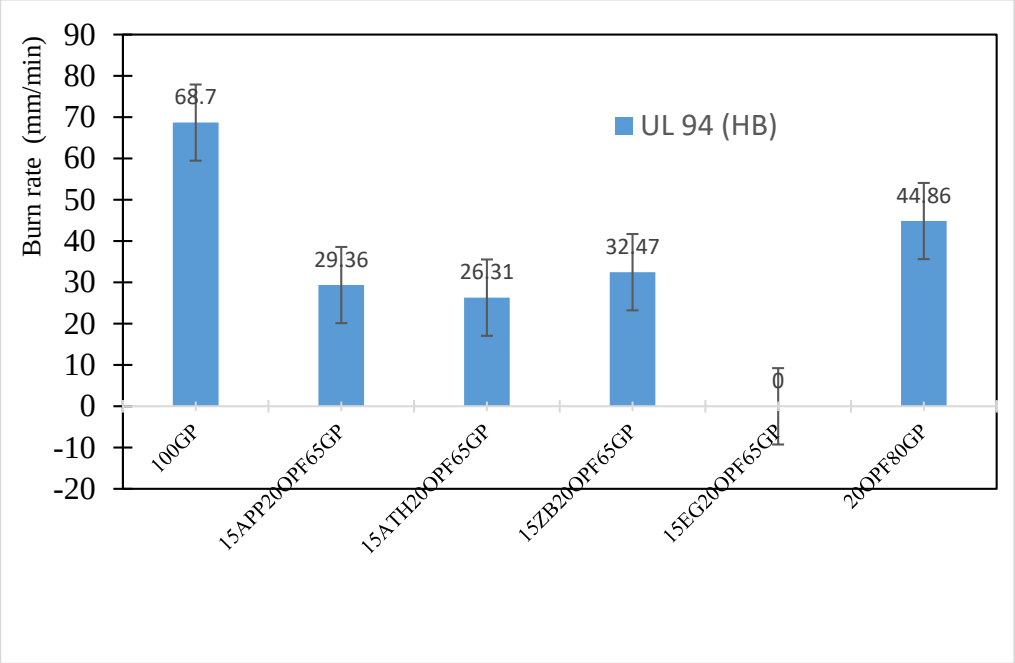

Figure 4-25: Horizontal burn rate of test samples with 15 wt.% FR and 20 wt.% OPF

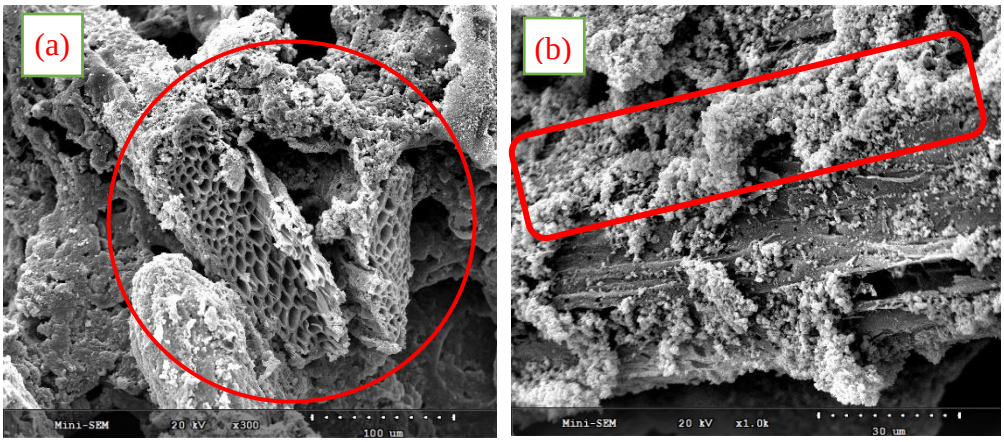

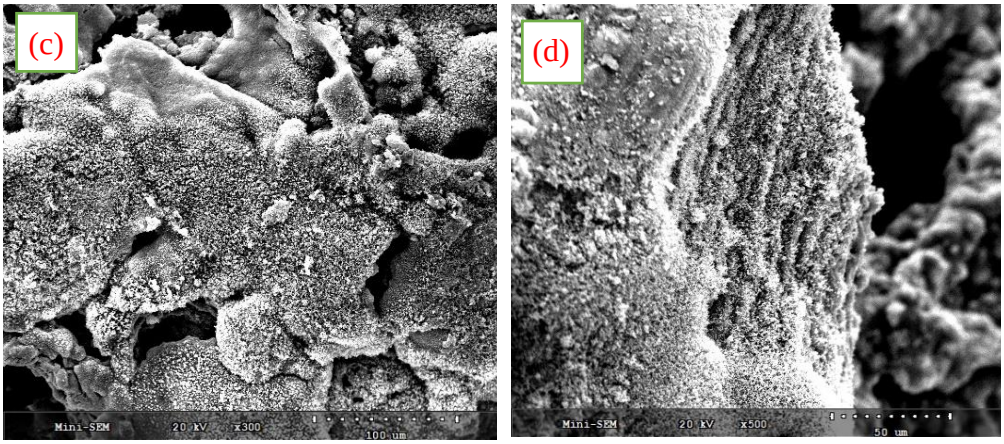

Figure 4-26: SEM images of (a) 20OPF80GP, (b) 15APP20OPF65GP, (c) 15ATH20OPF65GP and (d) 15ZB20OPF65GP

Some researchers reported that synergistic effects were observed when different types of FRs are mixed into natural fibre composites. Simionescu et al. revealed that organic montmorillonite and APP provide synergy in retarding flammability of ABS composites. The results of cone calorimeter tests indicated that higher reduction of the peak heat release rate and minimum mass reduction could be achieved [200]. P. Khalili et al. reported that by mixing 5% ATH and 10% APP into empty fruit bunch fibre reinforced epoxy composites, it could help to achieve 0 sec drip flame time and 0.5 sec total flame time in vertical bunsen burner test as well as contributing to the gross heat reduction from calorimetry test [6][180][7].

Hence, in this study, different FRs (APP, ATH and ZB) were mixed according to ratio 1:2 and then were added into OPF/ABS composites to investigate the fire resistant performance of test samples. As depicted in Figure 4-27, it can be observed that mixed FRs only able to reduce the horizontal burning rate of ABS composites by 32 – 52 %. As compared to single FR-ABS composites, the burning rate of mixed FRs test samples did not show further improvement. Conversely, the burn rate reduction of mixed FR-ABS composites was found even lower than single FR-ABS composites.

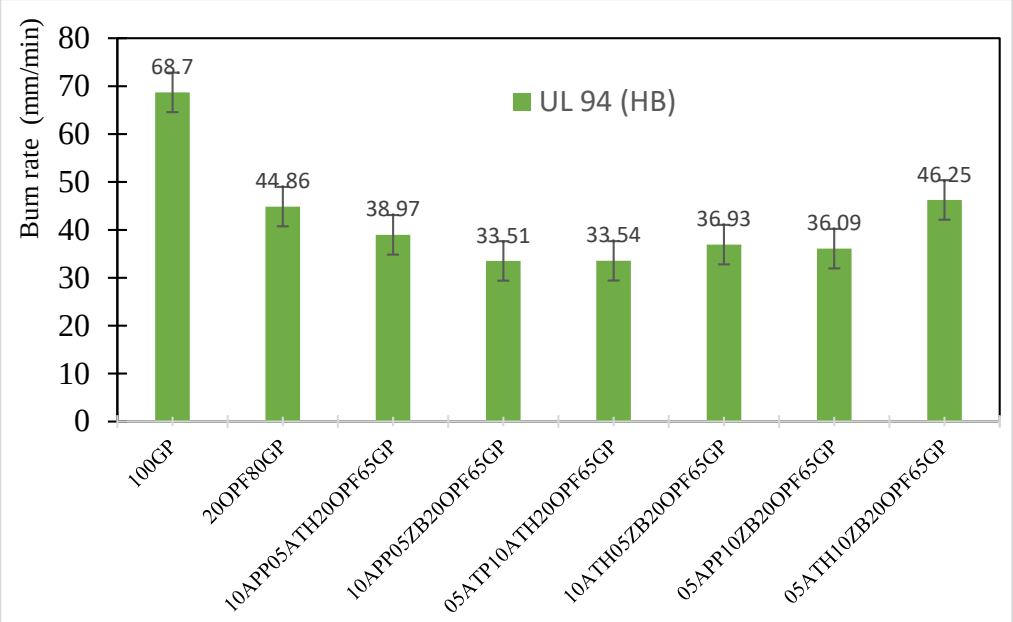

Figure 4-27: Horizontal burn rate of test samples with 15 wt.% mixed FRs and 20 wt.% OPF

As summarised in Table 4-20, all test samples were rated as 94HB as the burning rate was found not exceeding 75 mm min^{-1}. Specimens containing OPF and FRs capable to supress the burning rate of test samples. Higher loading of FRs able to provide better flame retardancy and EG was found to be the most effective FR in the current study. However, no synergistic effects of mixed FRs improving the flame retardancy were found in any test samples.

Table 4-20: UL 94 horizontal burning test (HB) result of different test samples

Specimen	Average Burnt Length (mm)	Average Burning Rate (mm/min)	Reduction in burning rate (%)	UL 94 flame classifications
100GP	75	68.7	-	94HB
05APP95GP	75	52	24.31	94HB
05ATH95GP	75	50.22	26.9	94HB
05ZB95GP	75	61.8	10.04	94HB
05EG95GP	75	42.28	38.46	94HB
15EG85GP	0	0	-	94HB
15APP20OPF65GP	75	29.36	57.26	94HB
15ATH20OPF65GP	75	26.31	61.7	94HB
15ZB20OPF65GP	75	32.47	52.74	94HB
15EG20OPF65GP	0	0	-	94HB
25EG20OPF45GP	0	0	-	94HB

20OPF80GP	75	44.86	34.7	94HB
10APP05ATH20OPF65GP	75	38.97	43.28	94HB
10APP05ZB20OPF65GP	75	33.51	51.22	94HB
05ATP10ATH20OPF65GP	75	33.54	51.18	94HB
10ATH05ZB20OPF65GP	75	36.93	46.24	94HB
05APP10ZB20OPF65GP	75	36.09	47.47	94HB
05ATH10ZB20OPF65GP	75	46.25	32.68	94HB

4.6 Limiting Oxygen Index

Selected specimens were tested to assess their flammability and test result was presented in Table 4-21 and Figure 4-28, it can be observed that neat ABS sample (100GP) is flammable at lower oxygen concentration (18.41%) environment. As compared to atmospheric oxygen level (20.95%)[201], this implied that ABS used in the study is combustible in an open-air condition [184]. Adding 20 wt.% of OPF into ABS matrix (20OPF80GP) able to slightly increase LOI value by 5.32%. This finding is in agreement with UL 94 burn test result. In the section 4.5.2, the UL 94 Horizontal Burning Test results showed that 20 wt.% of oil palm fibre (OPF) able to slow down the burning of ABS composites. Karunakaran et al. and Poonsub et al. reported that 10 wt.% natural fibre is unable to increase LOI value of natural fibre/ABS composites significantly. A threshold value of natural fibre loading is required so that natural fibre able to form highly conjugated char layer at elevated temperature and the char layer will provide a barrier to restrict air, heat and any pyrolysis product from entering material surface [183][182]. This suggested that effective protection layers such as char play an important role in inhibiting combustion.

LOI test result proved that APP, ATH, ZB and EG are effective flame retardants and able to further increase LOI value of OPF/ABS composites. The maximum LOI value (22.83%) was noticed in 15APP20OPF65GP. Its LOI value was increased remarkably after incorporating 15 wt.% of APP into OPF/ABS composites. Phosphorus-based flame retardants such as ammonium polyphosphate is well known as char promoter. They are able to improve char yield of natural fibre composites and thus lower the carbonic combustible gases generation [202]. Compact and intumescent char layer can separate the heat and mass transfer between the gas and condensed phases effectively [175]. Even in the mixed FR-ABS composites, test samples which consist of APP as part of the FR also shows better increment in LOI value. When 10 wt.% APP mixed with 5 wt.% of ATH (10APP05ATH20OPF65GP) and 5 wt.% of ZB (10APP05ZB20OPF65GP) respectively, the LOI values of above mixed FR-ABS composites increased to 21.97% and 21.63% respectively.

The second highest in LOI value improvement was noticed in 15EG20OPF65GP sample. 15 wt.% of EG able to increase LOI value of OPF/ABS composites from 19.39 % to 22.31 %. The improvement could be

attributed to mechanism of flame retardation of EG. Upon heating, EG will expand and form thermal insulation compound to protect underlying materials during fire [178]. ATH also demonstrated the ability of flame inhibition but the improvement is not significant as APP and EG. 15ATH20OPF65GP showed that LOI value was slightly increased to 20.61% after adding 15 wt.% of ATH into OPF/ABS composites. Water molecules in ATH was released during decomposition and thus quenched the materials and impeded the pyrolysis [6] [180].

The least effective FR in this study was zinc borate (ZB). Addition of 15 wt.% of ZB into OPF/ABS composites only able to increase LOI value to 20.17%. Zinc borate is good anti-dripping agent, smoke and afterglow suppressants. However, ZB is less effective in inhibiting the transfer of heat and gas between the materials and fire source [168][169]. ZB also did not show any significant synergistic effects after mixing with other FRs.

In a nutshell, it can be noted that 20 wt.% of OPF able to slightly increase LOI values of ABS composites and supress the combustion. Addition of FRs particularly APP capable of further increases the LOI values of OPF/ABS composites up to 17.74 %. However, no synergistic effects of mixed FRs on flame retardancy were found in any test samples. The surface characterisation of the burnt samples was previously discussed in *section 4.5* UL 94 Burn Test and illustrated in Figure 4-23 and Figure 4-26.

Table 4-21: Limiting oxygen index (LOI) of various OPF/ABS composites

Sample Name	LOI (%)	Increment in LOI (%) as compared with 100GP	Increment in LOI (%) as compared with 20OPF80GP
100GP	18.41	-	N/A
20OPF80GP	19.39	5.32	-
15APP20OPF65GP	22.83	24.01	17.74
15ATH20OPF65GP	20.61	11.95	6.29
15ZB20OPF65GP	20.17	9.56	4.02
15EG20OPF65GP	22.31	21.18	15.06
10APP05ATH20OPF65GP	21.97	19.34	13.31
10APP05ZB20OPF65GP	21.63	17.49	11.55
05APP10ATH20OPF65GP	21.29	15.64	9.80
10ATH05ZB20OPF65GP	20.31	10.32	4.74
05APP10ZB20OPF65GP	20.31	10.32	4.74
05ATH10ZB20OPF65GP	20.17	9.56	4.02

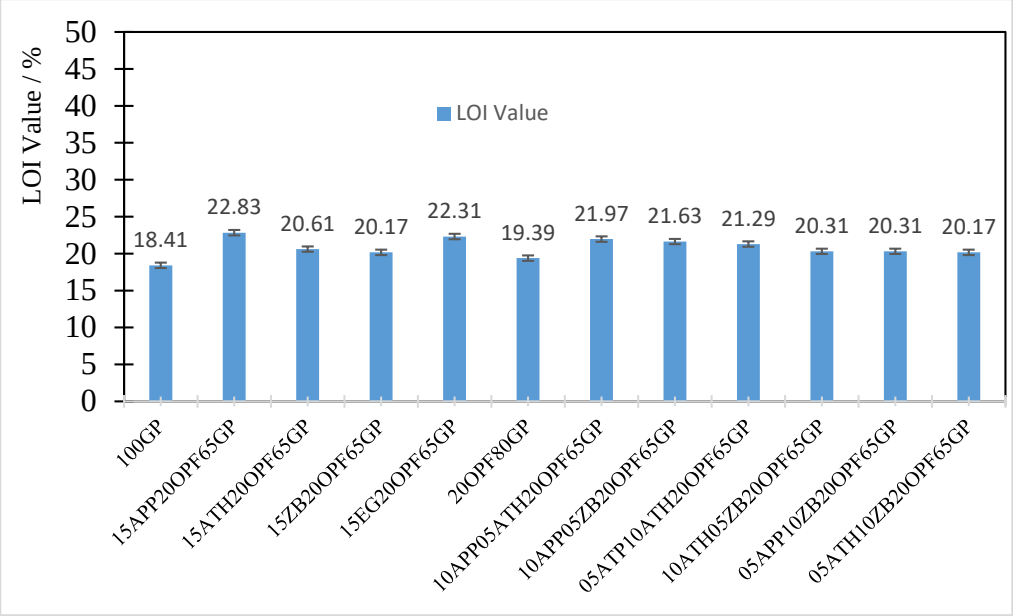

Figure 4-28: Limiting oxygen index (LOI) of various ABS/OPF composites

Chapter 5: Conclusion

5.1 Introduction

This study was conducted to evaluate the possibility of using natural fibre reinforced thermoplastic composites for aerospace interior components. At present, aircraft interior components such as aircraft seat, interior panel structures, floor covering, lining and windows are mainly fabricated by polymeric materials and composites. The face sheets of interior panels, floor covering, plastics moulding of aircraft seat and food tray are particularly suitable fabricated by polymer composites. Thermoset composites which reinforced by fibreglass, aromatic polyamides, graphite and carbon are often employed due to their outstanding properties and compliance with airworthiness standards. However, recycling of thermoset composites is generally considered less environmentally friendly compared to the recycling of thermoplastics due to limited end-of-life options.

It is essential to investigate the mechanical performance and flammability of the proposed natural fibre composites after applying natural fibre surface treatment, coupling agents and flame retardants. It is envisaged that natural fibre surface treatment and coupling agents able to enhance mechanical properties of natural fibre composites while flame retardants able to help natural fibre composites comply with FAR standards. Universally recognized standards and testing methods are implemented to verify the potential of proposed natural fibre composites.

5.2 Findings

During the initial phase of the study, the optimum process parameters for melt blending used in the fabricating OPF/ABS composites were justified through visual inspection, tensile test result and melt plastogram analysis. Visual inspection revealed that the compound exhibited a yellowish tint when processed at higher temperature (260 °C). The melt plastogram data indicated that a low rotor speed during compounding failed to attain preset temperature, whereas a high rotor speed tended to cause the temperature to exceed the preset value due to excessive shear heating. The melt plastogram data also indicated that a shorter mixing time is preferred to prevent thermal degradation, as long as the compound is fully melted. The results of both the tensile test and impact test corroborated that long mixing times would result in the deterioration of mechanical properties. Additionally, the incorporation of OPF into the ABS matrix demonstrated the potential to reduce energy consumption. The proposed process parameters were determined as follows: a mixer temperature of 220 °C, a rotor speed of 30 rpm, and a mixing duration of 5 minutes. These parameters were chosen to prevent the oxidative degradation of ABS, which can occur when exposed to high temperatures for extended periods.

The 2nd phase of study aims to explore the potential of nanocellulose as reinforcing filler for ABS composites. Nanocellulose was successfully extracted from oil palm fibre through delignification, alkali treatment and acid hydrolysis.

The optimum process parameters were justified through scientific approach. The nanocellulose was characterised by Fourier Transform Infrared Spectrometry (FTIR) analysis, Scanning Electron Microscopy (SEM) observation and particle size measurements and compared with commercial grade Celluforce cellulose nanocrystals (Celluforce NCC). FTIR analysis showed that both materials had the similar spectra. FESEM images showed that nanocellulose isolated from OPF has average size of 365.7 nm. The Zeta particle size test result revealed that nanocellulose isolated from OPF has an average particle size of 175.19 nm, whereas Celluforce NCC has an average particle size of 125.42 nm. Due to long synthesis time of nanocellulose, commercial grade Celluforce NCC was used for fabricating NCC/ABS composites.

The tensile test result indicates that, when coupled with appropriate coupling agents (maleic anhydride and silane) and right amount of NCC (3 wt.%), nanocellulose has the capacity to enhance the ultimate tensile strength of ABS by up to 11.97%. The reinforcing mechanism of NCC was discussed and subsequently validated through SEM images.

In the third part of the study, various types of chemically treated oil palm fibre (20 wt.%) were incorporated into ABS to study the effects of natural fibre surface treatment and coupling agents on the mechanical properties of OPF/ABS composites. The tensile result have demonstrated that fibre surface treatment (alkali treatment) and coupling agents (maleic anhydride and silane) are effective approaches for enhancing mechanical properties of natural fibre composites. The research findings indicated that maleic-treated OPF and silane-treated OPF can lead to a significant improvement of up to 35.59% in the ultimate tensile strength of the OPF/ABS composites when compared with raw OPF. On the other hand, chemically treated oil palm fibre/ABS composites is marginally improving the tensile properties of neat ABS up to 2.38%. SEM Images of the fracture surface of these ABS composites illustrated the gaps present at the interface between OPF and ABS were reduced with the aid of coupling agents.

In the fourth phase of the study, the effects of flame retardants on the mechanical properties and flammability of OPF/ABS composites were investigated. TGA analysis results showed that ATH and EG may initiate decomposition during the compounding of OPF/ABS composites as their onset degradation temperature is closely align with the processing temperature. OPF/ABS composites which containing 15 wt.% of flame retardants are unable to pass vertical burning test (VB). Expandable graphite is the most effective flame retardant in OPF/ABS composites. Addition of 15 wt.% EG able to achieve self-extinguish in the 1st burning but failed to stop the burning after second flame application. If the amount of EG increased to 25 wt.%, the OPF/ABS able to achieve V-0 rating. The flame retardation mechanism of expandable graphite was verified through SEM images. Results from horizontal burning test (HB) showed that both oil palm fibre and various flame retardants (APP, ATH, ZB and EG) able to slow down the burning rate of ABS composites. The incorporation of both OPF and flame retardants resulted in a further

reduction in the burning rate of ABS composites. However, it is important to note that there were no observed synergistic effects among the flame retardants in the ABS composites. This finding contradicts the results reported by other researchers. Limiting Oxygen Index (LOI) result revealed that OPF able to slightly increase LOI value by 5.32%. All FRs able to further increase LOI value of OPF/ABS composites up to 17.74%. APP is the most effective flame retardants which able to help to supress the combustion. The tensile properties of OPF/ABS composites are compromised after adding 15wt. % of flame retardants into OPF/ABS composites. The SEM images of test samples exhibits the failure mechanism of the OPF/ABS composites.

5.3 Limitation

OPF/ABS composites with sufficient flame retardants is possible to employ as aircraft interior materials. OPF/ABS composites with 25 wt. % of expandable graphite (25EG20OPF45GP) able to achieve V-0 rating. It means it is compliance with the requirements of FAR 25.853 (a). However, heat release rate test and smoke test as specified in FAR Part 25 cannot be conducted due to unavailability the required equipment.

Chapter 6: Recommendation

It can be observed the growing demand for composites in the aerospace industry. Industry leaders such as Airbus and Boeing are actively seeking new environmentally-friendly and sustainable materials to meet this demand. Natural fibre reinforced thermoplastic composites with addition of appropriate flame retardants has potential to be one of the alternative.

Using other fabrication methods, such as applying fire retardant coating on natural fibre reinforced thermoplastic composites is feasible approach. This coating can potentially be more effective in achieving fire resistance. It avoids the deterioration of the mechanical properties of natural fibre reinforced thermoplastic composites due to addition of flame retardants.

Durability testing of natural fibre reinforced thermoplastic composites is indeed worth investigating. It helps to assess the performance of natural fibre reinforced thermoplastic composites under various conditions over an extended period of time. This is crucial for understanding how the material will hold up and maintain their properties in real-world applications and thus providing valuable insights for design and engineering purposes.

References:

[1] Marketandmarkets, “Aircraft Cabin Interiors Market by Type (Aircraft Seating, IFEC, Aircraft Cabin Lighting, Aircraft Galley, Aircraft Lavatory, Aircraft Windows & Windshields, Aircraft Interior Panels), End User, Aircraft Type, Material, Region - Global Forecast 2025,” 2020.

[2] M. Standridge, “Aerospace materials: past, present and future,” *Introduction to Aerospace Materials*, pp. 15–38, 2012.

[3] D. Michaels, “New Materials for Airplanes,” *The Wall Street Journal*, pp. 1–5, 2013.

[4] W. D. Callister and D. G. Rethwisch, *Materials Science and Engineering: An Introduction, 10th Edition*. John Wiley and Sons, Incorporated, 2019.

[5] R. Sonnier, A. Taguet, L. Ferry, and J.-M. Lopez-Cuesta, *Towards Bio-based Flame Retardant Polymers*. Cham: Springer International Publishing, 2018.

[6] P. Khalili, K. Y. Tshai, I. Kong, J. H. Lee, and F. A. Mostafa, “The Synergistic Effect of Flame Retardants on Flammability, Thermal and Mechanical Properties of Natural Fiber Reinforced Epoxy Composite,” *Key Eng. Mater.*, vol. 701, pp. 281–285, 2016.

[7] P. Khalili, X. Liu, K. Y. Tshai, C. Rudd, X. Yi, and I. Kong, “Development of fire retardancy of natural fiber composite encouraged by a synergy between zinc borate and ammonium polyphosphate,” *Compos. Part B Eng.*, vol. 159, no. June 2018, pp. 165–172, 2019.

[8] L. Victor, S. Albert, T. Kim, and P. Khali, “Effect of Flame Retardants on Flammability , Thermal and Mechanical Performance of Palm Reinforced Composite fibre Reinforced Composite,” pp. 1–8, 2015.

[9] Y. A. El-Shekeil, M. S. Salit, K. Abdan, and E. S. Zainudin, “Development of a new kenaf bast fiber-reinforced thermoplastic polyurethane composite,” *BioResources*, vol. 6, no. 4, pp. 4662–4672, 2011.

[10] S. Shinoj, R. Visvanathan, S. Panigrahi, and M. Kochubabu, “Oil palm fiber (OPF) and its composites: A review,” *Ind. Crops Prod.*, vol. 33, no. 1, pp. 7–22, 2011.

[11] R. Ramli, R. M. Yunus, M. D. H. Beg, and D. M. R. Prasad, “Oil palm fiber reinforced polypropylene composites: Effects of fiber loading and coupling agents on mechanical, thermal, and interfacial properties,” *J. Compos. Mater.*, vol. 46, no. 11, pp. 1275–1284, 2012.

[12] J. G. Vijayan, T. N. Prabhu, and J. A. G., “Nanocellulose as an Ecofriendly Source in Nanoscience: Synthesis, Characterization, Properties, and Applications—A Review,” *Macromol. Symp.*, vol. 413, no. 2, Apr. 2024.

[13] A. James *et al.*, “A review of nanocellulose modification and compatibility barrier for various applications,” *J. Thermoplast. Compos.*

Mater., vol. 37, no. 6, pp. 2149–2199, Jun. 2024.

[14] A. Farooq *et al.*, "From farm to function: Exploring new possibilities with jute nanocellulose applications," *Carbohydr. Polym.*, vol. 342, p. 122423, Oct. 2024.

[15] U. Çelen, Y. Balçik Tamer, and H. Berber, "The potential use of natural expanded perlite as a flame retardant additive for acrylonitrile-butadiene-styrene based composites," *J. Vinyl Addit. Technol.*, vol. 30, no. 1, pp. 277–293, Jan. 2024.

[16] A. T. Phung, H. T. Dzung, N. P. D. Linh, V. M. Duc, and N. T. Liem, "Acrylonitrile butadiene styrene/wood sawdust particles composites: mechanical and morphological properties," *Iran. Polym. J.*, vol. 33, no. 1, pp. 67–78, Jan. 2024.

[17] I. Khan, N. Kumar, M. Choudhary, S. Kumar, and T. Singh, "Mechanical and dynamic mechanical behavior of 3D printed waste slate particles filled acrylonitrile butadiene styrene composites," *Arab. J. Chem.*, vol. 17, no. 2, p. 105559, Feb. 2024.

[18] F. Ghonjizade-Samani, L. Haurie, R. Malet, and V. Realinho, "Study of using cork powder as an adjuvant bio-flame retardant in acrylonitrile-butadiene-styrene flame retardant formulations," *Polym. Degrad. Stab.*, vol. 225, p. 110825, Jul. 2024.

[19] G. H. Douglas D. Stokke, Qinglin Wu, *Introduction to Wood and Natural Fiber Composites*. John Wiley and Sons Ltd., 2013.

[20] Todd Johnson, "Composites in Aerospace," *ThoughtCo*, 2019. [Online]. Available: https://www.thoughtco.com/composites-in-aerospace-820418. [Accessed: 06-Dec-2022].

[21] • Modern Airliners, "What are the Boeing 787 Dreamliner Specs?," 2015. [Online]. Available: https://modernairliners.com/boeing-787-dreamliner/boeing-787-dreamliner-specs/.

[22] V. Giurgiutiu, *Structural Health Monitoring of Aerospace Composites*. Elsevier, 2016.

[23] N. J. Arockiam, M. Jawaid, and N. Saba, "Sustainable bio composites for aircraft components," *Sustain. Compos. Aerosp. Appl.*, no. January, pp. 109–123, 2018.

[24] Federal Aviation Regulations, "Part 25-Airworthiness Standards: Transport Category Airplanes," *Fed. Aviat. Adm. (FAA), USA*, p. 86, 1989.

[25] A. Horner, "Aircraft Materials Fire Test Handbook," *Test*, no. April, p. 235, 2000.

[26] T. Edwards, "Composite materials revolutionise aerospace engineering," *Ingenia*, no. 36, pp. 25–27, 2008.

[27] S. Black, "Advanced materials for aircraft interiors Applications," Cincinnati, pp. 1–6, Nov-2006.

[28] R. D. Anandjiwala *et al.*, “Bio-based structural composite materials for aerospace applications,” *SAIAS Symp.*, no. September, pp. 1–6, 2008.

[29] “Potential of Sustainable Materials in Wing Structural Design,” in *Sustainable Composites for Aerospace Applications*, vol. 53, no. 9, Elsevier, 2018, pp. 109–123.

[30] M. Jawaid and M. Thariq, Eds., *Sustainable Composites for Aerospace Applications*, 1st ed. United kingdom: Woodhead Publishing, 2018.

[31] S. Black, “Looking to lighten up aircraft interiors? Try natural fibers!,” Cincinnati, Aug-2015.

[32] R. E. Lyon, “Materials with reduced flammability in aerospace and aviation,” *Adv. Fire Retard. Mater.*, pp. 573–598, 2008.

[33] C. LAUTENBERGER, J. TORERO, and C. FERNANDEZ-PELLO, “Understanding materials flammability,” in *Flammability Testing of Materials Used in Construction, Transport and Mining*, Elsevier, 2006, pp. 1–21.

[34] *UL Standard for Safety Tests for Flammability of Plastic Materials for Parts in Devices and Appliances*, 6th ed. Underwriters Laboratories Inc. (UL), 2013.

[35] “SIMONA Boltaron 9000 and 4000 Series Technical data Sheet.” [Online]. Available: https://www.boltaron.com/wp-content/uploads/2020/06/Boltaron-8.5_-x-8.5_-Aerospace_6-30-20.pdf.

[36] “Kydex® Technical Data Sheet.” [Online]. Available: https://www.professionalplastics.com/professionalplastics/KYDEX-Aircraft_Interiors.pdf.

[37] “Elastollan® Technical Data Sheet.” [Online]. Available: https://www.yumpu.com/en/document/read/45511444/elastollanar-aerospace-materials-from-basf.

[38] “Royalite® R57 Technical data sheet.” [Online]. Available: https://www.curbellplastics.com/Research-Solutions/Technical-Resources/Technical-Resources/Royalite-R57-Fire-Rated-Extruded-Sheet. [Accessed: 22-Sep-2021].

[39] “Royalite® R59 Technical data sheet.” [Online]. Available: https://www.curbellplastics.com/Research-Solutions/Technical-Resources/Technical-Resources/Royalite-R59-Fire-Rated-Extruded-Sheet. [Accessed: 22-Sep-2021].

[40] “ABS Flame Retardant SP790 Technical Data Sheet.” [Online]. Available: https://shuman-plastics.com/wp-content/uploads/2018/01/ABS-FLAME-RETARDANT-SP790-BLACK-AND-CUSTOM-COLORS.pdf.

[41] “Prime ABS 860 FR Technical data Sheet.” [Online]. Available: https://materials.ulprospector.com/en/profile/pdf?E=261503.

[42] J. Biagiotti, D. Puglia, and J. M. Kenny, “A Review on Natural Fibre-

Based Composites-Part I," *J. Nat. Fibers*, vol. 1, no. 2, pp. 37–68, Oct. 2004.

[43] I. S. Aji *et al.*, "KENAF FIBRES AS REINFORCEMENT FOR POLYMERIC COMPOSITES: A REVIEW," *Int. J. Mech. Mater. Eng.*, vol. 4, no. 2, pp. 239–248, 2009.

[44] R. Kozłowski and M. Władyka-Przybylak, "Flammability and fire resistance of composites reinforced by natural fibers," *Polym. Adv. Technol.*, vol. 19, no. 6, pp. 446–453, Jun. 2008.

[45] C. H. Lee, M. S. Salit, and M. R. Hassan, "A Review of the Flammability Factors of Kenaf and Allied Fibre Reinforced Polymer Composites," *Adv. Mater. Sci. Eng.*, vol. 2014, pp. 1–8, 2014.

[46] A. Hassan, A. A. Salema, F. N. Ani, and A. A. Bakar, "A review on oil palm empty fruit bunch fiber-reinforced polymer composite materials," *Polym. Compos.*, vol. 31, no. 12, pp. 2079–2101, Dec. 2010.

[47] T. Tuong An Tran, T. Kim Phung Le, T. Phong Mai, and D. Quan Nguyen, "Bioethanol Production from Lignocellulosic Biomass," in *Alcohol Fuels - Current Technologies and Future Prospect*, IntechOpen, 2020.

[48] H. P. S. Abdul Khalil, S. Hanida, C. W. Kang, and N. A. Nik Fuaad, "Agro-hybrid composite: The effects on mechanical and physical properties of oil palm fiber (EFB)/glass hybrid reinforced polyester composites," *J. Reinf. Plast. Compos.*, vol. 26, no. 2, pp. 203–218, 2007.

[49] M. S. Sreekala, M. G. Kumaran, and S. Thomas, "SREEKALA et al. (1997).pdf," pp. 821–835, 1997.

[50] M. Khalid, C. T. Ratnam, T. G. Chuah, S. Ali, and T. S. Y. Choong, "Comparative study of polypropylene composites reinforced with oil palm empty fruit bunch fiber and oil palm derived cellulose," *Mater. Des.*, vol. 29, no. 1, pp. 173–178, 2008.

[51] M. Jacob, S. Thomas, and K. T. Varughese, "Natural rubber composites reinforced with sisal/oil palm hybrid fibers: Tensile and cure characteristics," *J. Appl. Polym. Sci.*, vol. 93, no. 5, pp. 2305–2312, 2004.

[52] H. Ku, H. Wang, N. Pattarachaiyakoop, and M. Trada, "A review on the tensile properties of natural fiber reinforced polymer composites," *Compos. Part B Eng.*, vol. 42, no. 4, pp. 856–873, 2011.

[53] M. Brebu and C. Vasile, "Thermal degradation of lignin - A review," *Cellul. Chem. Technol.*, vol. 44, no. 9, pp. 353–363, 2010.

[54] Arno P. Schniewind, "Thermal Degradation," in *Concise Encyclopedia of Wood & Wood-based Materials*, Pergamon Press, 1989, pp. 271–273.

[55] F. Cardona, "Thermogravimetric Analysis of Bamboo Powder- Filled Epoxy Polymer Composites," no. February, 2017.

[56] F. Yao, Q. Wu, Y. Lei, W. Guo, and Y. Xu, "Thermal decomposition kinetics of natural fibers: Activation energy with dynamic

thermogravimetric analysis," *Polym. Degrad. Stab.*, vol. 93, no. 1, pp. 90–98, 2008.

[57] V. Fiore, T. Scalici, and A. Valenza, "Characterization of a new natural fiber from Arundo donax L. as potential reinforcement of polymer composites," *Carbohydr. Polym.*, vol. 106, no. 1, pp. 77–83, 2014.

[58] G. Luis, "a New Natural Fiber: Toquilla Straw a Potential Reinforcement in Thermoplastic Polymer Composites," *Article*, vol. 5, no. 1, p. 7, 2014.

[59] A. Gani and I. Naruse, "Effect of cellulose and lignin content on pyrolysis and combustion characteristics for several types of biomass," *Renew. Energy*, vol. 32, no. 4, pp. 649–661, Apr. 2007.

[60] H. Yang, R. Yan, H. Chen, D. H. Lee, and C. Zheng, "Characteristics of hemicellulose, cellulose and lignin pyrolysis," *Fuel*, vol. 86, no. 12–13, pp. 1781–1788, Aug. 2007.

[61] J. W. Kaczmar, J. Pach, and C. Burgstaller, "The chemically treated hemp fibres to reinforce polymers," *Polimery/Polymers*, vol. 56, no. 11–12, pp. 817–822, 2011.

[62] N. A. Rosli, I. Ahmad, and I. Abdullah, "Isolation and Characterization of Cellulose Nanocrystals from Agave angustifolia Fibre," *BioResources*, vol. 8, no. 2, Feb. 2013.

[63] Y. Y. Then, N. A. Ibrahim, N. Zainuddin, H. Ariffin, W. M. Z. Wan Yunus, and B. W. Chieng, "Surface Modifications of Oil Palm Mesocarp Fiber by Superheated Steam, Alkali, and Superheated Steam-Alkali for Biocomposite Applications," *BioResources*, vol. 9, no. 4, Oct. 2014.

[64] N. S. Lani, N. Ngadi, A. Johari, and M. Jusoh, "Isolation, Characterization, and Application of Nanocellulose from Oil Palm Empty Fruit Bunch Fiber as Nanocomposites," *J. Nanomater.*, vol. 2014, pp. 1–9, 2014.

[65] H. A. Silvério, W. P. Flauzino Neto, N. O. Dantas, and D. Pasquini, "Extraction and characterization of cellulose nanocrystals from corncob for application as reinforcing agent in nanocomposites," *Ind. Crops Prod.*, vol. 44, pp. 427–436, 2013.

[66] S. M. L. Rosa, N. Rehman, M. I. G. de Miranda, S. M. B. Nachtigall, and C. I. D. Bica, "Chlorine-free extraction of cellulose from rice husk and whisker isolation," *Carbohydr. Polym.*, vol. 87, no. 2, pp. 1131–1138, Jan. 2012.

[67] H. D. Nguyen, T. T. Thuy Mai, N. B. Nguyen, T. D. Dang, M. L. Phung Le, and T. T. Dang, "A novel method for preparing microfibrillated cellulose from bamboo fibers," *Adv. Nat. Sci. Nanosci. Nanotechnol.*, vol. 4, no. 1, 2013.

[68] C. Uma Maheswari, K. Obi Reddy, E. Muzenda, B. R. Guduri, and A. Varada Rajulu, "Extraction and characterization of cellulose microfibrils from agricultural residue - Cocos nucifera L," *Biomass and Bioenergy*, vol. 46, pp. 555–563, 2012.

[69] “TERLURAN GP-22 TECHNICAL DATASHEET.” .

[70] M. Suzuki and C. A. Wilkie, “The thermal degradation of acrylonitrile-butadiene-styrene terpolymei as studied by TGA/FTIR,” *Polym. Degrad. Stab.*, vol. 47, no. 2, pp. 217–221, Jan. 1995.

[71] L. Tong, H. Ma, and Z. Fang, “THERMAL DECOMPOSITION AND FLAMMABILITY OF ACRYLONITRILE-BUTADIENE-STYRENE/MULTI-WALLED CARBON NANOTUBES COMPOSITES,” *Chinese J. Polym. Sci.*, vol. 26, no. 03, p. 331, 2008.

[72] S. Aid, A. Eddhahak, Z. Ortega, D. Froelich, and A. Tcharkhtchi, “Experimental study of the miscibility of ABS/PC polymer blends and investigation of the processing effect,” *J. Appl. Polym. Sci.*, vol. 134, no. 25, pp. 1–9, Jul. 2017.

[73] M. A. PEYDRO, D. JUAREZ, S. SANCHEZ-CABALLERO, and F. PARRES, “STUDY OF THE THERMAL PROPERTIES OF ACRYLONITRILE BUTADIENE STYRENE – HIGH IMPACT POLYSTYRENE BLENDS WITH STYRENE ETHYLENE BUTYLENE STYRENE,” *Ann. ORADEA Univ. Fascicle Manag. Technol. Eng.*, vol. XXII (XII), no. 1, 2013.

[74] A. K. M. K. M. Moshiul Alam, M. D. H. D. H. Beg, D. M. M. Reddy Prasad, M. R. R. Khan, and M. F. F. Mina, “Structures and performances of simultaneous ultrasound and alkali treated oil palm empty fruit bunch fiber reinforced poly(lactic acid) composites,” *Compos. Part A Appl. Sci. Manuf.*, vol. 43, no. 11, pp. 1921–1929, Nov. 2012.

[75] M. Jacob, B. Francis, S. Thomas, and K. T. Varughese, “Dynamical mechanical analysis of sisal/oil palm hybrid fiber-reinforced natural rubber composites,” *Polym. Compos.*, vol. 27, no. 6, pp. 671–680, Dec. 2006.

[76] T. H. Nam, S. Ogihara, N. H. Tung, and S. Kobayashi, “Effect of alkali treatment on interfacial and mechanical properties of coir fiber reinforced poly(butylene succinate) biodegradable composites,” *Compos. Part B Eng.*, vol. 42, no. 6, pp. 1648–1656, 2011.

[77] M. Karina, H. Onggo, A. H. D. Abdullah, and A. Syampurwadi, “Effect of Oil Palm Empty Fruit Bunch Fiber on the Physical and Mechanical Properties of Fiber Glass Reinforced Polyester Resin,” *J. Biol. Sci.*, vol. 8, no. 1, pp. 101–106, Dec. 2007.

[78] M. M. Rahman and M. A. Khan, “Surface treatment of coir (Cocos nucifera) fibers and its influence on the fibers’ physico-mechanical properties,” *Compos. Sci. Technol.*, vol. 67, no. 11–12, pp. 2369–2376, 2007.

[79] J. Rout, M. Misra, S. S. Tripathy, S. K. Nayak, and A. K. Mohanty, “The influence of fibre treatment on the performance of coir-polyester composites,” *Compos. Sci. Technol.*, vol. 61, no. 9, pp. 1303–1310, Jul. 2001.

[80] R. Hu and J. K. Lim, “Fabrication and mechanical properties of

completely biodegradable hemp fiber reinforced polylactic acid composites," *J. Compos. Mater.*, vol. 41, no. 13, pp. 1655–1669, 2007.

[81] P. Threepopnatkul, N. Kaerkitcha, and N. Athipongarporn, "Effect of surface treatment on performance of pineapple leaf fiber–polycarbonate composites," *Compos. Part B Eng.*, vol. 40, no. 7, pp. 628–632, Oct. 2009.

[82] A. K. Bledzki, H. P. Fink, and K. Specht, "Unidirectional hemp and flax EP- and PP-composites: Influence of defined fiber treatments," *J. Appl. Polym. Sci.*, vol. 93, no. 5, pp. 2150–2156, 2004.

[83] Mohammad Mazedul Kabir, H. Wang, T. Aravinthan, F. Cardona, and K. tak Lau, "Effects of natural fibre surface on composite properties: a review," *eddBE2011 Proc.*, pp. 94–99, 2011.

[84] "Maleic anhydride - Spectra for FT-IR Raman." [Online]. Available: https://www.sigmaaldrich.com/deepweb/assets/sigmaaldrich/quality/spectra/377/883/RAIR013584.pdf. [Accessed: 23-Feb-2022].

[85] R. Bodîrlău and C. A. Teacă, "Fourier transform infrared spectroscopy and thermal analysis of lignocellulose fillers treated with organic anhydrides," *Rom. Reports Phys.*, vol. 54, no. 1–2, pp. 93–104, 2009.

[86] T. . J. Keener, R. . K. Stuart, and T. . K. Brown, "Maleated coupling agents for natural fibre composites," *Compos. Part A Appl. Sci. Manuf.*, vol. 35, no. 3, pp. 357–362, Mar. 2004.

[87] S. MOHD Jani, H. D. ROZMAN, Z. . MOHD ISHAK, A. ABUSAMAH, and S. RAHIM, "The Effect of PP/MAPP Blends On EFB Fibres For Improving Tensile And Dimensional Stability Properties," *J. Oil Palm Res.*, vol. 19, no. 1, pp. 338–349, 2007.

[88] M. J. Saad, "Effect of Maleated Polypropylene (MAPP) on the Tensile, Impact and Thickness Swelling Properties of Kenaf Core – Polypropylene Composites," *J. Sci. Technol.*, vol. 2, no. 1, pp. 33–44, 2010.

[89] M. Sain, S. H. Park, F. Suhara, and S. Law, "Flame retardant and mechanical properties of natural fibre-PP composites containing magnesium hydroxide," *Polym. Degrad. Stab.*, vol. 83, no. 2, pp. 363–367, 2004.

[90] Michael A Fuqua and Chad A Ulven, "Preparation and Characterization of Polypropylene Composites Reinforced with Modified Lignocellulosic Corn Fiber," in *2008 Providence, Rhode Island, June 29 - July 2, 2008*, 2008.

[91] V. Srebrenkoska, G. B. Gaceva, and Dimko Dimeski, "Preparation and characterization of lignocellulosic material filled eco-composites," no. 1, 2000.

[92] H. S. Kim, B. H. Lee, S. W. Choi, S. Kim, and H. J. Kim, "The effect of types of maleic anhydride-grafted polypropylene (MAPP) on the interfacial adhesion properties of bio-flour-filled polypropylene

composites," *Compos. Part A Appl. Sci. Manuf.*, vol. 38, no. 6, pp. 1473–1482, 2007.

[93] J. Z. Lu, I. I. Negulescu, and Q. Wu, "Maleated wood-fiber/high-density-polyethylene composites: Coupling mechanisms and interfacial characterization," *Compos. Interfaces*, vol. 12, no. 1–2, pp. 125–140, Jan. 2005.

[94] H. Demir, U. Atikler, D. Balköse, and F. Tihminlioğlu, "The effect of fiber surface treatments on the tensile and water sorption properties of polypropylene-luffa fiber composites," *Compos. Part A Appl. Sci. Manuf.*, vol. 37, no. 3, pp. 447–456, 2006.

[95] J. B. Naik and S. Mishra, "Esterification effect of maleic anhydride on swelling and mechanical properties of natural fiber / polystyrene composites," *North*, vol. 001.

[96] O. C. M., I. E. Y, and O. R. S., "Effects of Maleic Anhydride on the Mechanical Properties and Morphology of Wheat Straw Fibre Reinforced Polypropylene," *J. Innov. Res. Eng. Sci.*, vol. 3, no. 1, pp. 412–420, 2012.

[97] "3-(Trimethoxysilyl)propyl methacrylate - Spectra for FT-IR Raman." [Online]. Available: https://www.sigmaaldrich.com/deepweb/assets/sigmaaldrich/quality/spectra/283/663/RAIR004921.pdf. [Accessed: 23-Feb-2022].

[98] Y. Xie, C. A. S. Hill, Z. Xiao, H. Militz, and C. Mai, "Silane coupling agents used for natural fiber/polymer composites: A review," *Compos. Part A Appl. Sci. Manuf.*, vol. 41, no. 7, pp. 806–819, Jul. 2010.

[99] K. L. Pickering, M. G. A. Efendy, and T. M. Le, "A review of recent developments in natural fibre composites and their mechanical performance," *Compos. Part A Appl. Sci. Manuf.*, vol. 83, pp. 98–112, Apr. 2016.

[100] F. de Buyl, "Organo-Functional Silanes," *Inorg. Polym.*, pp. 88–93, 2007.

[101] L. Chotirat, K. Chaochanchaikul, and N. Sombatsompop, "On adhesion mechanisms and interfacial strength in acrylonitrile-butadiene-styrene/wood sawdust composites," *Int. J. Adhes. Adhes.*, vol. 27, no. 8, pp. 669–678, 2007.

[102] Z. A. Mohd Ishak, A. Ariffin, and R. Senawi, "Effects of hygrothermal aging and a silane coupling agent on the tensile properties of injection molded short glass fiber reinforced poly(butylene terephthalate) composites," *Eur. Polym. J.*, vol. 37, no. 8, pp. 1635–1647, 2001.

[103] X. Liu, Y. Han, G. Gao, Z. Li, and F. Liu, "Effect of Silane Coupling Agent on the Mechanical , Thermal Properties and Morphology of Tremolite / Pa1010 Composites," *Chinese J. Polym. Sci. Polym.*, vol. 26, no. 3, pp. 255–262, 2008.

[104] M. Müller, I. Radovanovic, T. Grüneberg, H. Militz, and A. Krause, "Influence of various wood modifications on the properties of polyvinyl

chloride/wood flour composites," *J. Appl. Polym. Sci.*, vol. 125, no. 1, pp. 308–312, Jul. 2012.

[105] N. Sombatsompop and K. Chaochanchaikul, "Average mixing torque, tensile and impact properties, and thermal stability of poly(vinyl chloride)/sawdust composites with different silane coupling agents," *J. Appl. Polym. Sci.*, vol. 96, no. 1, pp. 213–221, 2005.

[106] M. A. Gunning, L. M. Geever, J. A. Killion, J. G. Lyons, and C. L. Higginbotham, "Improvement in mechanical properties of grafted polylactic acid composite fibers via hot melt extrusion," *Polym. Compos.*, vol. 35, no. 9, pp. 1792–1797, 2014.

[107] M. A. Gunning *et al.*, "The effect of maleic anhydride grafting efficiency on the flexural properties of polyethylene composites," *J. Appl. Polym. Sci.*, vol. 49, no. 7, p. n/a-n/a, Jul. 2011.

[108] J. Z. Lu, "Chemical coupling in wood fiber and polymer composites: a review of coupling agents and treatments," *Wood Fiber Sci.*, vol. 32, no. 1, pp. 88–104, 2000.

[109] Z. Cao *et al.*, "Effect of Chemical Treatments and HDPE-g-MA on the Physical and Mechanical Behaviour of HDPE / Natural Fibre Composites," *Aust. J. Basic Appl. Sci.*, vol. 7, no. 5, pp. 128–139, 2013.

[110] S. W. Hwang *et al.*, "Grafting of maleic anhydride on poly(L-lactic acid). Effects on physical and mechanical properties," *Polym. Test.*, vol. 31, no. 2, pp. 333–344, Apr. 2012.

[111] J. Erdmann and J. Ganster, "Tailor-made PLA and PHB based cellulose fibre composites through coupling or anti-coupling agents," 2010.

[112] H. R. Saliu *et al.*, "The Effect of Epoxy Concentration and Fibre Loading on the Mechanical Properties of ABS/Epoxy-Coated Kenaf Fibre Composites," *Open J. Compos. Mater. Z.A. Open J. Compos. Mater.*, vol. 5, no. 5, pp. 41–48, 2015.

[113] M. A. Khan, M. Masudul Hassan, and L. T. Drzal, "Effect of 2-hydroxyethyl methacrylate (HEMA) on the mechanical and thermal properties of jute-polycarbonate composite," *Compos. Part A Appl. Sci. Manuf.*, vol. 36, no. 1, pp. 71–81, 2005.

[114] M. U. de la Orden, C. González Sánchez, M. González Quesada, and J. Martínez Urreaga, "Effect of different coupling agents on the browning of cellulose–polypropylene composites during melt processing," *Polym. Degrad. Stab.*, vol. 95, no. 2, pp. 201–206, Feb. 2010.

[115] H. Dong, K. E. Strawhecker, J. F. Snyder, J. A. Orlicki, R. S. Reiner, and A. W. Rudie, "Cellulose nanocrystals as a reinforcing material for electrospun poly(methyl methacrylate) fibers: Formation, properties and nanomechanical characterization," *Carbohydr. Polym.*, vol. 87, no. 4, pp. 2488–2495, Mar. 2012.

[116] A. Dufresne and M. N. Belgacem, "Cellulose-reinforced composites: From micro-to nanoscale," *Polímeros Ciência e Tecnol.*, vol. 20, no. 1,

pp. 1–10, 2010.

[117] M. Gama, P. Gatenholm, and D. Klemm, *Bacterial NanoCellulose: A Sophisticated Multifunctional Material*. CRC Press, 2016.

[118] C. Amara, A. El Mahdi, R. Medimagh, and K. Khwaldia, "Nanocellulose-based composites for packaging applications," *Curr. Opin. Green Sustain. Chem.*, vol. 31, p. 100512, Oct. 2021.

[119] H. Kargarzadeh, M. Ioelovich, I. Ahmad, S. Thomas, and A. Dufresne, "Methods for Extraction of Nanocellulose from Various Sources," in *Handbook of Nanocellulose and Cellulose Nanocomposites*, Weinheim, Germany: Wiley-VCH Verlag GmbH & Co. KGaA, 2017, pp. 1–49.

[120] P. Phanthong, P. Reubroycharoen, X. Hao, G. Xu, A. Abudula, and G. Guan, "Nanocellulose: Extraction and application," *Carbon Resour. Convers.*, vol. 1, no. 1, pp. 32–43, Apr. 2018.

[121] N. Lin and A. Dufresne, "Nanocellulose in biomedicine: Current status and future prospect," *Eur. Polym. J.*, vol. 59, pp. 302–325, Oct. 2014.

[122] Y. LU, H. L. TEKINALP, C. C. EBERLE, W. PETER, A. KUMAR NASKAR, and S. OZCAN, "Nanocellulose in polymer composites and biomedical applications," *TAPPI J.*, vol. 13, no. 6, pp. 47–54, Jul. 2014.

[123] R. Kumar, B. Rai, S. Gahlyan, and G. Kumar, "A comprehensive review on production, surface modification and characterization of nanocellulose derived from biomass and its commercial applications," *Express Polym. Lett.*, vol. 15, no. 2, pp. 104–120, 2021.

[124] J. D. P. de Amorim *et al.*, "Plant and bacterial nanocellulose: production, properties and applications in medicine, food, cosmetics, electronics and engineering. A review," *Environ. Chem. Lett.*, vol. 18, no. 3, pp. 851–869, May 2020.

[125] D. Trache *et al.*, "Nanocellulose: From Fundamentals to Advanced Applications," *Front. Chem.*, vol. 8, May 2020.

[126] B. L. Peng, N. Dhar, H. L. Liu, and K. C. Tam, "Chemistry and applications of nanocrystalline cellulose and its derivatives: A nanotechnology perspective," *Can. J. Chem. Eng.*, vol. 89, no. 5, pp. 1191–1206, 2011.

[127] Vijay Kumar Thakur and M. K. Thakur, *Handbook of Sustainable Polymers: Processing and Applications*, 1st ed. Singapore: Pan Stanford Publishing Pte. Ltd., 2015.

[128] A. Chakrabarty and Y. Teramoto, "Recent Advances in Nanocellulose Composites with Polymers: A Guide for Choosing Partners and How to Incorporate Them," *Polymers (Basel).*, vol. 10, no. 5, p. 517, May 2018.

[129] M. Börjesson and G. Westman, *Cellulose - Fundamental Aspects and Current Trends*. InTech, 2015.

[130] H.-M. Ng *et al.*, "Extraction of cellulose nanocrystals from plant sources for application as reinforcing agent in polymers," *Compos. Part B Eng.*,

vol. 75, pp. 176–200, Jun. 2015.

[131] M. Rajinipriya, M. Nagalakshmaiah, M. Robert, and S. Elkoun, “Importance of Agricultural and Industrial Waste in the Field of Nanocellulose and Recent Industrial Developments of Wood Based Nanocellulose: A Review,” *ACS Sustain. Chem. Eng.*, vol. 6, no. 3, pp. 2807–2828, Mar. 2018.

[132] E. Espino, M. Cakir, S. Domenek, A. D. Román-Gutiérrez, N. Belgacem, and J. Bras, “Isolation and characterization of cellulose nanocrystals from industrial by-products of Agave tequilana and barley,” *Ind. Crops Prod.*, vol. 62, pp. 552–559, 2014.

[133] A. I. Akinjokun, L. F. Petrik, A. O. Ogunfowokan, J. Ajao, and T. V. Ojumu, “Isolation and characterization of nanocrystalline cellulose from cocoa pod husk (CPH) biomass wastes,” *Heliyon*, vol. 7, no. 4, p. e06680, Apr. 2021.

[134] D. M. do Nascimento *et al.*, “A comprehensive approach for obtaining cellulose nanocrystal from coconut fiber. Part I: Proposition of technological pathways,” *Ind. Crops Prod.*, vol. 93, pp. 66–75, Dec. 2016.

[135] Z. Kassab, I. Kassem, H. Hannache, R. Bouhfid, A. E. K. Qaiss, and M. El Achaby, “Tomato plant residue as new renewable source for cellulose production: extraction of cellulose nanocrystals with different surface functionalities,” *Cellulose*, vol. 27, no. 8, pp. 4287–4303, May 2020.

[136] F. N. N. M. Hussin, N. Attan, and R. A. Wahab, “Extraction and Characterization of Nanocellulose from Raw Oil Palm Leaves (Elaeis guineensis),” *Arab. J. Sci. Eng.*, vol. 45, no. 1, pp. 175–186, Jan. 2020.

[137] C. Liu *et al.*, “Properties of nanocellulose isolated from corncob residue using sulfuric acid, formic acid, oxidative and mechanical methods,” *Carbohydr. Polym.*, vol. 151, pp. 716–724, Oct. 2016.

[138] Z. Kassab, F. Aziz, H. Hannache, H. Ben Youcef, and M. El Achaby, “Improved mechanical properties of k-carrageenan-based nanocomposite films reinforced with cellulose nanocrystals,” *Int. J. Biol. Macromol.*, vol. 123, pp. 1248–1256, Feb. 2019.

[139] L. N. Megashah, H. Ariffin, M. R. Zakaria, and M. A. Hassan, “Properties of Cellulose Extract from Different Types of Oil Palm Biomass,” *IOP Conf. Ser. Mater. Sci. Eng.*, vol. 368, p. 012049, Jun. 2018.

[140] X. J. Shen, P. L. Huang, J. H. Chen, Y. Y. Wu, Q. Y. Liu, and R. C. Sun, “Comparison of acid-hydrolyzed and TEMPO-oxidized nanocellulose for reinforcing alginate fibers,” *BioResources*, vol. 12, no. 4, pp. 8180–8198, 2017.

[141] M. R. K. Sofla, R. J. Brown, T. Tsuzuki, and T. J. Rainey, “A comparison of cellulose nanocrystals and cellulose nanofibres extracted from bagasse using acid and ball milling methods,” *Adv. Nat. Sci. Nanosci. Nanotechnol.*, vol. 7, no. 3, p. 035004, Jul. 2016.

[142] V. Nang An, H. T. Chi Nhan, T. D. Tap, T. T. T. Van, P. Van Viet, and L. Van Hieu, "Extraction of High Crystalline Nanocellulose from Biorenewable Sources of Vietnamese Agricultural Wastes," *J. Polym. Environ.*, vol. 28, no. 5, pp. 1465–1474, May 2020.

[143] X. Yang *et al.*, "Effects of preparation methods on the morphology and properties of nanocellulose (NC) extracted from corn husk," *Ind. Crops Prod.*, vol. 109, pp. 241–247, Dec. 2017.

[144] A. Bahloul *et al.*, "Micro- and nano-structures of cellulose from eggplant plant (Solanum melongena L) agricultural residue," *Carbohydr. Polym.*, vol. 253, p. 117311, Feb. 2021.

[145] M. L. Foo, C. R. Tan, P. D. Lim, C. W. Ooi, K. W. Tan, and I. M. L. Chew, "Surface-modified nanocrystalline cellulose from oil palm empty fruit bunch for effective binding of curcumin," *Int. J. Biol. Macromol.*, vol. 138, pp. 1064–1071, Oct. 2019.

[146] N. A. Nordin, O. Sulaiman, R. Hashim, and M. H. Mohamad Kassim, "Oil Palm Frond Waste for the Production of Cellulose Nanocrystals," *J. Phys. Sci.*, vol. 28, no. 2, pp. 115–126, Aug. 2017.

[147] K. Xu *et al.*, "Isolation of nanocrystalline cellulose from rice straw and preparation of its biocomposites with chitosan: Physicochemical characterization and evaluation of interfacial compatibility," *Compos. Sci. Technol.*, vol. 154, pp. 8–17, Jan. 2018.

[148] M. Antonio, "Nanocrystalline Cellulose: Production, Opportunities, and Challenges," 2014. [Online]. Available: http://blog.luxresearchinc.com/blog/2014/11/nanocrystalline-cellulose-production-opportunities-and-challenges/. [Accessed: 22-Aug-2016].

[149] M. Özgür Seydibeyoğlu and K. Oksman, "Novel nanocomposites based on polyurethane and micro fibrillated cellulose," *Compos. Sci. Technol.*, vol. 68, no. 3–4, pp. 908–914, Mar. 2008.

[150] M. A. Saïd Azizi Samir, F. Alloin, M. Paillet, and A. Dufresne, "Tangling Effect in Fibrillated Cellulose Reinforced Nanocomposites," *Macromolecules*, vol. 37, no. 11, pp. 4313–4316, Jun. 2004.

[151] M. Jonoobi, J. Harun, A. P. Mathew, and K. Oksman, "Mechanical properties of cellulose nanofiber (CNF) reinforced polylactic acid (PLA) prepared by twin screw extrusion," *Compos. Sci. Technol.*, vol. 70, no. 12, pp. 1742–1747, Oct. 2010.

[152] S. Boufi, H. Kaddami, and A. Dufresne, "Mechanical Performance and Transparency of Nanocellulose Reinforced Polymer Nanocomposites," *Macromol. Mater. Eng.*, vol. 299, no. 5, pp. 560–568, May 2014.

[153] B. Montero, M. Rico, S. Rodríguez-Llamazares, L. Barral, and R. Bouza, "Effect of nanocellulose as a filler on biodegradable thermoplastic starch films from tuber, cereal and legume," *Carbohydr. Polym.*, vol. 157, pp. 1094–1104, Feb. 2017.

[154] S. Shankar and J.-W. Rhim, "Preparation of nanocellulose from micro-

crystalline cellulose: The effect on the performance and properties of agar-based composite films," *Carbohydr. Polym.*, vol. 135, pp. 18–26, Jan. 2016.

[155] N. Peng, D. Huang, C. Gong, Y. Wang, J. Zhou, and C. Chang, "Controlled Arrangement of Nanocellulose in Polymeric Matrix: From Reinforcement to Functionality," *ACS Nano*, vol. 14, no. 12, pp. 16169–16179, Dec. 2020.

[156] J. Jose, V. Thomas, V. Vinod, R. Abraham, and S. Abraham, "Nanocellulose based functional materials for supercapacitor applications," *J. Sci. Adv. Mater. Devices*, vol. 4, no. 3, pp. 333–340, Sep. 2019.

[157] G. K. Gupta and P. Shukla, "Lignocellulosic Biomass for the Synthesis of Nanocellulose and Its Eco-Friendly Advanced Applications," *Front. Chem.*, vol. 8, Dec. 2020.

[158] DATTATREYA MANDAL, "6 potential future uses of nanocellulose – the ultimate 'wonder material,'" 2014. [Online]. Available: https://www.hexapolis.com/2014/09/02/6-potential-future-uses-nanocellulose-ultimate-wonder-material/. [Accessed: 30-May-2022].

[159] J. G. Speight, "Sources and Types of Organic Pollutants," in *Environmental Organic Chemistry for Engineers*, Elsevier, 2017, pp. 153–201.

[160] A. B. Morgan and J. W. Gilman, "An overview of flame retardancy of polymeric materials: application, technology, and future directions," *Fire Mater.*, vol. 37, no. 4, pp. 259–279, Jun. 2013.

[161] Huber Engineered Materials, "Alumina Trihydrate (ATH)," *Huber Engineered Materials*, 2017. [Online]. Available: https://www.hubermaterials.com/products/alumina-trihydrate-ath-magnesium-hydroxide-mdh/flame-retardants-smoke-suppressants/alumina-trihydrate.aspx. [Accessed: 28-Nov-2017].

[162] The R.J. Marshall Company, "Alumina Trihydrate (ATH)," *The R.J. Marshall Company*, 2016. [Online]. Available: http://www.rjmarshall.com/wp-content/uploads/2016/08/ATH_Brochure_2016-web.pdf. [Accessed: 28-Nov-2017].

[163] The R.J. Marshall Company, "Alumina Trihydrate (ATH)," *The R.J. Marshall Company*, 2017. [Online]. Available: https://www.rjmarshall.com/bayer-alumina-trihydrate-ath. [Accessed: 28-Nov-2017].

[164] D. E. Gardner, B. Walker Jr, G. Orians, and M. T. Clegg, *Toxicological Risks of Selected Flame-Retardant Chemicals*. Washington, D.C.: National Academies Press, 2000.

[165] Polymerinsights, "APP," *Polymerinsights*, 2017. [Online]. Available: http://fr.polymerinsights.com/fr-types/phosphorous/app. [Accessed: 28-Nov-2017].

[166] Connect Chemicals, “Ammonium polyphosphate,” *Connect Chemicals*, 2017. [Online]. Available: http://www.connectchemicals.com/en/products-finder/ammonium-polyphosphate-68333-79-9-24/?from=function-flame-retardant. [Accessed: 28-Nov-2017].

[167] K.-S. Lim *et al.*, “A review of application of ammonium polyphosphate as intumescent flame retardant in thermoplastic composites,” *Compos. Part B Eng.*, vol. 84, pp. 155–174, Jan. 2016.

[168] National Center for Biotechnology Information, “Compound Summary - ZINC Borate,” *National Center for Biotechnology Information*, 2017. [Online]. Available: https://pubchem.ncbi.nlm.nih.gov/compound/zinc_borate#section=Top. [Accessed: 28-Nov-2017].

[169] The Chemical Company, “Zinc Borate,” *The Chemical Company*, 2022. [Online]. Available: https://thechemco.com/chemical/zinc-borate/. [Accessed: 04-Apr-2022].

[170] Arthur Mack, “Zinc Borate,” 2012. [Online]. Available: http://fr.polymerinsights.com/fr-types/mineral/zinc-borate.

[171] Graftech International Holdings LTD, “Expandable Graphite Flake as an Additive for a New Flame Retardant Resin,” 2012. [Online]. Available: http://graftechaet.com/wp-content/uploads/2015/03/GRAFGUARD-Expandable-Graphite-Flake-as-an-Additive-for-a-New-Flame-Retardant-Resin.pdf.

[172] M. Modesti, A. Lorenzetti, F. Simioni, and G. Camino, “Expandable graphite as an intumescent flame retardant in polyisocyanurate–polyurethane foams,” *Polym. Degrad. Stab.*, vol. 77, no. 2, pp. 195–202, Jan. 2002.

[173] M. E. Mngomezulu, A. S. Luyt, S. A. Chapple, and M. J. John, “Effect of expandable graphite on thermal and flammability properties of poly(lactic acid)-starch/poly(ε-caprolactone) blend systems,” *Polym. Eng. Sci.*, vol. 58, no. 9, pp. 1619–1629, Sep. 2018.

[174] S. Chapple and R. Anandjiwala, “Flammability of natural fiber-reinforced composites and strategies for fire retardancy: A review,” *J. Thermoplast. Compos. Mater.*, vol. 23, no. 6, pp. 871–893, 2010.

[175] Z. Xu, Z. Chu, L. Yan, H. Chen, H. Jia, and W. Tang, “Effect of chicken eggshell on the flame-retardant and smoke suppression properties of an epoxy-based traditional APP-PER-MEL system,” *Polym. Compos.*, pp. 1–12, 2018.

[176] M. J. Suriani, F. S. M. Radzi, R. A. Ilyas, M. Petrů, S. M. Sapuan, and C. M. Ruzaidi, “Flammability, Tensile, and Morphological Properties of Oil Palm Empty Fruit Bunches Fiber/Pet Yarn-Reinforced Epoxy Fire Retardant Hybrid Polymer Composites,” *Polymers (Basel).*, vol. 13, no. 8, p. 1282, Apr. 2021.

[177] P. Khalili, K. Y. Tshai, and I. Kong, “Effects of organophosphorus and

mineral based flame retardants on combustibility and mechanical performances of natural fiber reinforced composites," *World J. Eng.*, vol. 13, no. 3, pp. 193–198, 2016.

[178] P. Khalili, K. Y. Tshai, and I. Kong, "Natural fiber reinforced expandable graphite filled composites: Evaluation of the flame retardancy, thermal and mechanical performances," *Compos. Part A Appl. Sci. Manuf.*, vol. 100, pp. 194–205, 2017.

[179] P. Khalili, K. Y. Tshai, I. Kong, and C. H. Yeoh, "The Effects of Graphene and Flame Retardants on Flammability and Mechanical Properties of Natural Fibre Reinforced Polymer Composites," *Key Eng. Mater.*, vol. 701, pp. 286–290, 2016.

[180] P. Khalili, K. Y. Tshai, D. Hui, and I. Kong, "Synergistic of ammonium polyphosphate and alumina trihydrate as fire retardants for natural fiber reinforced epoxy composite," *Compos. Part B Eng.*, vol. 114, pp. 101–110, 2017.

[181] A. Toldy, B. Szolnoki, and G. Marosi, "Flame retardancy of fibre-reinforced epoxy resin composites for aerospace applications," *Polym. Degrad. Stab.*, vol. 96, no. 3, pp. 371–376, 2011.

[182] S. Karunakaran, D. L. Majid, and M. L. M. Tawil, "Flammability of self-extinguishing kenaf/ABS nanoclays composite for aircraft secondary structure," *IOP Conf. Ser. Mater. Sci. Eng.*, vol. 152, no. 1, 2016.

[183] P. Threepopnatkul, T. Krachang, and C. Kulsetthanchalee, "Phosphate Derivative Flame Retardants on Properties of Pineapple Leaf Fiber/Abs Composites," *Polym. Polym. Compos.*, vol. 22, no. 7, pp. 591–598, Sep. 2014.

[184] H. Cirmad, S. Tirkes, and U. Tayfun, "Evaluation of flammability, thermal stability and mechanical behavior of expandable graphite-reinforced acrylonitrile–butadiene–styrene terpolymer," *J. Therm. Anal. Calorim.*, vol. 147, no. 3, pp. 2229–2237, Feb. 2022.

[185] D. Amrishraj and T. Senthilvelan, "Acrylonitrile butadiene styrene composites reinforced with nanozirconia and PTFE: Mechanical and thermal behavior," *Polym. Compos.*, vol. 39, no. S3, pp. E1520–E1530, Jun. 2018.

[186] H. Ma, J. Wang, and Z. Fang, "Cross-linking of a novel reactive polymeric intumescent flame retardant to ABS copolymer and its flame retardancy properties," *Polym. Degrad. Stab.*, vol. 97, no. 9, pp. 1596–1605, Sep. 2012.

[187] H. Demir, D. Balköse, and S. Ülkü, "Influence of surface modification of fillers and polymer on flammability and tensile behaviour of polypropylene-composites," *Polym. Degrad. Stab.*, vol. 91, no. 5, pp. 1079–1085, 2006.

[188] J. da S. Rocha, V. A. Escócio, L. L. Visconte, and É. B. Pacheco, "Thermal and flammability properties of polyethylene composites with fibers to replace natural wood," *J. Reinf. Plast. Compos.*, vol. 40, no. 19–

20, pp. 726–740, Oct. 2021.

[189] A. Schirp and A. Hellmann, “Fire retardancy improvement of high-density polyethylene composites based on thermomechanical pulp treated with ammonium polyphosphate,” *Polym. Compos.*, 2018.

[190] H. Blom, R. Yeh, R. Wojnarowski, and M. Ling, “Detection of degradation of ABS materials via DSC,” *J. Therm. Anal. Calorim.*, vol. 83, no. 1, pp. 113–115, Jan. 2006.

[191] J. TOMASZEWSKA, T. STERZYNSKI, and K. PISZCZEK, “The influence of the chamber temperature in the Brabender measuring mixer on the state of equilibrium of the torque of rigid poly(vinyl chloride),” *Polimery*, vol. 53, no. 09, pp. 678–680, Sep. 2008.

[192] Shao-Yun Fu, B. Lauke, and Yiu-Wing Mai, *Science and Engineering of Short Fibre Reinforced Polymer Composites*, 3nd ed. Woodhead Publishing, 2019.

[193] B. . Tiganis, L. . Burn, P. Davis, and A. . Hill, “Thermal degradation of acrylonitrile–butadiene–styrene (ABS) blends,” *Polym. Degrad. Stab.*, vol. 76, no. 3, pp. 425–434, Jun. 2002.

[194] N. Joudeh and D. Linke, “Nanoparticle classification, physicochemical properties, characterization, and applications: a comprehensive review for biologists,” *J. Nanobiotechnology*, vol. 20, no. 1, p. 262, Jun. 2022.

[195] Y. K. Song, I. M. Leng Chew, T. S. Yaw Choong, J. Tan, and K. W. Tan, “Isolation of Nanocrystalline Cellulose from oil palm empty fruit bunch – A response surface methodology study,” *MATEC Web Conf.*, vol. 60, p. 04009, Jun. 2016.

[196] S. Naduparambath, M. P. Sreejith, T. V. Jinitha, V. Shaniba, K. B. Aparna, and E. Purushothaman, “Development of green composites of poly (vinyl alcohol) reinforced with microcrystalline cellulose derived from sago seed shells,” *Polym. Compos.*, vol. 39, no. 9, pp. 3033–3039, Sep. 2018.

[197] Y. C. Ching, A. Rahman, K. Y. Ching, N. L. Sukiman, and C. H. Chuah, “Preparation and characterization of polyvinyl alcohol-based composite reinforced with nanocellulose and nanosilica,” *BioResources*, vol. 10, no. 2, pp. 3364–3377, 2015.

[198] S. Fu, P. Song, and X. Liu, “Thermal and flame retardancy properties of thermoplastics/natural fiber biocomposites,” in *Advanced High Strength Natural Fibre Composites in Construction*, Elsevier, 2017, pp. 479–508.

[199] B. Baltaci, G. Ö. Çakal, G. Bayram, I. Eroglu, and S. Özkar, “Surfactant modified zinc borate synthesis and its effect on the properties of PET,” *Powder Technol.*, vol. 244, pp. 38–44, Aug. 2013.

[200] T. M. Simionescu, A. A. Minea, and P. N. B. dos Reis, “Fire Properties of Acrylonitrile Butadiene Styrene Enhanced with Organic Montmorillonite and Exolit Fire Retardant,” *Appl. Sci.*, vol. 9, no. 24, p. 5433, Dec. 2019.

[201] R. Vitali, C. M. Belcher, J. O. Kaplan, and A. J. Watson, “Increased fire activity under high atmospheric oxygen concentrations is compatible with the presence of forests,” *Nat. Commun.*, vol. 13, no. 1, p. 7285, Nov. 2022.

[202] R. Sonnier, A. Taguet, L. Ferry, and J.-M. Lopez-Cuesta, “Flame Retardancy of Natural Fibers Reinforced Composites,” 2018, pp. 73–98.